UNIVERSITY OF THESSALY

SCHOOL OF ENGINEERING

MECHANICAL AND INDUSTRIAL ENGINEERING DEPARTMENT

Master Thesis

PASSIVE CONTROL OF STRUCTURES: EXPERIMENTAL VERIFICATION USING TUNED MASS DAMPERS

By

KARAISKOS K. GRIGORIOS

Diploma in Mechanical & Aeronautical Engineering

University of Patras 2005

A Thesis
Submitted in Partial Fulfillment of the
Requirements for the Degree of
Master of Science
(in Mechanical & Industrial Engineering)

2008

ΠΑΝΕΠΙΣΤΗΜΙΟ ΘΕΣΣΑΛΙΑΣ

ΠΟΛΥΤΕΧΝΙΚΗ ΣΧΟΛΗ

ΤΜΗΜΑ ΜΗΧΑΝΟΛΟΓΩΝ ΜΗΧΑΝΙΚΩΝ ΒΙΟΜΗΧΑΝΙΑΣ

Μεταπτυχιακή Εργασία

ΠΑΘΗΤΙΚΟΣ ΕΛΕΓΧΟΣ ΤΩΝ ΚΑΤΑΣΚΕΥΩΝ: ΠΕΙΡΑΜΑΤΙΚΗ ΠΙΣΤΟΠΟΙΗΣΗ ΑΠΟΣΒΕΣΤΗΡΩΝ ΕΛΕΓΧΟΜΕΝΗΣ ΜΑΖΑΣ

υπό

ΚΑΡΑΪΣΚΟΥ Κ. ΓΡΗΓΟΡΙΟΥ

Διπλωματούχου Μηχανολόγου & Αεροναυπηγού Μηχανικού

Πανεπιστήμιο Πατρών 2005

Υπεβλήθη για την εκπλήρωση μέρους των
απαιτήσεων για την απόκτηση του
Μεταπτυχιακού Διπλώματος Ειδίκευσης

2008

Η έγκριση της Μεταπτυχιακής Εργασίας από το Τμήμα Μηχανολόγων Μηχανικών Βιομηχανίας της Πολυτεχνικής Σχολής του Πανεπιστημίου Θεσσαλίας δεν υποδηλώνει αποδοχή των απόψεων του συγγραφέα (Ν. 5343/32 αρ. 202 παρ. 2)

Εγκρίθηκε από τα Μέλη της Πενταμελούς Εξεταστικής Επιτροπής:

Πρώτος Εξεταστής (Επιβλέπων)	Δρ. Κωνσταντίνος Παπδημητρίου Καθηγητής, Τμήμα Μηχανολόγων Μηχανικών Βιομηχανίας, Πανεπιστήμιο Θεσσαλίας
Δεύτερος Εξεταστής (Συνεπιβλέπων)	Δρ. Παναγιώτης Παπανικολάου Επίκουρος Καθηγητής, Τμήμα Πολιτικών Μηχανικών, Πανεπιστήμιο Θεσσαλίας
Τρίτος Εξεταστής	Δρ. Σπύρος Καραμάνος Επίκουρος Καθηγητής, Τμήμα Μηχανολόγων Μηχανικών Βιομηχανίας, Πανεπιστήμιο Θεσσαλίας
Τέταρτος Εξεταστής	Δρ. Τάσος Σταματέλλος Καθηγητής, Τμήμα Μηχανολόγων Μηχανικών Βιομηχανίας, Πανεπιστήμιο Θεσσαλίας
Πέμπτος Εξεταστής	Δρ. Γεώργιος Πετρόπουλος Επίκουρος Καθηγητής, Τμήμα Πολιτικών Μηχανικών, Πανεπιστήμιο Θεσσαλίας

Ευχαριστίες

Από τη θέση αυτή θέλω να ευχαριστήσω κάποιους ανθρώπους οι οποίοι έχουν σταθεί δίπλα μου στην προσπάθεια ολοκλήρωσης επιτυχώς των μεταπτυχιακών μου σπουδών.

Αρχικά θέλω να ευχαριστήσω τον Καθηγητή και Δάσκαλό μου, Καθηγητή Κώστα Παπαδημητρίου, ο οποίος πίστεψε στις ικανότητές μου και με δέχτηκε στο Εργαστήριο Δυναμικής των Κατασκευών το οποίο και διευθύνει. Τον ευχαριστώ θερμά για την αμεσότητα και συνεργασιμότητα σε οποιοδήποτε θέμα προέκυπτε αλλά και για τις εποικοδομητικές συζητήσεις μαζί του εντός και εκτός του Εργαστηρίου.

Παράλληλα θέλω να ευχαριστήσω τον συνεπιβλέποντα και συντοπίτη Καθηγητή Παναγιώτη Παπανικολάου για τις εύστοχες και χρήσιμες παρατηρήσεις και συμβουλές του κατά τη διάρκεια των πειραματικών διεργασιών.

Επίσης οφείλω ένα μεγάλο ευχαριστώ στο συνάδελφο και υποψήφιο Διδάκτορα Βαγγέλη Ντότσιο ο οποίος με βοήθησε κυρίως σε θέματα μορφικής ανάλυσης των κατασκευών αλλά και για την ανιδιοτελή χορήγηση του αξιόπιστου κώδικα που έχει αναπτύξει για τη μορφική ανάλυση κατασκευών βασιζόμενη σε μετρήσεις επιταχύνσεων.

Τελειώνοντας, θέλω να εκφράσω το βαθύτερο μου σεβασμό και αγάπη στους γονείς μου οι οποίοι με στηρίζουν σε όλες μου τις προσπάθειες, στόχους και επιλογές ανιδιοτελώς. Εντούτοις, αν και κάποιες φορές έχουμε αντίθετη γνώμη εκείνοι εξακολουθούν και πιστεύουν σε εμένα και τις δυνατότητές μου προσπαθώντας πάντα για το καλύτερο.

Στους Γονείς μου

Abstract

The focus of this thesis is to review and experimentally verify the effect of vibrational control systems applied in tall and flexible structures. The installation of these systems on new and existing structures aim at the spectacular improvement of the structural dynamic behavior under different types of manmade and ambient excitations on the concepts of structural safety and operational conditions.

The control theory of this thesis is applied for the design of Passive Control Systems and more specifically for the design of Tuned Mass Damper (TMD) installed properly on the main structure. The main mass of the Tuned Mass Damper, which is named as secondary system, is significantly smaller than the main mass of the primary system which is a Single Degree of Freedom (SDOF) system.

A series of experiments with one and two TMDs installed on a SDOF modeled small laboratory structure are designed, constructed and performed. The structural behavior of the laboratory structure was tested by subjecting to artificially induced harmonic excitation and one of the components available during the strong El Centro earthquake. The main modal characteristics of the combined primary-secondary system studied are the modal frequencies, the damping coefficients and the mass ratios between primary and secondary systems.

A smart laboratory technique for damping improvement of structures was also employed to both primary and secondary systems and it is shown that sensibly contributes to vibration attenuation of the primary system.

All the experimental concepts and results are discussed herein and demonstrate the effectiveness and reliability of Passive Control Systems installed on tall and flexible structures that are susceptible to strong winds and earthquake events.

Contents

List of Figures

Chapter 4

Chapter 5

List of Tables

CHAPTER 1

INTRODUCTION

1.1 Introduction

Continued urbanization and localization of people into massive city centers fuel the desire to reach the sky. Taller buildings are required to satisfy space requirements in such a clustered environment. As buildings increase in height, flexibility will become critical in defining their structural integrity. The current trend toward structures of ever increasing heights and the use of lightweight and high-strength materials have led to very flexible and lightly damped structures. Understandably, these structures are very sensitive to manmade and environmental excitations such as wind and earthquakes. Under the action of one or a combination of these loads, a structure may experience dynamic load effects which may lead to structural failure, fatigue, occupant discomfort and operational difficulty of supporting equipment of the structure (Nyawako and Reynolds (2007)).

From the early years of industrialization the humanity tried to protect its creations against those manmade excitations and hazard natural phenomena like strong winds and earthquakes which threat their existence and safe operation. The earliest method to do that was any kind of Passive Control Systems which alleviate energy dissipation demand on the primary structure by reflecting or absorbing part of the input energy, thereby reducing possible structural damage (Housner et al. (1997)).

Any structure that is built must be designed with certain forces in mind. Some of the forces that buildings must withstand are live and some others are dead loads. On the one hand live loads refer to loads that move and on the other hand dead loads refer to loads that are permanent and do not move. The structural flexibility compromises human comfort levels in the building to a far greater degree than structural integrity (Lametrie (2001), Fujino et al. (1996)).

Today, one of the main challenges in structural engineering is to develop innovative design concepts to better protect civil structures, including their material contents and human occupants, from these hazards of strong wind and earthquakes. Conventionally,

structures have been designed to resist natural hazards through a combination of strength, deformability and energy absorption. These structures may deform well beyond the elastic limit, for example in a severe earthquake. They may remain intact only due to their ability to deform inelastically, as this deformation results in increased flexibility and energy dissipation. Unfortunately, this deformation also results in local damage to the structure, as the structure itself must absorb much of the earthquake input energy. It is ironic that the prevention of the devastating effects from these natural hazards, including structural damage, is frequently attained by allowing certain structural damage.

Alternatively, some types of structural protective systems may be implemented to mitigate the damaging effects of these environmental forces. These systems work by absorbing or reflecting a portion of the input energy that would otherwise be transmitted to the structure itself. Considering the following energy conservation relationship (Uang and Bertero (1988)) as an illustration of this approach:

$$E = E_k + E_s + E_h + E_d$$

where

E = total energy input from environmental and manmade forces,

E_k = absolute kinetic energy

E_s = recoverable elastic strain energy

E_h = irrecoverable energy dissipated by the structural system through inelastic or other inherent forms of damping and

E_d = energy dissipated by structural protective systems.

From this equation, with certain input energy, the demand on energy dissipation through inelastic deformation can be reduced by using structural protective systems. As a result of this approach, many new and innovative concepts for structural protection have been advanced and are at various stages of development. These concepts can be divided into three main categories, namely *Passive Control Systems*, *Active Control Systems*, *Semi-*

Active Control Systems and *Hybrid Control Systems* (Housner et al. (1997), Symans and Comstantinou (1999), Fujino et al. (1996)).

Vibration Control is the design or modification of a system to suppress unwanted vibrations or to reduce force or motion transmission. The design parameters include inertia properties, stiffness properties, damping properties, and even the system configuration including the number of degrees of freedom.

To be more specific, Active, Semi-Active and Hybrid structural control systems are a natural evolution of Passive control technologies. The possible use of Active Control Systems and some combinations of Passive and Active Systems as a means of structural protection against ambient and manmade excitations has received considerable attention in recent years.

Damping is the dissipation of energy from an oscillating system, primarily through friction. The kinetic energy is transformed into heat. Dampers, as mechanical systems can be installed to increase the damping rate. Attention has been devoted to active control of engineering structures for earthquake hazard mitigation.

A significant number of tall buildings and towers, particularly in Japan, are fitted with a variety of those systems to reduce the dynamic response caused by environmental loads such as wind and earthquake. Although it is not yet routine design practice to design damping capacity into a structural system, or to consider the need for other mechanical means to increase the damping capacity of a building, this has become increasingly more common in the new generation of tall and super tall buildings. The selection of a particular type of vibration control device is governed by a number of factors which include efficiency, compactness and weight, capital cost, operating cost, maintenance requirements and safety.

Serviceability is an extremely important issue in the design of tall buildings under wind loading. There are primarily two types of serviceability problems caused by winds. The first type concerns large deflections causing architectural damage to nonstructural members like glass panes and fatigue damage to structural elements. The other one is the oscillatory motion which may cause discomfort or even panic to the occupants due to the acceleration and the rate of change of acceleration which are the main causes of human discomfort.

In evaluating the performance of the vibration control system, fundamental characteristics of the device should be examined and the general measures for performance evaluation should be prepared. Fundamental characteristics of the device are examined based on the following parameters.

- Dimensions of the device
- Weight of device, including moving parts
- Maximum stroke and maximum speed
- Number of moving masses and driver units
- Power of driver unit
- Number, type, characteristics and mechanism of sensors
- Number and system of computer and method of detecting abnormal operation
- Provision of software (number of subprograms)
- Number of control modes or control frequency range
- Control method and algorithms
- Countermeasures to malfunctions
- Countermeasures to accidents and abnormal operation
- Countermeasures to environmental effects and maintenance
- Economy (initial and running costs)
- Result of response in the time domain

For vibration control of ambient-induced responses, uncertainty exists in mathematical models of the building, vibration control system and in the monitoring system. These uncertainties affect the efficiency of the control system and may lead to malfunctions or failure. Errors or uncertainties in mathematical modeling consist of inaccuracy of identified system parameters and a lack of information of higher modes due to simplification, which causes spill-over problems. Uncertainties in the monitoring system include time delay, noise and failures.

Many buildings have been built as passive structures. Passive structures use their mass and solidity to resist external forces. As passive structures, they can not adapt to a changing environment. Many factors have surfaced as keys to building better buildings.

These factors are: flexibility, safety, material and lower costs. Thus, structural control takes on a new technology that permits the design of lighter structures with control. Structural control is now an area of heavy research for its means of controlling systems through an external energy supply or not in order to extend their life.

1.2 Overview of the Thesis

The focus of this thesis is to review and experimentally verify the effect of Tuned Mass Dampers (TMD) on the dynamic behavior of tall and flexible structures being excited by different types of excitations. All the concepts of designing and performing a passive control experiment on a small laboratory structure are presented and the results of the experiments are discussed.

Chapter 2 presents a structural control review. All the main categories of Structural Control Systems are briefly presented and their advantages and disadvantages are discussed.

In Chapter 3 the equations of motion that describe a Single Degree of Freedom (SDOF) system with the presence either one Tuned Mass Damper (TMD) or Multiple Tuned Mass Dampers (MTMD) connected in parallel with the main SDOF system are presented. A methodology for optimal design and selection of the parameters of the TMD is given.

In Chapter 4 a detailed presentation of the whole design and instrumentation process of the experiment is given. Data acquisitioning problems encountered during the experiments are also pointed out and discussed. Additionally, experimental modern modal analysis method is introduced for the extraction of the modal parameters of the tested structure.

In Chapter 5 modal analysis is applied at main and secondary systems and the results are presented. In addition, the implementation of one or two TMDs installed on the main system and subjected to different excitation scenarios is experimentally verified. Finally, the effect of adding some extra damping for both the main and secondary system is investigated by repeating some of the experiments.

Conclusions and future work on Structural Control close the present thesis in Chapter 6.

CHAPTER 2

STRUCTURAL CONTROL REVIEW

2.1 Passive Control Systems

Passive Control Systems alleviate energy dissipation demand on the primary structure by reflecting or absorbing part of the input energy, thereby reducing possible structural damage (Housner et al. (1997)). They do not require power to operate, so they are very reliable since they are unaffected by power outages which are common during earthquakes. They dissipate energy using the structure's own motion to produce relative movement within the control device (Symans et al. (1994)) or by converting kinetic energy to heat. Since they do not inject energy into the system they are unable to destabilize it, their maintenance requirements are very low and they are low in cost and effective for support of buildings in low structural risk areas (Housner et al. (1997), Soong and Spencer (2002)).

They are simple and generally low in cost, but are unable to adapt changing needs. Passive Control Systems are most commonly used in new and existing buildings that are in low seismic areas.

There have been numerous investigations, both analytical/numerical and experimental, into the area of passive vibration control of tall buildings. The basic concept of these devices is to increase the effective structural damping of the structure near a critical mode of vibration by dynamically coupling the structure to an absorber system as well as increasing its inherent stiffness and strength. In general such systems are characterized by their capability to enhance energy dissipation in the structural systems in which they are installed.

There are many reasons for installing Passive Control Systems in buildings. The ability to guarantee a certain amount of damping by auxiliary damping devices significantly improves structural design reliability whereas uncertainty of inherent structural damping reduces it. In designing ambient-excited sensitive buildings, possibly employing auxiliary damping devices, designers have to choose the most suitable device based on their

judgment of its effectiveness and on the various design conditions (Tamura (1998)). To accomplish this, it is necessary to do the following:

- Establish a basic policy for structural design of buildings employing damping devices
- Clarify the purposes of vibration control
- Estimate excitation levels
- Model the dynamic characteristics of the structure by establishing an analytical model
- Select response prediction methods according to the excitations and the analytical model
- Select an appropriate damping device
- Confirm and evaluate damping efficiency
- Evaluate system reliability
- Establish system maintenance and administration methods

However, Passive Control Systems are limited in that they can not deal with the change of either external loading conditions or usage patterns. These devices generally operate on principles such as frictional sliding, yielding of metals, phase transformation in metals, deformation of viscoelastic solids or fluids and fluid orificing.

The effectiveness of a Passive Control System is usually measured in terms of structural safety, human comfort and minimum cost. Structural safety can be ensured by imposing a constraint on the maximum allowable deflection and/or acceleration at a critical location of the structure. In addition, a human comfort requirement dictates that the acceleration should not violate some acceptable criterion. The cost of Passive Control imposes a third constraint and it can usually be expressed as a function of the magnitude of the control forces applied to the structure. While it is desirable to maximize the safety and to minimize the cost, both requirements cannot be achieved simultaneously.

In what follows, basic principles of Passive Control Systems are illustrated using a single-degree-of-freedom (SDOF) structural model (Soong and Spencer (2002)). Consider the lateral motion of the SDOF model consisting of a mass m, supported by

springs with total linear elastic stiffness k, and a damper with damping coefficient c. This SDOF system is then subjected to an earthquake load (stochastic load) where $\ddot{x}_g(t)$ is ground acceleration. The excited model responds with a lateral displacement $x(t)$ relative to the ground which satisfies the equation of motion

$$m\ddot{x} + c\dot{x} + kx = -m\ddot{x}_g \tag{2.1}$$

and schematically presented in Fig. 2.1

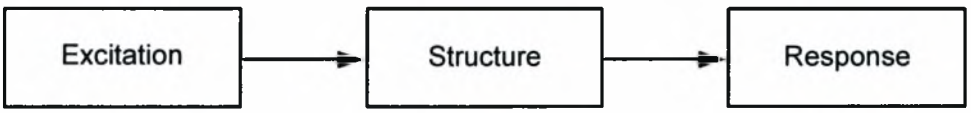

Figure 2.1: Conventional structure under external loading

Consider now the addition of a generic Passive Control System into the SDOF model. The above equation of motion for the extended SDOF model, which is schematically presented by Fig. 2.2

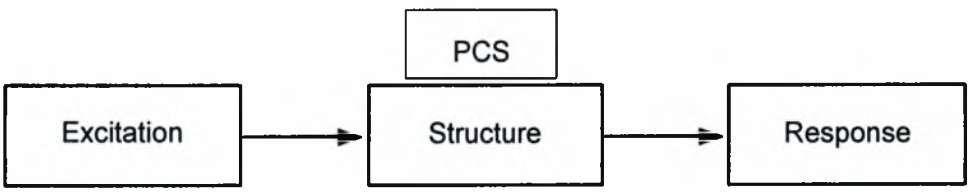

Figure 2.2: Schematic diagram of Passive Control Systems (PCS)

then Eq. (2.1) becomes

$$m\ddot{x} + c\dot{x} + kx + \Gamma x = -\left(m + \bar{m}\right)\ddot{x}_g \tag{2.2}$$

where $\bar{m}$ is the mass of the Passive Control System and the force corresponding to the device is written as Γx, where Γ represents a generic integrodifferential operator. The specific form of Γx needs to be specified before Eq. (2.2) can be analyzed, which is necessarily highly dependent on the device type. It is seen that from the addition of the Γx term in Eq. (2.2), the structural properties have modified so that it can respond more favorably to the designed or anticipated ground motion.

Generally speaking, Passive Control Systems include base isolation systems, bracing systems, friction dampers, metallic yield dampers, viscoelastic dampers, viscous fluid dampers, tuned mass dampers (TMD), tuned liquid dampers (TLD) and tuned liquid column dampers (TLCD).

On the one side there are Passive Control Systems which employ passive supplemental damping devices. These devices protect a structure by increasing its energy dissipation capacity. A supplemental damping system works by absorbing a portion of the input energy to a structure, thereby reducing energy dissipation demands and preventing damage to the primary structure. This effect is achieved either by conversion of kinetic energy to heat or through the transfer of energy among vibration modes.

That method utilizes devices that operate on principles such as frictional sliding, yielding of metals, phase transformation in metals and deformation of viscoelastic solids or fluids (Soong and Dargush (1997), Soong and Spencer (2002)). Examples include metallic yield dampers (Clark et al. (1999), Dargush and Soong (1995), Ou and Wu (1995), Scholl (1993), Tsai et al. (1993), Wada et al. (1999), Whittaker et al. (1993), Xia and Hanson (1992)), friction dampers (Aiken and Kelly (1990), Colajanni and Papia (1997), Filiatrault and Cherry (1990), Filiatrault et al. (2000), Levy et al. (2000), Li and Reinhorn (1995), Nims et al. (1993), Pall and Marsh (1982), Scholl (1993)), viscoelastic dampers (Aprile et al. (1997), Crosby et al. (1994), Ferry (1980), Higgins and Kasai (1998), Makris and Dargush (1994), Shen and Soong (1995)), viscous fluid dampers (Constantinou et al. (1993), Constantinou and Symans (1993), Makris (1991),Makris et al. (1995), (1996) and (1997), Reinhorn et al. (1995), Taylor and Constantinou (1996)), viscous damping walls (Arima (1988), Miyazaki and Mitsusaka (1992), Reinhorn and Li (1995)) which attenuate the force due to external and seismic loads.

Base isolation systems are typically placed at the foundation of a structure and the isolation system introduces flexibility and energy absorption capabilities, thereby reducing the levels of energy and floor acceleration which can be transmitted to the structure. The most important requirements for an isolation system are its flexibility to lengthen the natural period and produce an isolation effect, its sufficient rigidity under service loads against ambient vibrations and its energy dissipation capability (Buckle and Mayes (1990)).

Bracing systems are used to permanently stabilize buildings from external forces such as wind loads and earthquakes.

Friction dampers consist of a steel plate and two plates holding the steel plate from both sides. All plates work together to absorb energy by friction as the building deforms due to seismic activity.

Metallic yield dampers rely on the inelastic deformation of metals to dissipate energy. Many of these devices use mild steel plates with triangular or X shapes so that yielding is spread almost uniformly throughout the material. Some particularly desirable features of these devices are their stable hysteretic behavior, low-cycle fatigue property, long term reliability, and relative insensitivity to environmental temperature. Hence, numerous analytical and experimental investigations have been conducted to determine these characteristics of individual devices. These devices were first implemented in New Zeland and Japan and later used to retrofit structures in Mexico and the United States (Soong and Spencer Jr. (2002)).

Viscoelastic (VE) dampers used in structural applications are usually made of materials like copolymers or glassy substances that dissipate energy through shear deformation. A typical VE damper, which consists of VE layers bonded with steel plates is shown in the Fig. 2.3 (Housner et al. (1997), Soong and Spencer (2002)). When mounted in a structure, shear deformation and hence energy dissipation takes place when structural vibration induces relative motion between the outer steel flanges and the center plates.

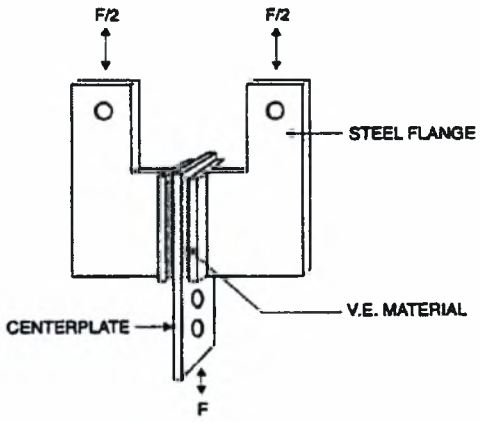

Figure 2.3: Typical VE damper configuration

A viscous fluid (VF) damper is very similar to an automotive shock absorber, consisting of a cylinder filled with a liquid such as silicone or oil and a piston with small openings through which the fluid passes from one side to another. Thus, VF dampers dissipate energy through the movement of a piston in a highly VF based on the concept of fluid orificing.

On the other side, there are famous methods of energy dissipation which incorporate dynamic vibration absorbers, such as Tuned Mass Dampers (TMD) (Abe and Fujino (1994), Clark (1988), den Hartog (1947), Jangid (1999), Li (2000), Sadek et al (1997), Tsai and Lin (1993)). Through intensive research and development in recent years, the TMD has been accepted as an effective vibration control device for both new structures and existing ones to enhance their reliability against winds, earthquakes and human activities.

TMD theory has been adopted to reduce vibrations of tall buildings and also other civil engineering structures. TMDs can be incorporated into an existing structure with less interference compared with other passive energy dissipation devices. However, it is found that the vibration control effectiveness of a TMD depends not only on the controlled modal parameters of the main structure but also on the installed location and moving direction of the TMD as well as the direction of excitation. The TMD is designed to control the mode which makes most contribution to the largest response of the structure. The spring and damping components are tuned to a specific frequency,

resulting in the TMD's control being limited to a single structural mode. Those components cause the energy to dissipate resulting in the reduction of the structure's dynamic response through which the TMD transfers inertial force to the building. Its optimum installation location and moving direction are determined from the mode shape values of controlled mode. It is applied to the structure at the location of maximum dynamic response, typically at the top of it. The optimal system parameters of TMD are then calculated by minimizing the mean-square total modal displacement response ratio of controlled mode between the structure with and without TMD under any type of excitation from critical direction.

2.1.1 Tuned Mass Damper (TMD)

One of the simplest and most reliable control measures at present is the Tuned Mass Damper (TMD). A TMD is a mass that is supported by a pendulum arrangement such as a simple pendulum which is designed to reduce building motions by applying inertial and damping forces opposite to the direction of building motions.

Basically, a TMD is a device consisting of a mass m attached on the top of a building or a structure such that it oscillates at the same frequency as the structure but with a phase shift (90^o). The mass is usually attached to the building via a spring-dashpot system and energy is dissipated as relative motion develops between the mass and the structure as well as it can be made of any material such as concrete and/or steel, while damping is typically provided by viscous damping devices such as large shock absorbers. The space envelope for a TMD is a combination of the physical size of the TMD mass plus the additional space required to accommodate the necessary amplitude of the swinging mass, the supporting structure and the viscous damping devices (Housner et al. (1997)).

The mechanism of suppressing structural vibrations by attaching a TMD to the structure is to transfer the vibration energy of the structure to the TMD and to dissipate the energy at the damper of the TMD. In order to enlarge the dissipation energy in a TMD, it is essential to tune the natural frequency of the TMD to that of the structural motion and to select the appropriate capacity of the damper. This means that there exist optimum parameters of a TMD and the optimization of a TMD for different types of structural

oscillations, such as harmonically forced oscillation, randomly forced oscillation, free vibration and self-excited vibration, has been investigated by many researchers.

The TMD has many advantages compared with other damping devices: compactness, reliability, efficiency, low maintenance cost amongst others. Hence, in recent years it has been widely used in civil engineering structures (Chang (1999), Rahul and Soong (1998), Kwok and Samali (1995)).

TMDs have proven to be effective for certain applications but they are not perfect and are limited in the magnitude of motion reduction they can achieve. To be more specific, in order to have the best results in vibration attenuation of the structure, the main eigenfrequency of the ambient excitation should be very close to one of the first natural frequencies of the structure that is to be damped (Papadimitriou (2006)). In any other case, either the TMD has no meaning or it acts against the structure. For this reason, the optimal design of a TMD is only possible when the frequency of the induced force is known. In addition to this, by increasing the mass ratio of the TMD and main system and by increasing the damping ratio of the TMD these result in the vibration attenuation of the main system. When the excitation frequency is unknown, like in an earthquake, it is impossible to design an effective, let alone optimal, TMD to control the vibrations.

There are, however, some disadvantages in a TMD. The sensitivity of a TMD's effectiveness to a fluctuation in the natural frequency of the structure and/or that in the damping ratio of the TMD is one of the disadvantages. The effectiveness of a TMD is decreased significantly by the mistuning or the off-optimum damping of the TMD. That is, a TMD is not robust at all.

Conclusively, the vibration attenuation of the Main System mass M can be achieved by these ways:

- By choosing the eigenfrequency of secondary system very close to the eigenfrequency of the primary system.
- By choosing the mass m of the secondary system to be about 2% mass M of the primary system.

- By increasing the damping ratio $\zeta = \frac{c}{2m\omega} = \frac{c}{2m\sqrt{k/m}} = \frac{c}{2mk}$ of the secondary system.
- By increasing the mass $\mu = \frac{m}{M}$ ratio of the system.

Consider a one-degree-of-freedom system fitted with a TMD, as shown in Fig. 2.4 (Kwok and Samali (1995))

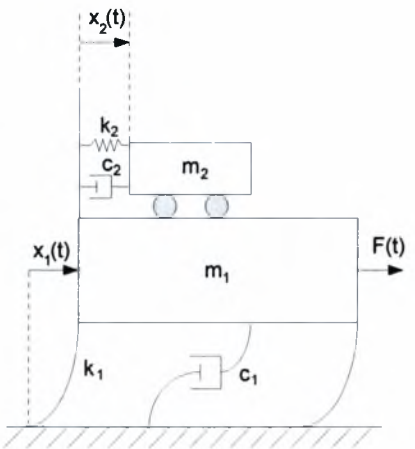

Figure 2.4: One-degree-of-freedom system fitted with TMD

The equations of motion of the resultant two-degree-of-freedom system subjected to an external excitation F can be written in the form

$$m_1\ddot{x}_1 + c_1\dot{x}_1 + k_1x_1 + c_2\left(\dot{x}_1 - \dot{x}_2\right) + k_2\left(x_1 - x_2\right) = F \tag{2.3}$$

$$m_2\ddot{x}_2 + c_2\left(\dot{x}_2 - \dot{x}_1\right) + k_2\left(x_2 - x_1\right) = 0 \tag{2.4}$$

in which m_1, c_1, k_1, $x_1(t)$ are the mass, the damping capacity, the stiffness and the response of the main system, m_2, c_2, k_2, $x_2(t)$ are the mass, the damping capacity, the stiffness and the response of the TMD.

As a single TMD cannot provide vibration control for more than one mode therefore, investigations have been made regarding controlling multiple structural modes using Multiple Tuned Mass Dampers (MTMD). The multiple passive-damping systems would be another alternative to control more than one mode of vibration in a building. They however found that adding TMDs tuned to the second and third modes deteriorated the first mode response and that the use of multiple TMDs for multiple mode control was not effective.

When a TMD is installed in the structure to control a particular mode, properties of the finally obtained system become different from those of the original structure. Now, if an additional TMD tuned to another mode is also to be installed, it may not perform as expected because of this effective change in structural parameters. Also, the addition of a TMD may affect the performance of TMD(s) already present.

2.1.2 Multiple Tuned Mass Damper (MTMD)

Some researchers (Igusa and Xu (1991)) demonstrated that a series of lightly damped oscillators, whose frequencies are distributed over a small range around the natural frequency of a SDOF system, can be more effective and more robust than a single TMD with equal total mass when the system is excited by a wideband random disturbance. It was found that the multiple oscillators are equivalent to a single 'moderately damped' TMD.

MTMDs consisting of N TMDs are considered for the control of a specific single mode vibration of a structure, and the analytical model is shown in Fig. 2.5 in which the main system is modeled as a SDOF system is set to have different dynamic characteristics. Especially the natural frequencies of MTMDs are to be distributed around the natural frequency of the structural vibration mode which is to be suppressed.

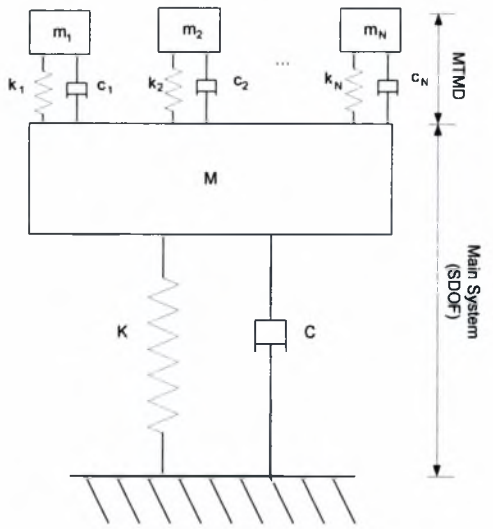

Figure 2.5: Analytical model of main system with MTMD

For earthquake application, several investigators (Chowdhury and Iwuchukwu (1987), Clark (1988), Xu and Igusa (1994)) have shown that a single TMD is not so effective in reducing seismic responses. There are two reasons for this. First, earthquake loads are typically impulsive and reach the maximum values rapidly. A TMD, subjected to a dynamic load filtered by the building structure, usually is not set into significant motion yet in such a short period. As a result, its energy-absorbing is not fully developed when it is needed the most. The heavier the TMD, the slower it reaches its full potential. Second, earthquake ground motions include a wide spectrum of frequency components and often induce significant vibration in the fundamental and higher modes of a tall building structure. Therefore, a single TMD may fail to reduce the total responses of the structures. It was reported (Chowdhury and Iwuchukwu (1987)) that a TMD tuned to the fundamental mode of a structural system can even amplify the responses of higher modes due to a coupling effect. Recognizing these shortcomings of a single TMD, it was proposed the multistage TMDs with the intent of reducing the inertia of each damper and decoupling the fundamental and higher modes of the structure. However, the multistage dampers scheme-distributed single TMDs around the main structure is not optimum for the reduction of structural responses.

Other investigators also studied MTMDs that are tuned to different modes and placed at various locations to enhance the damper's performance (Clark (1988)). These research findings have confirmed the merit of MTMD systems in seismic applications. In addition to its superior performance, MTMD consists of distributed dampers of small masses and often does not require any devoted space to house them. Therefore, engineers can make full use of the spare space at different places of the structure and design them in a cost-effective way. Due to its lightweight, malfunction of any damper will not cause detrimental effects on the structural responses so that the MTMD strategy is very robust.

2.1.3 Practical considerations of TMD

There are a number of factors which influence the selection of vibration control system for tall buildings and structures, namely:

- Efficiency
- Size and compactness
- Capital cost
- Operating cost
- Maintenance and
- Safety

In the engineering design of a TMD, the amount of dynamic response reduction that can be economically achieved is dictated by several practical design considerations.
First and foremost is the amount of additional mass, usually no more than about 2% of the modal mass of the main system, that can be practically placed at the top of a building (Papadimitriou (2006)). It is not uncommon to have the damper mass weighing up to $400t$. The damper mass is usually made up of steel or concrete and the TMD has to be allocated to a dedicated space which has to be designed to accommodate the extra weight. Water storage tanks, which are essential to building services, have been successfully integrated into the design of TMDs in which case the extra space and strength requirements are largely avoided.

Another major engineering problem is the necessity to allow for the TMD mass to move relative to the building, even at small building movements at low levels of excitation, and to allow for tuning. The simplest arrangement is to suspend the mass in the form of a pendulum, where the oscillation frequency is simply a function of the length of suspension. For buildings with a low natural frequency, the length of suspension of the pendulum can be quite large in which case extra headroom is required for the TMD to be hung. Inverted pendulums have also been used in which coil springs are usually employed to provide stability and stiffness. Since the natural frequencies of a building are sensitive to design changes and are often difficult to predict accurately, the required tuning frequency is usually determined by full-scale measurement after the building is completed.

Modern pendulum-type TMDs are mostly designed to be adjustable in the field. The suspension length is adjusted by sliding clamps to allow for fine tuning to the desirable tuning frequency. Pendulum-type TMDs are occasionally augmented by coil springs for fine tuning. Mechanically guided slide tables, hydrostatic bearings and laminated rubber bearings have also been used to provide a low friction platform for the damper mass to respond to the movement of the building. Coil springs or variable stiffness pneumatic springs provide stiffness for the tuning of the TMDs. For TMDs fitted with laminated rubber bearings, the bearings act as horizontal springs. These types of TMDs are generally more compact with no special requirement for a large headroom compared to that for a conventional pendulum-type TMD but they are more complex and hence more expensive.

2.1.4 Tuned Liquid Damper (TLD)

Another type of passive control device utilizes the motion of a sloshing fluid to reduce responses of a structure. Dampers having the mechanism similar to a TMD but utilizing liquid motion were proposed for vibration control of civil engineering structures several years ago. The Tuned Liquid Damper (TLD) (Fujino et al. (1988), (1989) and (1992)) consists of one or a group of rigid tanks which can have a wide variety of geometries, from toroidal ring to rectangular or circular shaped, partially filled with liquid, usually

water. It relies upon liquid sloshing forces or moments to change the dynamical characteristics of a structure and to dissipate the vibration energy through the amplitude of fluid motion and the wave braking on the free surface which mimics the motion of the TMD mass. TLD is a special class of TMD where the mass is replaced by liquid, which most of the times is water. In a TLD the liquid in a sloshing tank is used to add damping to the structural system (Modi and Munshi (1998)).

By properly designing the size of the TLD tanks as well as the water depth inside, the natural sloshing frequency of the TLD can be tuned to that of the structure. In practice, a group of tanks with the same size and the same water depth is often used in order that the total mass of the liquid can amount to about one or several per cent of the structural mass, which is the value of the mass ratio usually used for a TMD. In some TLD designs, they may carry additional internal devices, for instance nets, baffles and moving spheres, which are installed in the liquid to increase the damping of sloshing to a certain value with which the TLD can work efficiently. Since the TLD has some advantages over the TMD, such as low cost, easily adjustable natural frequency, suitability for temporary use, low trigger level, easily installation into existing structures etc., it has become a popular vibration control device. However, research on TLD is complicated because unlike the TMDs, which have a linear response, that of TLDs is highly nonlinear due to the fluid motion. Based on shallow water wave theory, it has been proposed analytical models for the TLD to suppress horizontal vibrations. However, in civil engineering it is also often necessary to suppress structural vibrations of vertical or pitching motions, for instance galloping or fluttering of a deck of suspended-span bridge under wind loading.

The fact that standing waves may exist on the surface of an infinite expanse of liquid raises the question of whether standing waves may exist on the surface of a liquid which is contained in a vessel of finite extent. At this point rectangular vessels will be considered, and it will be shown, as might be expected, that only standing whose wavelengths coincide with a discrete spectrum of values may exist on such liquid surfaces. Fig. 2.6 shows a two-dimensional rectangular container of width $2l$ which contains a liquid of average depth h (Currie (1974)).

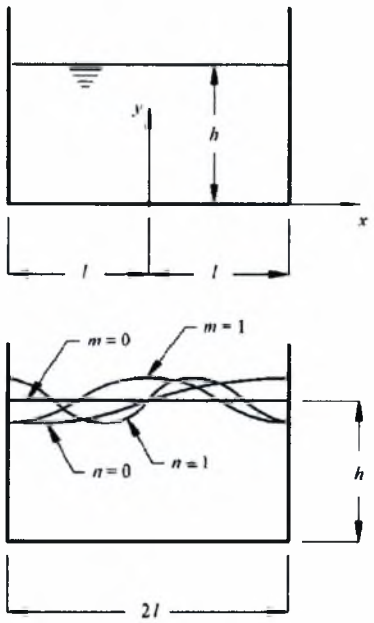

Figure 2.6: Geometry for liquid in a rectangular container and the first four fundamental modes of surface oscillation

Any waves which may exist will have to satisfy the following partial differential equation and boundary conditions:

$$\frac{\partial^2\phi}{\partial x^2}+\frac{\partial^2\phi}{\partial y^2}=0 \tag{2.5a}$$

$$\frac{\partial^2\phi}{\partial t^2}(x,h,t)+g\frac{\partial\phi}{\partial y}(x,h,t)=0 \tag{2.5b}$$

$$\frac{\partial\phi}{\partial y}(x,0,t)=0 \tag{2.5c}$$

$$\frac{\partial\phi}{\partial x}(\pm l,y,t)=0 \tag{2.5d}$$

From the above equations, the eigenfrequency of the liquid depends on the geometric form of the water tank, the height of the water filling and the length of the water tank. The eigenfrequency can estimated to be

$$f = \frac{1}{2\pi}\sqrt{\xi \frac{g}{2l} \tanh\left(\xi \frac{h}{2l}\right)} \tag{2.6}$$

Hereby g denotes the coefficient of gravity, h denotes the height of the fluid in the water tank, $2l$ denotes the length of the tank and ξ denotes a coefficient which represents the geometry of the tank. For a rectangular tank the value $\xi = \pi$ can be used. So, by adjusting the height of the tank you can preferably adjust the eigenfrequency of the TLD.

The water in a vessel absorbs energy of vibration of a main structure as kinetic energy of sloshing motion, and dissipates it through the shear of the water, friction between water and wall, collision of floating particles and so on. The energy is converted into heat based on the principle of the dissipation of energy through sloshing liquid.

The effectiveness of a TLD for suppressing vibrations depends not only on the mass of liquid in the TLD but also on the configuration of the liquid as well as upon the position where the TLD is located. If the configuration of the liquid, i.e. the liquid depth and the TLD tank size, is designed suitably, the TLD can have a large suppressing moment and can be very effective even with a small mass of liquid.

Large-scale civil engineering structures such as tall buildings, towers and bridges are usually flexible and have relatively low natural frequency, so a TLD is usually filled with shallow liquid to tune its sloshing frequency to the structural natural frequency. The damping of the liquid sloshing is an important parameter in the study of a TLD as it affects the efficiency of the TLD. The pressure forces acting on the side walls and the bottom of the TLD tank and the moments due to liquid sloshing will act as interaction forces between the TLD and the structure to suppress structural vibrations.

During free-vibration tests, the TLD is subjected to angular vibrations (Modi and Munshi (1998)). The amplitude of vibration affects the dynamics of liquid motion inside the damper. For small displacements $\left(\theta_0 \le 1^o\right)$, almost imperceptible surface ripples are observed traveling back and forth inside the damper. There is negligible energy dissipation. For moderate displacements $\left(1^o \le \theta_0 \le 2.5^o\right)$, a single large wave accompanied by small ripples are created. There is a small amount of energy dissipation

due to partial breaking of the liquid near the walls of the damper. For large displacements $(\theta_0 \geq 2.5^o)$, a significant portion of the liquid mass is accelerated. Due to the combined action of large angular motion and high kinetic energy of the accelerated liquid mass, there is considerable sloshing accompanied by overturning of the wave during impact against the side wall of the tank and breaking of the free surface. This results in much greater energy dissipation.

Implementation of such devices occurred primarily in Japan for the control of wind-induced vibrations in airport towers and tall buildings (Tamura et al. (1988), Wakahara et al. (1992), Soong and Spencer Jr. (2002)). Although effective in reducing wind-induced responses by up to 70% (Wakahara et al. (1992)), TLDs were found to be less effective than TMDs.

2.1.5 Tuned Liquid Column Damper (TLCD)

A Tuned Liquid Column Damper (TLCD) is a special type of TLD which relies on the inertia of a liquid column in a U-tube to counteract the forces acting on the structure. A passive TLCD is a mass of liquid (typically water), enclosed in a custom U-shaped tank, which is designed to reduce building motions by applying inertial and damping forces opposite to the direction of building motions. The U-shaped tank is designed to allow the liquid to oscillate freely at a frequency that optimally matches one or more of the structure's natural frequencies. Damping is provided by adjusting the turbulence levels in the moving water. Generally, a single TLCD is capable of providing damping along a single building axis. The big advantage of this system is the distance the liquid is able to move.

Damping in the TLCD is introduced as a result of headloss experienced by the liquid column moving through an orifice. It relies on the sloshing of the liquid column in a U-tube to counteract the forces acting on the structure, with damping introduced in the oscillating liquid column through an orifice. To change its properties and therefore its natural frequency, different strategies have been proposed, such as changing the length of the liquid column (Lou et al. (1994)), the cross section of the sloshing tank, or even using a variable orifice within the liquid column (Haroun et al. (1994)). The effective damping

in the TLCD is obtained by changing the orifice opening of the valve. In the fully closed position no liquid oscillations take place and the system becomes a single degree of freedom (SDOF) system (Gao et al. (1999), Adeli (2004), Adeli and Kim (2006)).

The potential of liquid dampers in their passive state is not fully realized due to the dependence of their damping on the motion amplitudes (or the level of excitation) and their inability to respond quickly to suddenly applied loads such as earthquakes and gust of winds. It has been observed that at lower amplitudes of excitation, higher damping was achieved by constructing the liquid flow through the orifice and at higher amplitudes of excitation opening of the orifice and higher liquid velocity contributed to the appropriate level of damping.

The main advantages of TLDs / TLCDs are their low initial and maintenance costs and the fact that most tall buildings need water tanks for the building water supply for occupant's usage and fire-fighting purposes making them a viable and attractive choice over other mechanical vibration absorbers.

2.2 Active Control Systems

To develop a more versatile alternative, the concept of active control was introduced several years ago (Yao (1972)). Active Control Systems operate by using external power in the order of tens of kilowatts (Symans et al. (1994)) supplied to operate actuators to impart control forces on the structure in a prescribed manner. They have the ability to adapt to different loading conditions and to control different vibration modes of the structure (Housner et al. (1997)).

These forces can be used to both add and dissipate energy in the structure and have the possibility to destabilize the overall system. They are more effective than passive devices because of their ability to adapt to different loading conditions and to control different modes of vibration (Housner et al. (1997)).

However, since the large amount of power required for their operation may not always be available during seismic events, they are not as reliable. Cost and maintenance of such systems is also significantly higher than that of passive control systems. Therefore, a number of serious challenges need to be solved before active control technology can gain

general acceptance by the engineering and construction community. These challenges include:

1. reducing capital cost and maintenance
2. eliminating reliance on external power
3. increasing system reliability and robustness and
4. gaining acceptance of nontraditional technology.

The appropriate control action is typically determined based on measurements of the structural responses and/or the disturbance in order to calculate appropriate control signals to be sent to actuators, as shown schematically in Fig. 2.7. Because the control forces are not entirely dependent on the local motion of the structure (although there is some dependence on the local response due to the effects of the control-structure interaction), the control systems are considerably more flexible in their ability to reduce the structural responses for a wide variety of loading conditions (Soong and Spencer (2002)).

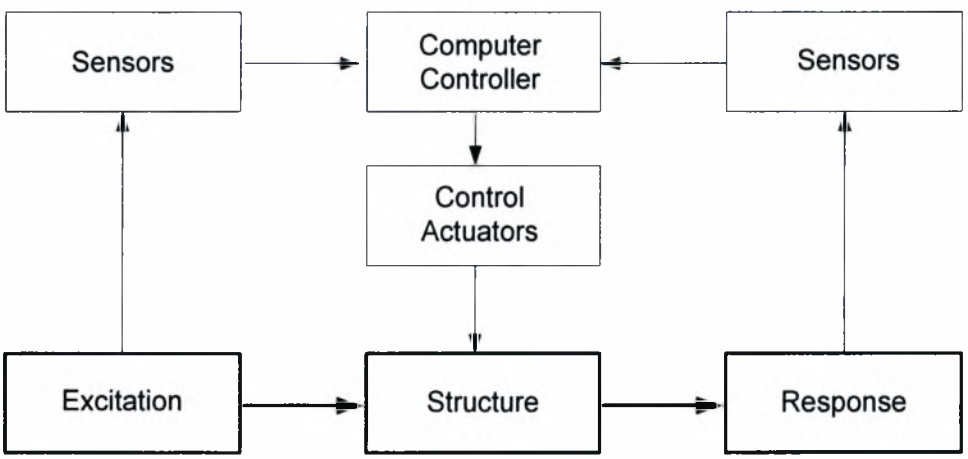

Figure 2.7: Schematic diagram of Active Control Systems

In this system, the signals sent to control actuators are a function of responses of the system measured with physical sensors (Housner et al. (1997)).

When only the structural response variables are measured, the control configuration is referred to as *feedback control* since the structural response is continually monitored and this information is used to make continual corrections to the applied control forces. A *feedforward control* results when the control forces are regulated only by the measured excitation, which can be achieved, for earthquake inputs, by measuring accelerations at the structural base. In the case where the information on both the response quantities and excitation are utilized for control design, the term *feedback-feedforward* control is used.

Most of the current research on active structural control for aseismic protection has focused on either full state feedback strategies or velocity feedback strategies. However, accurate measurement of the necessary displacements and velocities of the structure is difficult to achieve directly, particularly during seismic activity. Displacements and velocities are not absolute, but dependent upon the inertial reference frame in which they are taken, their direct measurement at arbitrary locations on large-scale structures is difficult to achieve. During seismic activity, this difficulty is exacerbated, because the foundation to which the structure is attached is moving with the ground and does not provide an inertial reference frame. Alternatively, because accelerometers are inexpensive and can readily provide reliable measurement of the structural accelerations at strategic points on the structure, development of control methods based on acceleration feedback is an ideal solution to this problem. Active Control works well with the use of new materials and new construction methods. It also safeguards against structures with excessive vibrations.

Active Control Systems encompass active mass dampers, active mass drivers, active tendon systems, pulse thrusters and active variable stiffness systems and they use computer controlled actuators to produce the best performance.

The active mass damper (AMD), the most commonly used active control device, is similar to the TMD, since it also uses a spring-mass-damper system. It does, however, include an actuator that is used to position the mass at each instant, to increase the amount of damping achieved and the operational frequency range of the device. They suppress the oscillation of a building by actuating a weight to control axial forces. The first implementation of this control method and of active control in general was performed in 1989, in the Kyobashi Seiwa building in Tokyo, Japan, by the Kajima

Corporation (Korobi et al. (1991), Spencer Jr. and Soong (1999), Soong and Spencer Jr (2002)).

Active mass dampers are very effective in controlling oscillations in high winds and in medium-sized earthquakes. Researching each control system is necessary to determine which will produce the required performance. Structural control systems have and will allow for new designs that produce safer, comfortable and earthquake protected civil engineering structures.

Although the effect of the damping device is theoretically expressed by the control force $F_C(t)$, the actual mathematical model differs depending on the device. The damping device and the building cannot always be modeled separately. An active vibration control system model must take into account the machine part which generates the control force, the controller which calculates the control force based on the control algorithm and sensors which measure response and excitation.

2.3 Semi-Active Control Systems

A compromise between passive and active control systems has been developed in the form of Semi-Active Control Systems as depicted in Fig. 2.8, which are based on semi-active devices. A semi-active control device has mechanical properties, such as damping or stiffness that can be adjusted in real time to improve its performance but can not inject energy into the controlled system (Housner et al. (1997), Spencer Jr. and Sain (1997)). Typically, a semi-active control device is defined as one that cannot increase the mechanical energy in the controlled system but has properties that can be dynamically varied, so they do not have the potential to destabilize the system. Changes in the system's mechanical properties are based on feedback from measured responses and/or ground excitation (Spencer et al. (1997), Jansen and Dyke (1999), Soong and Spencer (2002)).

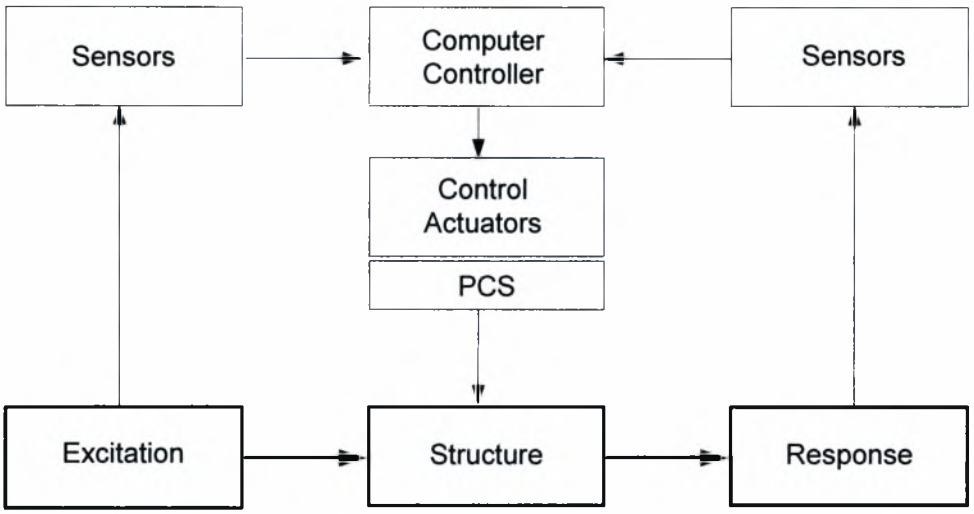

Figure 2.8: Schematic diagram of Semi-Active Control Systems

Since external power is only used to change device's properties and not to generate a control force, power requirements are very low, on the order of tens of watts (Symans et al. (1994), Symans and Constantinou (1997)). So, they can operate on battery power alone making them quite advantageous during seismic events when the main power may fail. Semi-active control systems offer another alternative in structural control. A variety of semi-active control devices have been proposed, including variable orifice devices, variable stiffness control devices, variable friction devices, semi-active TMDs, adjustable TLCDs, controllable fluid dampers such as magnetorheological (MR) dampers and electrorheological (ER) dampers. These systems have attracted much attention recently because they possess the adaptability of active control systems, yet are intrinsically stable and operate using very low power. Because these devices are adaptable, they are expected to be quite effective for structural response reduction over a wide range of loading conditions. The control strategy of a semi-active control system is based on the feedback of structural motions. Different control algorithms can be adopted directly from active control systems. However, semi-active control systems are typically nonlinear due to the intrinsic nonlinearities of semi-active devices.

Variable orifice dampers can achieve variable damping by changing the hydraulic fluid flow resistance of a conventional hydraulic fluid damper using an electromechanical variable orifice and therefore alter the amount of damping provided to the structure

(Symans et al. (1994), Spencer Jr. and Soong (1999)). A schematic of such a device is given in Fig. 2.9 (Spencer and Nagarajaiah (2003)).

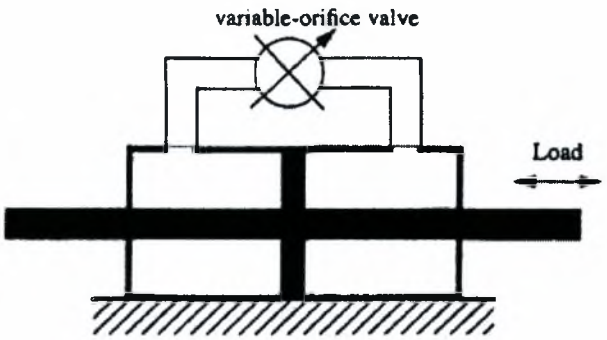

Figure 2.9: Schematic of variable orifice damper

Variable stiffness control devices have also been proposed as a form of semi-active control system. These systems have the ability to modify the structure's stiffness and therefore its natural frequency, to avoid resonant conditions (Symans and Constantinou (1997)). They are installed in bracing systems and engaged or released to change building stiffness, as necessary. They are also designed to be fail-safe, that is, in the case of power failure, the devices automatically engage themselves, increasing the structure's stiffness (Kobori et al. (1993).

Variable friction dampers dissipate vibration energy in a structural system by utilizing force generated by surface friction. These devices consisting of a preloaded friction shaft rigidly connected to the structural bracing. Operation of the brace is controlled by the preload on the friction interface, which in turn is actively regulated through commands generated by the controller during ambient excitations.

Semi-active TMDs have also been developed for wind vibration reduction. These devices are similar to the TMDs, but with the capability of varying their level of damping. Simulations showed that the performance of these semi-active devices outperform that of TMDs and was comparable to that of AMDs.

Controllable fluid dampers form another class of semi-active devices, consisting of controllable fluids in a fixed orifice damper. Unlike the semi-active control devices

mentioned previously, which employ electrically-controlled valves or mechanisms, controllable fluid dampers contain no moving parts other than the damper piston. This feature makes them inherently more reliable and maintainable (Spencer Jr. and Soong (1999), Soong and Spencer Jr. (2002)). Controllable fluid dampers generally utilize controllable fluids either electrorheological (ER) fluids or magnetorheological (MR) fluids. In comparison with semi-active dampers (variable orifice dampers) described above, an advantage of controllable fluid devices is that the contain no moving parts other than the piston, which makes them simple and potentially very reliable. These fluids are unique in their ability to reversibly change their viscosity from free-flowing linear viscous fluids to semi-solids with a controllable yield strength in only a few milliseconds when exposed to an electric (for ER fluids) or magnetic field (for MR fluids). These fluids are consisted of dielectric polarizable or magnetically polarizable particles suspended in a mineral or silicone oil medium and can be modeled as Newtonian fluids in the absence of the applied field. Although the discovery of ER and MR fluids dates back to the 1940's, only recently have they been applied to structural engineering applications (Makris et al. (1995), (1996), Makris (1997), Spencer et al. (1997), Dyke et al. (1998), Jansen and Dyke (2000)).

On the one hand, ER dampers for structural control applications have been developed and investigated by several researchers but their commercial application is limited. This happens due to the following reasons:

1. ER dampers are only able to achieve yield stresses of 3.0 to 3.5 kPa
2. ER fluid capacity is greatly reduced by the introduction of impurities or contaminants such as moisture during manufacturing or use and
3. The voltage required for their operation, approximately 4000 volts, is quite high and may not be available or may be too costly (Yang et al. (2002), Soong and Spencer Jr. (2002)).

On the other hand, MR dampers, seem to be a more feasible alternative. Their maximum yield stresses are higher, approximately 50 to 100 kPa, impurities do not affect fluid performance, and their voltage requirements are quite smaller, around 12 to 24 volts, as are their power requirements less than 50 watts (Yang et al. (2002), Soong and Spencer Jr. (2002)).

2.4 Hybrid Control Systems

Active and Passive Control systems may be combined to form Hybrid Control Systems as shown in Fig. 2.10. Since a portion of the control objective is accomplished by the Passive System, less Active Control effort implying less power resource is required. By operating both systems together enhances the robustness of the passive system and reduces the energy requirements of the active system (Soong and Spencer (2002)).

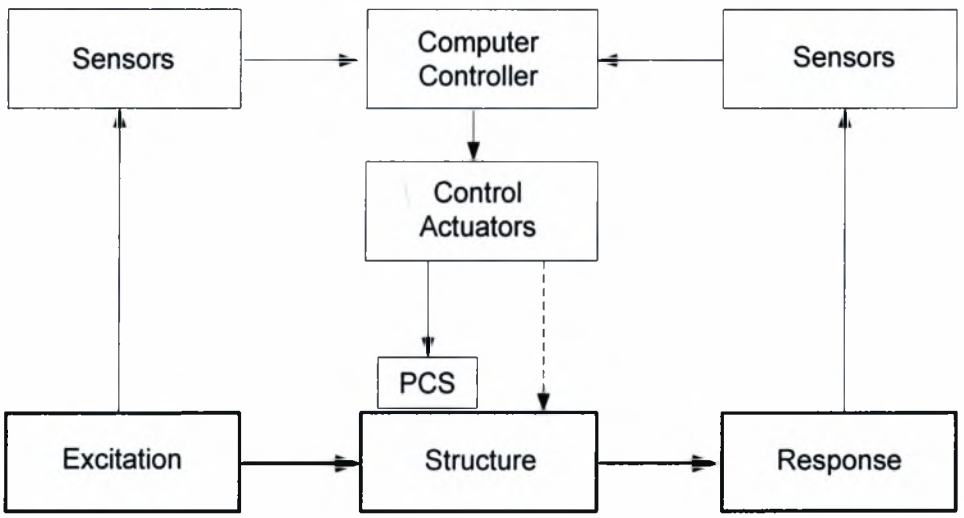

Figure (2.10): Schematic diagram of Hybrid Control Systems

There are two main approaches for the implementation of hybrid systems: the hybrid mass damper (HMD) and the hybrid seismic isolation system. HMD systems have recently been introduced to exploit the benefits of both the conventional TMD system and the AMD system. A HMD is programmed to function as either a conventional TMD system or as an AMD system according to the wind conditions and the resultant building and damper mass vibration characteristics. This restricts the operation of the active mode of control to only when an optimum increase in damping and a large reduction in wind-induced response are required. At other times when moderate increase in damping and reduction in the wind-induced response are adequate, the system operates in a passive mode. While the initial capital cost would remain high because of the added cost of the active capacity, there is a considerable saving in operating and maintenance cost.

A hybrid mass damper combines a tuned mass damper with an active actuator to enhance its robustness to reduce structural vibrations under different loading conditions. Usually, the energy required by an HMD is far less than that required by an AMD with comparable performance.

In fact, HMDs are the most common full-scale implementation of control devices in civil structures and rely mainly on the natural motion of the TMD. The actuator force is only used to increase efficiency and robustness to changes in structural dynamic characteristics (Spencer Jr and Soong (1999), Yang et al. (2002)). Structures with such control strategy include, among others, the Kansai International Airport in Osaka, Japan, the Mitsubishi Heavy Industry in Yokohama, Japan, and the RIHGA Royal Hotel in Hirosima, Japan (Spencer Jr. and Soong (1999)).

Hybrid seismic isolation systems through the installation of additional active devices into seismic isolation systems can achieve the isolation effect while keeping the base displacement at low levels. They are consisted of the introduction of active devices in base-isolated structures. Although base isolation has the ability to reduce interstory drifts and structural accelerations, it increases base displacement, hence the need for an active device (Spencer Jr. and Sain (1997)).

CHAPTER 3

ANALYSIS OF SDOF SYSTEMS WITH TMDs

3.1 Introduction

At the present Chapter we will extract the equations of motion that describe a Single Degree of Freedom (SDOF) System with the presence either one Tuned Mass Damper (TMD) or Multiple Tuned Mass Dampers (MTMD) connected in parallel with the main SDOF system. Also, a methodology for the optimal design of the parameters of the TMD will be given. The theory developed in this Chapter will be applied in Chapter 4 to analyze and optimally design the laboratory SDOF system with one and two TMDs.

3.2 Single Degree of Freedom (SDOF) System with one Tuned Mass Damper (TMD)

The SDOF main system (primary system) with one TMD (secondary system) is shown in Fig. 3.1. The main system includes the mass M supported to the ground through the spring with stiffness K and dashpot of viscous damping C. The Secondary System can also be viewed as a SDOF oscillator that consists of a body of mass m which is supported to the main mass M through the spring of stiffness k and a dashpot of viscous damping c. The mass m of the TMD is much smaller than the mass M of the main system and the mass m has a leading role in vibration attenuation of mass M when the whole structure is subjected to base excitation $\ddot{x}_g(t)$.

The response of the total system is described by the absolute displacements z_p and z_s of the system masses M and m correspondingly, as it is depicted in Fig. 3.1 (Papadimitriou (2006)).

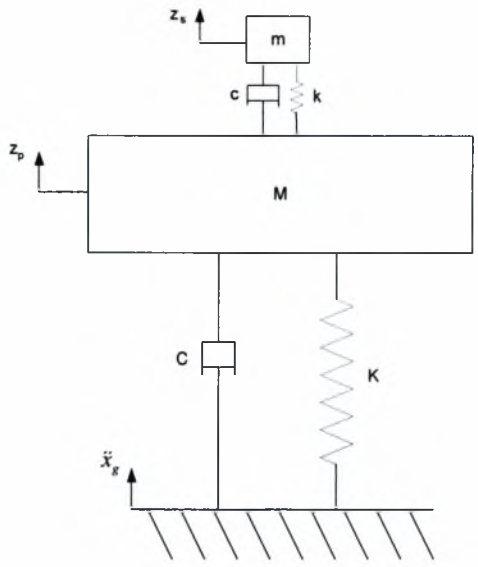

Figure 3.1: Simple mechanical model of two degrees of freedom system subjected to ground acceleration $\ddot{x}_g$

For convenience, the relative displacements x_p and x_s of the above masses with respect to the ground motion x_g are introduced as follows

$$x_p = z_p - x_g \tag{3.1a}$$

$$x_s = z_s - x_g \tag{3.1b}$$

Calculating the first and second time derivative of the Eq. (3.1a) and (3.1b) one derives the relative velocities and relative accelerations of the system masses

$$\dot{x}_p = \dot{z}_p - \dot{x}_g \tag{3.2a}$$

$$\dot{x}_s = \dot{z}_s - \dot{x}_g \tag{3.2b}$$

$$\ddot{x}_p = \ddot{z}_p - \ddot{x}_g \tag{3.2c}$$

$$\ddot{x}_s = \ddot{z}_s - \ddot{x}_g \tag{3.2d}$$

In order to create the equations of motion it is necessary to design the free body diagrams of the two system masses. The free body diagram for the main system of mass M is shown in Fig. 3.2

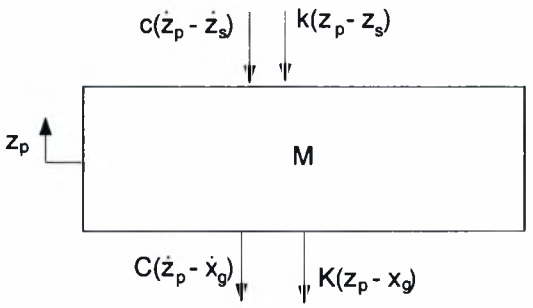

Figure 3.2: Free body diagram of mass M

Applying Newton's Law, one derives the equation of motion in the form

$$M \cdot \ddot{z}_p = -k \cdot \left(z_p - z_s\right) - c \cdot \left(\dot{z}_p - \dot{z}_s\right) - K \cdot \left(z_p - x_g\right) - C \cdot \left(\dot{z}_p - \dot{x}_g\right) \tag{3.3}$$

Substituting the Eq. (3.1) and Eq. (3.2) of relative displacements, relative velocities and relative accelerations into the Eq. (3.3), it results in the following equation of motion

$$M \cdot \ddot{x}_p + \left(C + c\right) \cdot \dot{x}_p + \left(K + k\right) \cdot x_p - c \cdot \dot{x}_s - k \cdot x_s = -M \cdot \ddot{x}_g \tag{3.4}$$

The free body diagram for the secondary system of mass m is shown in Fig. 3.3

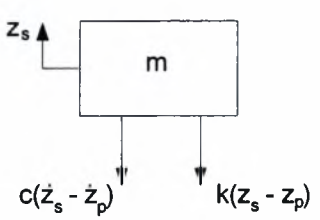

Figure 3.3: Free body diagram of mass m

Applying Newton's Law, one derives the equation of motion in the form

$$m \cdot \ddot{z}_s = -k \cdot (z_s - z_p) - c \cdot (\dot{z}_s - \dot{z}_p) \tag{3.5}$$

Substituting the Eq. (3.1) and Eq. (3.2) of relative displacements, relative velocities and relative accelerations into the Eq. (3.5), it results in the following equation of motion

$$m \cdot \ddot{x}_s + c \cdot \dot{x}_s + k \cdot x_s - c \cdot \dot{x}_p - k \cdot x_p = -m \cdot \ddot{x}_g \tag{3.6}$$

So, the equations of motion that describe the whole system are given by the Eqs. (3.4) and (3.6) which can be written in the following matrix form:

$$\begin{pmatrix} M & 0 \\ 0 & m \end{pmatrix} \cdot \begin{pmatrix} \ddot{x}_p \\ \ddot{x}_s \end{pmatrix} + \begin{pmatrix} C+c & -c \\ -c & c \end{pmatrix} \cdot \begin{pmatrix} \dot{x}_p \\ \dot{x}_s \end{pmatrix} + \begin{pmatrix} K+k & -k \\ -k & k \end{pmatrix} \cdot \begin{pmatrix} x_p \\ x_s \end{pmatrix} = -\begin{pmatrix} M \\ m \end{pmatrix} \cdot \ddot{x}_g \tag{3.7}$$

Introducing the vectors of relative displacement, velocity and acceleration of the system

$$\underline{x} = \begin{pmatrix} x_p \\ x_s \end{pmatrix}, \quad \underline{\dot{x}} = \begin{pmatrix} \dot{x}_p \\ \dot{x}_s \end{pmatrix}, \quad \underline{\ddot{x}} = \begin{pmatrix} \ddot{x}_p \\ \ddot{x}_s \end{pmatrix}$$

the mass, damping and stiffness matrices

$$\boldsymbol{M} = \begin{pmatrix} M & 0 \\ 0 & m \end{pmatrix}, \qquad \boldsymbol{C} = \begin{pmatrix} C+c & -c \\ -c & c \end{pmatrix}, \qquad \boldsymbol{K} = \begin{pmatrix} K+k & -k \\ -k & k \end{pmatrix}$$

and the vector $\underline{L}$

$$\underline{L} = \boldsymbol{M} \cdot \underline{\Gamma} = \begin{pmatrix} M & 0 \\ 0 & m \end{pmatrix} \cdot \begin{pmatrix} 1 \\ 1 \end{pmatrix}$$

the system of equations of motion can be written in the following matrix form

$$\boldsymbol{M}\cdot\ddot{\underline{x}}+\boldsymbol{C}\cdot\dot{\underline{x}}+\boldsymbol{K}\cdot\underline{x}=-\boldsymbol{M}\cdot\underline{\Gamma}\cdot\ddot{x}_g \tag{3.8}$$

3.3 Single Degree of Freedom (SDOF) System with Multiple Tuned Mass Dampers (MTMD) Connected in Parallel

A single TMD cannot provide effective vibration control when the excitation contains harmonics with frequency away from the resonant frequency of the main system. In fact a simple TMD provides very effective control for harmonics with frequencies very close to the resonant frequency of the main system. In order to improve the effectiveness of Passive Control in a wider frequency range around the resonant frequency of the main system, Multiple Tuned Mass Dampers (MTMD) connected in parallel with the main SDOF system are employed. The MTMD could also be used to control more than one modes of vibration in a structure (Yamaguchi and Harnpornchai (1993)). The system with MTMD in parallel connection with the main mass M is shown in Fig. 3.4. It consists of a SDOF main system for which we want to control its vibrations and N secondary systems which compose the MTMD.

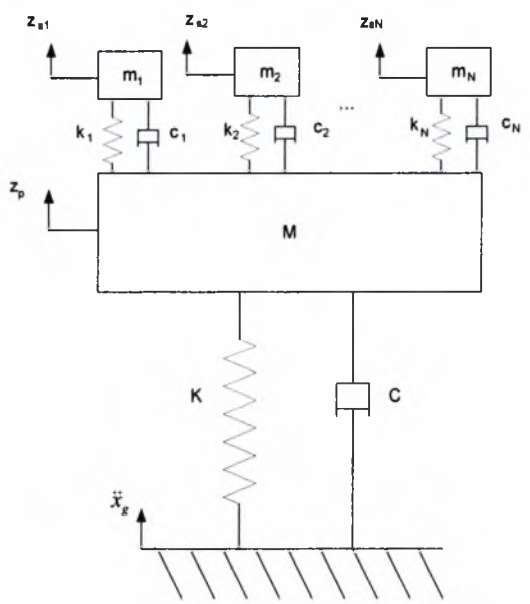

Figure 3.4: Simple mechanical model of $N+1$ degrees of freedom system subject to ground acceleration $\ddot{x}_g$

The main system behaves as a SDOF oscillator and consists of a concentrated body of mass M supported to the ground through a spring of stiffness K and dashpot of viscous damping C. The n secondary system can also be viewed as a SDOF oscillator that consist of a body of mass m_n, a spring of stiffness k_n and a dashpot of viscous damping c_n. The Secondary Systems are attached to the mass M of the main system in parallel as shown in Fig. 3.4.

The masses of the secondary systems are much smaller than the mass M of the main system. The dynamic characteristics of the secondary systems will be selected so that vibrations of the main system are significantly reduced. The combined system of a single main system and N secondary systems behave as a mechanical system of $N+1$ degrees of freedom. The combined system is subjected to base excitation $\ddot{x}_g(t)$.

The response of the system is described by the absolute displacements z_p and $z_{sn}, n=1,\ldots,N$ of the system masses M and m_n, respectively, as shown in Fig. 3.4. For convenience, the relative displacements x_p and $x_{sn}, n=1,\ldots,N$ of the masses with respect to the ground motion x_g are introduced as follows

$$x_p = z_p - x_g \tag{3.9a}$$

$$x_{sn} = z_{sn} - x_g \tag{3.9b}$$

In order to create the equations of motion it is necessary to design the free body diagrams of the $N+1$ system masses. The free body diagram for the main system of mass M is shown in Fig. 3.5

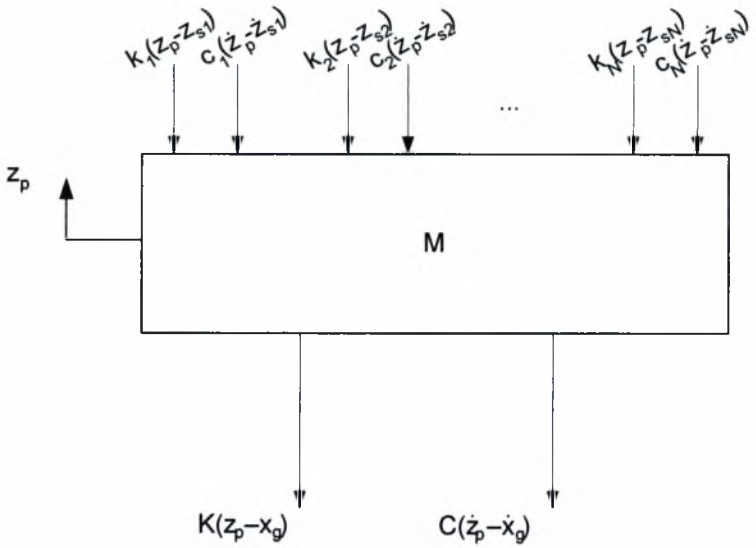

Figure 3.5: Free body diagram of mass M

Applying Newton's Law, it results in the following equation of motion

$$\begin{aligned} M\cdot\ddot{z}_p = &-k_1\cdot\left(z_p-z_{s1}\right)-k_2\cdot\left(z_p-z_{s2}\right)-\ldots-k_N\cdot\left(z_p-z_{sN}\right)- \\ &-c_1\cdot\left(\dot{z}_p-\dot{z}_{s1}\right)-c_2\cdot\left(\dot{z}_p-\dot{z}_{s2}\right)-\ldots-c_N\cdot\left(\dot{z}_p-\dot{z}_{sN}\right)- \\ &-K\cdot\left(z_p-x_g\right)-C\cdot\left(\dot{z}_p-\dot{x}_g\right) \end{aligned} \tag{3.10}$$

Substituting the Eq. (3.9a) and Eq. (3.9b) of relative displacements into the Eq. (3.10), it results in the following equation of motion

$$\begin{aligned} &M\cdot\ddot{x}_p+\left(C+c_1+c_2+\ldots+c_N\right)\cdot\dot{x}_p+\left(K+k_1+k_2+\ldots+k_N\right)\cdot x_p- \\ &-c_1\cdot\dot{x}_{s1}-c_2\cdot\dot{x}_{s2}-\ldots-c_N\cdot\dot{x}_{sN}- \\ &-k_1\cdot x_{s1}-k_2\cdot x_{s2}-\ldots-k_N\cdot x_{sN}=-M\cdot\ddot{x}_g \end{aligned} \tag{3.11}$$

The free body diagram for the secondary system of mass m_n is shown in Fig. 3.6

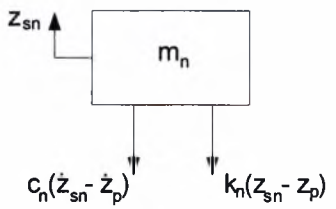

Figure 3.6: Free body diagram of mass m_n

Applying Newton's Law, it results in the following equation of motion for the n^{th} secondary body of mass m_n

$$m_n \cdot \ddot{z}_{sn} = -k_n \cdot \left(z_{sn} - z_p\right) - c_n \cdot \left(\dot{z}_{sn} - \dot{z}_p\right) \tag{3.12}$$

Substituting the Eq. (3.9a) and Eq. (3.9b) of relative displacements into the Eq. (3.12), it results in the following equation of motion

$$m_n \cdot \ddot{x}_{sn} + c_n \cdot \dot{x}_{sn} + k_n \cdot x_{sn} - c_n \cdot \dot{x}_p - k_n \cdot x_p = -m_n \cdot \ddot{x}_g \tag{3.13}$$

So, the equations of motion that describe the whole system are the Eq. (3.11) and N equations of Eq. (3.13). These previous equations can be written in the following matrix form

$$\begin{pmatrix} M & 0 & 0 & \dots & 0 \\ 0 & m_1 & 0 & \dots & 0 \\ \vdots & & \ddots & \dots & 0 \\ 0 & 0 & & \dots & m_N \end{pmatrix} \cdot \begin{pmatrix} \ddot{x}_p \\ \ddot{x}_{s1} \\ \vdots \\ \ddot{x}_{sN} \end{pmatrix} + \begin{pmatrix} C + c_1 + \ldots + c_N & -c_1 & \dots & -c_N \\ -c_1 & c_1 & \dots & 0 \\ \vdots & \vdots & \dots & 0 \\ -c_N & 0 & \dots & c_N \end{pmatrix} \cdot \begin{pmatrix} \dot{x}_p \\ \dot{x}_{s1} \\ \vdots \\ \dot{x}_{sN} \end{pmatrix} +$$
$$+ \begin{pmatrix} K + k_1 + \ldots + k_N & -k_1 & \dots & -k_N \\ -k_1 & k_1 & \dots & 0 \\ \vdots & \vdots & \dots & 0 \\ -k_N & 0 & \dots & k_N \end{pmatrix} \cdot \begin{pmatrix} x_p \\ x_{s1} \\ \vdots \\ x_{sN} \end{pmatrix} = - \begin{pmatrix} M \\ m_1 \\ \vdots \\ m_N \end{pmatrix} \cdot \ddot{x}_g \tag{3.14}$$

Introducing the vectors of relative displacement, velocity and acceleration of the system

$$\underline{\ddot{x}} = \begin{pmatrix} \ddot{x}_p \\ \ddot{x}_{s1} \\ \vdots \\ \ddot{x}_{sN} \end{pmatrix}$$

$$\underline{\dot{x}} = \begin{pmatrix} \dot{x}_p \\ \dot{x}_{s1} \\ \vdots \\ \dot{x}_{sN} \end{pmatrix}$$

$$\underline{x} = \begin{pmatrix} x_p \\ x_{s1} \\ \vdots \\ x_{sN} \end{pmatrix}$$

the mass, damping and stiffness matrices

$$\boldsymbol{M} = \begin{pmatrix} M & 0 & 0 & \dots & 0 \\ 0 & m_1 & 0 & \dots & 0 \\ \vdots & & \ddots & \dots & 0 \\ 0 & 0 & & \dots & m_N \end{pmatrix}, \qquad \boldsymbol{C} = \begin{pmatrix} C + c_1 + \dots + c_N & -c_1 & \dots & -c_N \\ -c_1 & c_1 & \dots & 0 \\ \vdots & \vdots & \dots & 0 \\ -c_N & 0 & \dots & c_N \end{pmatrix},$$

$$\boldsymbol{K} = \begin{pmatrix} K + k_1 + \dots + k_N & -k_1 & \dots & -k_N \\ -k_1 & k_1 & \dots & 0 \\ \vdots & \vdots & \dots & 0 \\ -k_N & 0 & \dots & k_N \end{pmatrix}$$

and the vector $\underline{L}$

$$\underline{L} = \boldsymbol{M} \cdot \underline{\Gamma} = \begin{pmatrix} M & 0 & 0 & \dots & 0 \\ 0 & m_1 & 0 & \dots & 0 \\ \vdots & & \ddots & \dots & 0 \\ 0 & 0 & & \dots & m_N \end{pmatrix} \cdot \begin{pmatrix} 1 \\ 1 \\ \vdots \\ 1 \end{pmatrix}$$

The system of equations of motion can be written in the following matrix form

$$\boldsymbol{M}\cdot\ddot{\underline{x}}+\boldsymbol{C}\cdot\dot{\underline{x}}+\boldsymbol{K}\cdot\underline{x}=-\boldsymbol{M}\cdot\underline{\Gamma}\cdot\ddot{x}_g \tag{3.15}$$

which is exactly the same as Eq. (3.8).

3.4 Method of Solution of Equations of Motion

The final system of Eq. (3.9) or Eq. (3.15) is a system of second order ordinary differential equations (ODE). For constant mass, stiffness, and damping matrices, the system of ODE becomes a system of linear ODE with constant coefficients and can be solved in MATLAB using the State Space Method.

In order to use the State Space Method available in MATLAB, the final second-order system of equations is transformed to a single order one as follows

$$\dot{\underline{y}}=\boldsymbol{A}\cdot\underline{y}+\boldsymbol{B}\cdot\underline{u} \tag{3.16}$$

$$\underline{z}=\boldsymbol{C}\cdot\underline{y}+\boldsymbol{D}\cdot\underline{u}$$

This is achieved by introducing the state space vector

$$\underline{y}=\begin{pmatrix}\underline{x}\\ \dot{\underline{x}}\end{pmatrix} \tag{3.17}$$

and the output vector

$$\underline{z}=\begin{pmatrix}\underline{x}\\ \dot{\underline{x}}\\ \ddot{\underline{x}}\end{pmatrix} \tag{3.18}$$

which includes the variables of the problem that are desirable to calculate. The above output vector has been chosen specifically for this problem in order to calculate at any time the displacement, velocity and acceleration vectors of the two masses of the system. In addition, $\underline{u}$ is the excitation vector and the matrices $\boldsymbol{A}$, $\boldsymbol{B}$, $\boldsymbol{C}$ and $\boldsymbol{D}$ are depended upon the second-order system of equations and the output vector $\underline{z}$.

The matrices $\boldsymbol{A}$, $\boldsymbol{B}$, $\boldsymbol{C}$ and $\boldsymbol{D}$ are estimated as follows. Starting from the initial system of Eq. (3.9) or Eq. (15) one has that

$$\ddot{\underline{x}} = -\boldsymbol{M}^{-1} \cdot \boldsymbol{C} \cdot \dot{\underline{x}} - \boldsymbol{M}^{-1} \cdot \boldsymbol{K} \cdot \underline{x} - \underline{\Gamma} \cdot \ddot{x}_g \tag{3.19}$$

Differentiating the state space vector given in Eq. (3.17) and using the Eq. (3.19) one derives that

$$\dot{\underline{y}} = \begin{pmatrix} \dot{\underline{x}} \\ \ddot{\underline{x}} \end{pmatrix} = \begin{pmatrix} \dot{\underline{x}} \\ -\boldsymbol{M}^{-1} \cdot \boldsymbol{C} \cdot \dot{\underline{x}} - \boldsymbol{M}^{-1} \cdot \boldsymbol{K} \cdot \underline{x} - \underline{\Gamma} \cdot \ddot{x}_g \end{pmatrix}$$

or equivalently

$$\dot{\underline{y}} = \begin{pmatrix} \underline{\mathbf{0}} & I \\ -\boldsymbol{M}^{-1} \cdot \boldsymbol{K} & -\boldsymbol{M}^{-1} \cdot \boldsymbol{C} \end{pmatrix} \cdot \dot{\underline{x}} + \begin{pmatrix} \underline{\mathbf{0}} \\ -\underline{\Gamma} \end{pmatrix} \cdot \ddot{x}_g \tag{3.20}$$

Next, taking the output vector in Eq. (3.18) and using the Eq. (3.19) one has that

$$\underline{z} = \begin{pmatrix} \underline{x} \\ \dot{\underline{x}} \\ \ddot{\underline{x}} \end{pmatrix} = \begin{pmatrix} \underline{x} \\ \dot{\underline{x}} \\ -\boldsymbol{M}^{-1} \cdot \boldsymbol{C} \cdot \dot{\underline{x}} - \boldsymbol{M}^{-1} \cdot \boldsymbol{K} \cdot \underline{x} - \underline{\Gamma} \cdot \ddot{x}_g \end{pmatrix}$$

or equivalently

$$\underline{z} = \begin{pmatrix} I & \underline{0} \\ \underline{0} & I \\ -\boldsymbol{M}^{-1} \cdot \boldsymbol{K} & -\boldsymbol{M}^{-1} \cdot \boldsymbol{C} \end{pmatrix} \cdot \begin{pmatrix} \underline{x} \\ \underline{\dot{x}} \end{pmatrix} + \begin{pmatrix} \underline{0} \\ \underline{0} \\ -\underline{\Gamma} \end{pmatrix} \cdot \ddot{x}_g \tag{3.21}$$

Comparing the Eq. (3.16) with (3.20) and (3.21), it is easy to conclude that the matrices $\boldsymbol{A}, \boldsymbol{B}, \boldsymbol{C}$ and $\boldsymbol{D}$ are given as follows

$$\boldsymbol{A} = \begin{pmatrix} \underline{0} & I \\ -\boldsymbol{M}^{-1} \cdot \boldsymbol{K} & -\boldsymbol{M}^{-1} \cdot \boldsymbol{C} \end{pmatrix}$$

$$\boldsymbol{B} = \begin{pmatrix} \underline{0} \\ \underline{\Gamma} \end{pmatrix}$$

$$\boldsymbol{C} = \begin{pmatrix} I & \underline{0} \\ \underline{0} & I \\ -\boldsymbol{M}^{-1} \cdot \boldsymbol{K} & -\boldsymbol{M}^{-1} \cdot \boldsymbol{C} \end{pmatrix}$$

$$\boldsymbol{D} = \begin{pmatrix} \underline{0} \\ \underline{0} \\ \underline{\Gamma} \end{pmatrix}$$

while the excitation vector is given by $\underline{\boldsymbol{u}} = \ddot{x}_g$.

3.5 Optimal Design of TMDs

Next, the method for designing the characteristics of the TMDs is presented. These characteristics may include stiffness, k_n, damping, c_n, and mass, m_n, parameters of the TMDs. The design is highly dependent on the characteristics of the main structure, that is, its stiffness K, its damping C and its mass M. For this, we introduce a parameter set $\underline{\theta}$ that includes all the design variables related to the characteristics of the TMDs.

Specifically, in this application, the parameter set $\underline{\theta}$ is selected to include the stiffness k_n and the viscous damping c_n of the TMDs, i.e.

$$\underline{\theta} = \left(k_1, \ldots, k_n, c_1, \ldots, c_n\right) \tag{3.22}$$

The masses of the TMDs are kept fixed and selected to be a certain percentage of the mass of the main system. For the n TMD, its mass ratio is introduced as follows

$$\mu_n = \frac{m_n}{M} \tag{3.23}$$

to denote the ratio of the mass m_n of the TMD to the mass M of the main system. The higher the mass ratio, the higher the reduction of vibrations. However, from the practical point of view, the designer would like to achieve the highest reduction in the vibration of the main system with the lowest mass ratio. So the TMD masses are usually selected to be a few percent of the mass of the main system.

In the optimal design of the parameters of the TMDs, the objective is to find the values of the parameter set $\underline{\theta}$ that optimize a scalar performance function. This performance function is related to the vibration levels of the main system. In this work, the performance is related to the vibration levels of the main mass which are characterized by the peak of the transfer function between the input acceleration and the acceleration of the mass M of the main system. Thus, let $H\left(\omega;\underline{\theta}\right)$ be the transfer function which is a function of frequency ω and the design variables $\underline{\theta}$. The optimal design values of the model parameters are selected to minimize the maximum value of the transfer function over a frequency range of interest $\omega \in \left[\omega_{\min}, \omega_{\max}\right]$, that is, the optimal parameter values $\underline{\theta}$ of the parameter set $\underline{\theta}$ is given by

$$\hat{\underline{\theta}} = \arg\min_{\underline{\theta}} \left[\max_{\omega \in [\Omega_{\min}, \Omega_{\max}]} H\left(\omega;\underline{\theta}\right) \right] \tag{3.24}$$

This is an optimization problem that is carried out in MATLAB using available gradient-based optimization algorithms. Also, genetic algorithms have been used to better search the parameter space and find the multiple local and global optima in case these optima exist. In the optimization, the characteristics of the main structure and the characteristics of the TMDs that are not included in the parameter set $\underline{\theta}$ are kept constant to their pre-selected values or to the values identified from experiments as it will be seen in Chapter 4.

CHAPTER 4

EXPERIMENT DESIGN

4.1 Introduction

This Chapter gives details of the structures that have been developed in the laboratory for validating the performance of TMDs for passive control of structures. Two type of systems have been developed. The first system is used to simulate the behavior of a main system under the action of one TMD and the second system is used to simulate the behavior of the main system under the action of two TMDs connected in parallel with the main system. The details of the design of the individual components, that is, the main system and the secondary systems are given in Sections 4.2, 4.3 and 4.4. Sections 4.5 and 4.6 give a summary of the equipment used for carrying out the dynamic experiment and obtaining the transfer functions of the whole system as well as the modal dynamic properties. Also, the data acquisition hardware and software that are used to collect and analyze the dynamic data is described in Section 4.7. Section 4.8 gives a review of the methodology used for obtaining the modal properties of the structure from the experimentally obtained transfer functions. Results validating the performance of the TMDs for Passive Control will be presented in Chapter 5.

4.2 Experimental Setup for Structure with one TMD

In the following paragraphs, the whole process of designing the experimental structure is described in detail. The experimental setup included one or two prototype TMDs connected in parallel to a SDOF main system. The laboratory structure that is used to simulate a SDOF main system consists of a rectangular body of mass M that is attached to one end of a slender beam of length L and rectangular cross-section. When the other end of the slender beam is attached to a fixed support, the system behaves as a SDOF oscillator for excitations containing low frequencies in the vicinity of the first modal frequency. The mass of the rectangular body provides the inertia in the oscillator, while

the slender beam provided the stiffness of the oscillator. The motion of the body in the horizontal direction is the main motion of the system. Similarly, the laboratory structure used to simulate the secondary system also consists of a body of mass m that is attached to one end of the slender beam of length ℓ and rectangular cross section. This secondary system when attached to a fixed support behaves also as a SDOF oscillator for excitation frequencies close to the vicinity of the lowest modal frequency of the secondary system. The mass m of the secondary system is selected to be a small percentage of the mass M of the main system.

The combined system consisting of the main and the secondary system is shown in Fig. 4.1 for one TMD. The whole structure of the main system and one TMD is mounted on an electromagnetic shaking table. As shown in Fig. 4.1 for one TMD, accelerometers positioned on the basement of the structure and on the highest point of it. The first one measures the ground excitation of the structure and the other one the acceleration response of the main mass M .

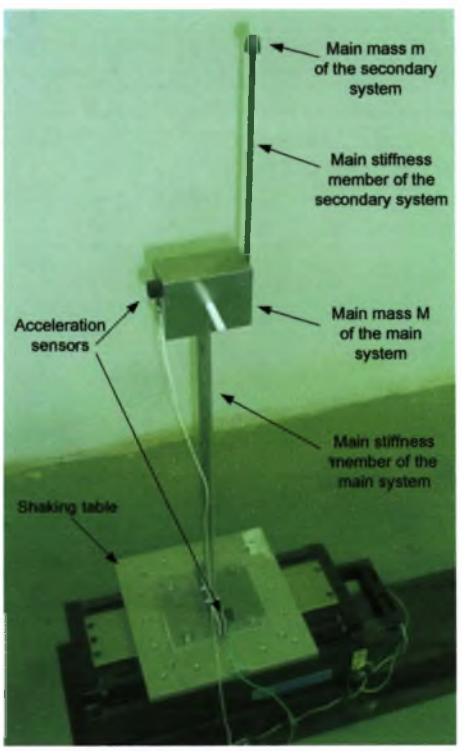

Figure 4.1: Experimental setup with one TMD

The objective here is to select the mass of the main system and design the beam of the primary system so that during the motion that will be experienced by the base excitation, the structure will behave as a linear SDOF oscillator. This requires checking for buckling of the rectangular cross-section beam that supports the main body of mass M, as well as checking for possible high stresses that could be developed due to high horizontal motions at the resonance of the main system and could exceed yield stresses. Also, the mass and the beam should be designed so that the fundamental frequency of the primary structure is in a range that can be measured from the experimental dynamics equipment available in the laboratory. For this reason it was decided that the fundamental frequency of the main system be within the frequency range 1 to 5 Hz. The aforementioned design criteria are next used to select the size of the body and the dimensions of the beam.

Design Criterion 1: Safety against Buckling

In the design of the continuum beam of the main system, account was taken so that the vertical beam supports the weight of mass M. The critical mode of failure due to the slenderness of the beam is buckling along the weak axis of the cross-section of the beam. According to the buckling theory, the critical buckling load P_{cr} of a vertical cantilever beam like the one in Fig 4.2 is

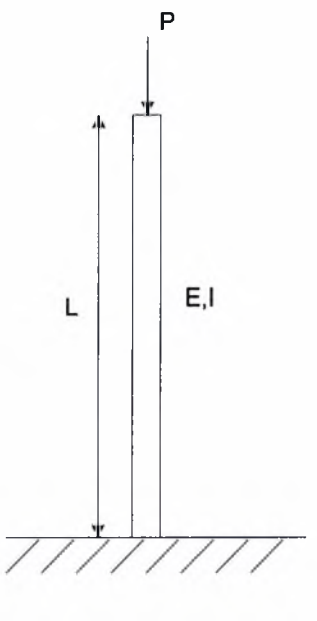

Figure 4.2: Vertically cantilever beam subject to coaxial pressing load

$$P_{cr} = \frac{\pi^2 EI}{4L^2} \tag{4.1}$$

where E is the modulus of elasticity of the main stiffness member, I is the second moment of inertia of the main stiffness member, and L is the length of the main stiffness member.

In the present system, the cross-sectional profile of the main stiffness member is orthogonal like the one shown in Fig 4.3 where $I_{zz} = \frac{bh^3}{12}$ is the second moment of inertia along the z axis, and $I_{yy} = \frac{hb^3}{12}$ is the second moment of inertia along the y axis. In the present situation the system buckling is governed by the smallest second moment of inertia which is I_{zz}.

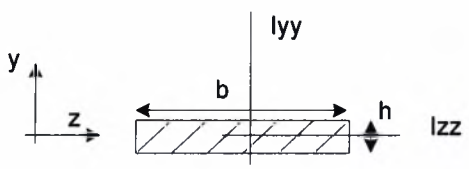

Figure 4.3: Cross-sectional profile of the main stiffness member

So, in order to avoid a disastrous buckling failure of our system, the beam dimensions were designed so that the buckling load that had to withstand had to be a times the total weight of the structure, that is

$$P_{cr} = a(M + m) \cdot g \tag{4.2}$$

where a was taken to be at least in the range $a \geq 2$.

Substituting Eq. (4.1) into Eq. (4.2) the first design equation becomes

$$\frac{\pi^2 EI_{zz}}{4L^2} = a(M+m)g \tag{4.3}$$

Using the value of $I_{zz} = \frac{bh^3}{12}$ in Eq. (4.3) and solving with respect to bh^3, the design equation takes the form

$$bh^3 = \frac{48a(M+m)gL^2}{\pi^2 E} \tag{4.4}$$

Design Criterion 2: Range of Fundamental Frequency

Neglecting the weight of the beam, the analytical expression for the natural eigenfrequency ω_p of the main system is

$$\omega_p = \sqrt{\frac{K}{M}} \tag{4.5}$$

It is known that in a cantilever beam, the stiffness constant is given by

$$K = \frac{3EI}{L^3} \tag{4.6}$$

Substituting Eq. (4.6) into Eq. (4.5) one obtain the second design equation

$$\frac{3EI}{L^3} = \omega_p^2 M \tag{4.7}$$

Design Criterion 3: Safety against Yielding

One more constraint that it is necessary to be checked is the possible failure due to plastic deformation at the base of the main system where it is the most critical point for this kind

of failure at this specific system. To be more specific, when the load P has the direction shown in Fig. 4.4, then the maximum tensional stresses are applied at the point A and the maximum compressive stresses are applied at the point B of the whole system.

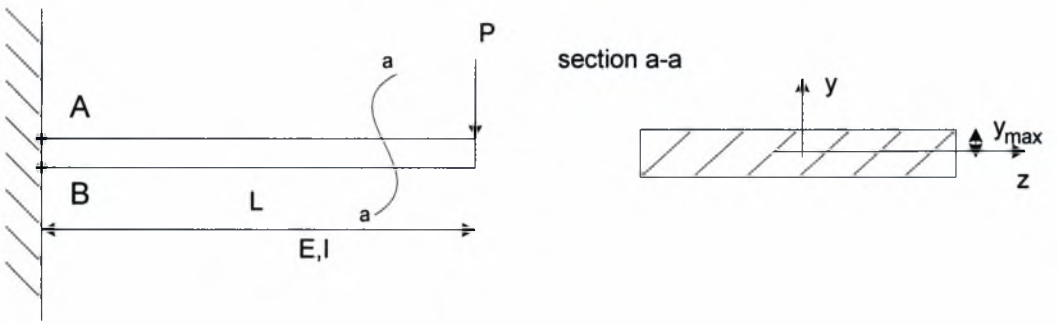

Figure 4.4: Cantilever beam subject to load P

The maximum bending stress should be less than the critical yield stress, that is

$$\sigma_{max} = \frac{M_{max}}{I_{zz}} y_{max} \leq \frac{\sigma_y}{n} \tag{4.8}$$

where M_{max} is the bending moment at the base of the beam, given by

$$M_{max} = PL \tag{4.9}$$

y_{max} is the distance between the neutral axis and the external area of the main stiffness member profile, σ_y is the yield stress limit of the main stiffness member material, n is the safety factor of the system against that kind of loading and the maximum inertia force P is generated from the vibration of the main mass M. Assuming that the system vibrates at its resonant frequency $\Omega \approx \omega_p$ and the magnitude of the sinusoidal excitation is F_o, then the inertia force is

$$P = \frac{MF_o\Omega^2}{2\zeta K} = \frac{F_o\Omega^2}{2\zeta\omega_p^2} \approx \frac{F_o}{2\zeta} \tag{4.10}$$

where ζ is the damping ratio of the primary oscillator

Throughout the design process the mass of the main stiffness member of the main system was neglected compared to the mass M of the main system in order to simplify the design.

The first two design criteria were used to select the length of the beam specifically, assuming $m \ll M$ and using equations estimation of the final design of main system, Eqs. (4.3) and (4.7) one derives the following result

$$\frac{\frac{\pi^2 EI}{4L^2}}{\frac{3EI}{L^3}} = \frac{a((M+m)g)}{\omega_p^2 M} \quad \Rightarrow \quad L = \frac{12ag}{\pi^2\omega_p^2} \tag{4.11}$$

According to the Eq. (4.11), the length L of the main system is depended on the constant a and the natural eigenfrequency ω_p of the main system. The selection of both constants depends on designer's judgment.

Setting values of a and ω_p at Eq. (4.11) we calculated the corresponding values of the length L. In Table 4.1 we have gathered the results that were computed from Eq. (4.11) for various values of a and ω_p.

Table 4.1: Results of length L for different values of a and ω_p

a	ω_p (Hz)	L (m)
2	1	0.6160
	2	0.1540
	2.5	0.0986
5	1	1.5399
	2	0.3850
	2.5	0.2464
10	1	3.0798
	2	0.7699
	2.5	**0.4928**

From the results of Table 4.1, the length of the beam was chosen to be $\mathbf{L = 0.5m}$ which is a logical length for small scale dynamic laboratory experiment.

The first design criterion given by Eq. (4.4) and the third design criterion given by Eq. (4.8) were used to design the sides b and h of the cross-section of the beam, as well as select the mass M so that the final fundamental frequency ω_p of the main system remains in the range of 1 to 5 Hz. Although the choices are not unique, the values of the parameters that were selected are shown in Table 4.2 using the fact that the beam will be made by aluminum, which is not only a lightweight material with density $\rho_{Al} = 2700 kg/m^3$ but also very flexible and stress resistant material.

Table 4.2: Selection of Design Parameters of main system

Type	Symbol	Values
Length of beam	L	$0.5\,m$
Modulus of elasticity	E	$70e9\,Pa$
Density	ρ	$2700\,kg/m^3$
Width of beam	b	$0.05\,m$
Thickness of beam	h	$0.004\,m$
Mass of Primary System	M	$1\,kg$

4.3 Detailed Drawings of the Primary System

Next, the structural drawings of all the parts of the primary and the secondary systems of the experimental setup are given. Firstly, the whole experimental setup is based on an appropriate aluminum made basement which consists of two pieces with the construction drawing given in Fig. 4.5.

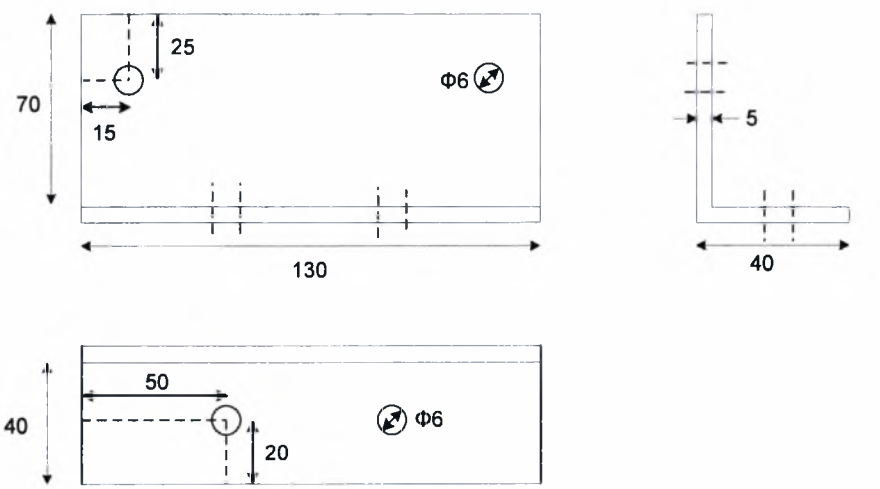

Figure 4.5: Mechanical drawing of the base of the whole experimental setup

The main stiffness member of the main system is a beam that is made of aluminum and it consists of one piece with the construction drawing given in Fig. 4.6.

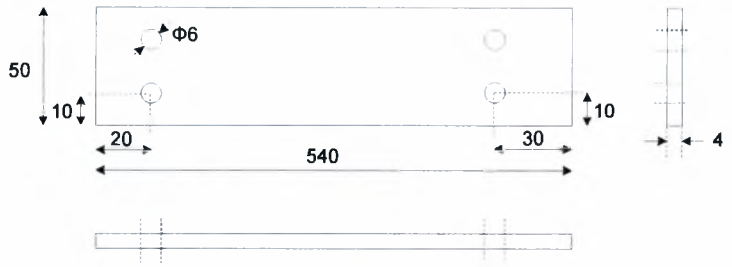

Figure 4.6: Mechanical drawing of the main system stiffness member

Finally, at the tallest point of the main system there is the mass M of the main system which is made of aluminum and its construction drawing is given in Fig. 4.7.

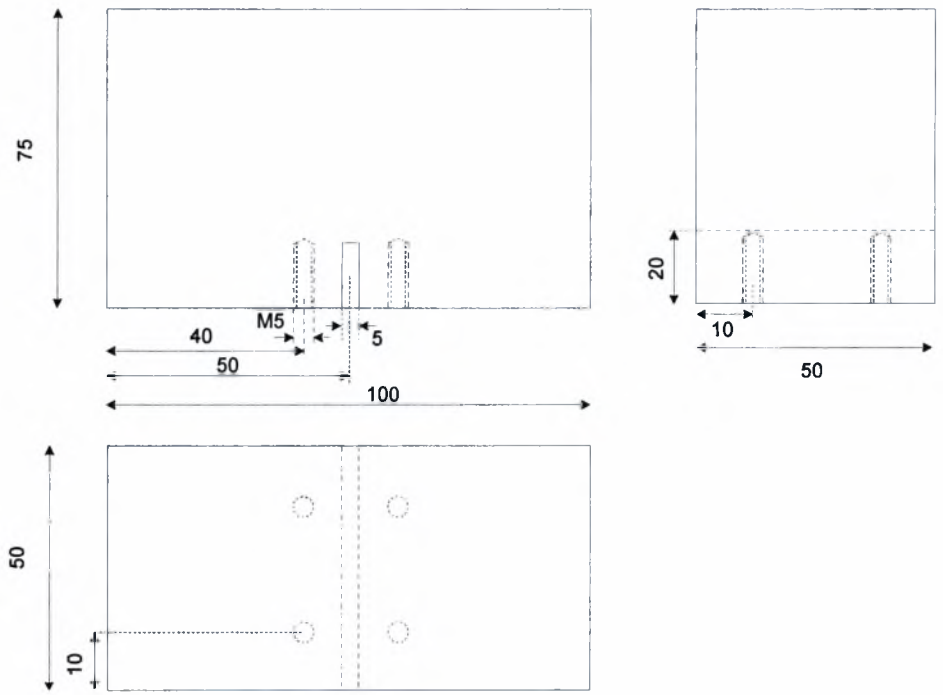

Figure 4.7: Mechanical drawing of the main system mass M

4.4 Design of the Secondary System

It is clear that, in the first mode of the main system, the highest point of it will undergo the largest steady-state deflection subjected to harmonic excitation. Therefore, the TMD should be placed at the highest point of the main system for best control of its first mode. Now, the TMD that it is used in the experiments also consists of its mass m which is attached to the end of a slender beam used as the basic stiffness member k. In reality, the secondary system of our structure is a miniature of the main system.

As it is already known from the theory of TMD reduction in the response of the main system mass M can be achieved by choosing the eigenfrequency of secondary system to be very close to the eigenfrequency of the main system. The mass m of the TMD is selected be about 2% of the main system mass M. Thus given that $M = 1kg$ the mass m of the TMD is selected to be $m = 20g$.

The mass m is made of lead, because of its high density that allows having compactness. As it is shown in Fig. 4.8 the mass m is a cylinder shaped mass which is very compact and is fitted tautly on the edge of the main stiffness member of the TMD.

Figure 4.8: Mass of the secondary system m

The optimal value k of the TMD is selected using the optimal design method presented in Section 3.5. For this, it is assumed that the damping ratio of the TMD is 1%. The optimal value of k, given that $\omega_s = 0.43 rad/s$, was estimated by the optimal design methodology to be $k = 0.15 N/m$. This optimal k value is used to design the beam of the TMD that provides the main stiffness. The main stiffness member of the TMD is selected to be very flexible and simultaneously stress resistant in order to avoid failure due to the

harsh vibrations that would be subjected to. After screening some materials we selected high tensile and strength steel for constructing the main stiffness member.

The dimensions of the cross-section of the beam are shown in Fig. 4.9. The length of the beam is then chosen so that the stiffness of the beam considered as cantilever, is equal to the optimal stiffness value. This is the theoretical value of the length of the beam. Its actual value was obtained by using experiments. Specifically, the optimal length of the TMD was chosen so that the fundamental frequency of the TMD obtained from experiments corresponds to stiffness value $k = \omega_s^2 m$ equal to the optimal value.

The final optimal value of the length of the beam is shown in Fig. 4.9

Figure 4.9: Mechanical drawing of one TMD main stiffness member

Next, the laboratory structure with two TMDs is presented. The laboratory structure that is used to simulate a SDOF main system is chosen to be the same as in Section 4.2. The two TMDs are designed from the same material as in Section 4.2. The masses of the TMDs are selected to be 1% of the mass M of the main system so that the total mass of the two TMDs is equal to the total mass $m = 20gr$ selected for the single TMD in Section 4.2. The cross-sectional dimensions of the main beam members providing the stiffness in the two TMDs are same as the dimensions used for the single TMD in Section 4.2. However, the lengths of the two TMDs are designed so that the stiffness values of the two TMDs are the optimal values computed using the optimal design formulation presented in Section 3.5.

In the optimal design, the damping ratios of the TMDs were considered to be equal to 1%. The optimal values of k_1 and k_2, given that $\omega_{s1} = 0.33 rad/s$ and $\omega_{s2} = 0.37 rad/s$, were estimated by the optimal design methodology to be $k_1 = 0.07 N/m$ and $k_2 = 0.09 N/m$. Using these values, the optimal values of the lengths of the two TMD beams were selected. However, since these lengths are only theoretical, the actual values

of the TMD beam lengths were selected using experiments. Specifically, the optimal lengths L_1 and L_2 of the two TMDs were selected so that the fundamental frequencies of the TMDs obtained from experiments correspond to the stiffness values $k_1 = \omega_{s1} m_1$ and $k_2 = \omega_{s2} m_2$, respectively, that are equal to the optimal stiffness values obtained from the optimal design methodology presented in Section 3.5. The optimal values of the lengths of the TMDs are shown in Figs. 4.10 and 4.11. The laboratory structure with two TMDs is shown in Figure 4.12.

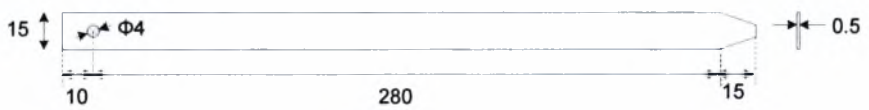

Figure 4.10: Mechanical drawing of first TMD main stiffness member

Figure 4.11: Mechanical drawing of second TMD main stiffness member

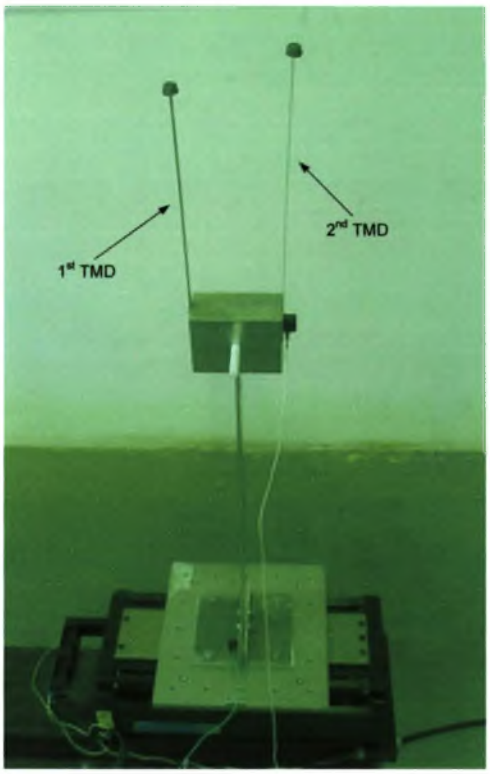

Figure 4.12: Experimental setup with two TMDs

4.5 Description of Experimental Equipment

4.5.1 Electrodynamic Shaker

In order to apply any type of base acceleration, we fit the whole structure on the shaking table of an ELECTRO-SEIS long stroke shaker. To be more specific, the APS Dynamics ELECTRO-SEIS shaker shown in Fig. 4.13 is a force generator specifically designed to be used for exciting various structures. In particular, it can be used as a seismic shaking table in the present application in order to excite at the base the combined main-secondary system.

It has also been optimized for driving structures to their natural resonant frequencies and as an electrodynamic force generator, the outputs are directly proportional to the instantaneous value of the applied current, independent of frequency and load response. It can also deliver random or transient as well as sinusoidal waveforms of force to the load.

The ample armature stroke allows driving antinodes of large structures at low frequencies and permits rated force at low frequencies when operating in a free body mode. The unit employs permanent magnets and is configured such that the armature coil remains in a uniform magnetic field over the entire stroke range - assuring force linearity. The enclosed, self-cooled construction provides safety and minimum maintenance.

Figure 4.13: Model 113-APS Dynamics ELECTRO-SEIS shaker

The basic technical characteristics of the electrodynamic shaker are given in Table 4.3.

Table 4.3: Characteristics of the electrodynamic shaker

Technical characteristic	**Unit**	**Value**
Frequency Range	*Hz*	0…200
Maximum Force Vector	*N*	133
Maximum Stroke, p-p	*mm*	158
Armature Weight	*kg*	2.2
Total Weight	*kg*	38

4.5.2 Power Amplifier

In order to amplify the desirable signal from the PC it needs to pass the signal from a specifically designed amplifier, such as the APS Dynamics 124-EP DUAL-MODE Power Amplifier shown in Fig. 4.14. It may be operated in either a voltage or current amplifier

mode, selectable from the front panel. This operating mode selector switch facilitates shaker drive power interruption, in either a current or voltage mode, for observation of resonance decay in structures.

Figure 4.14: APS 124-EP DUAL-MODE Power Amplifier

The basic technical characteristics of the Power Amplifier are given in Table 4.4.

Table 4.4: Characteristics of the power amplifier

Technical characteristic	**Unit**	**Value**
Power Output RMS	$V-A$	250
Power Output Peak	$V-A$	750
Current Output RMS	A	8
Current Output Peak	A	18
Frequency Range	Hz	0…2000
Noise	dB	−90
Input Power	W	600

4.5.3 Impulse Force Hammer

Next, we are going to describe the data acquisition system which consists of the impulse force hammer, the accelerometers and their power supply coupler.

The dynamic response of a mechanical structure while either in a development phase or an actual use environment can readily be determined by impulse force testing. Using a FFT analyzer, the transfer function of the structure can be determined from a force pulse generated by the impact of a hammer and the response signal measured with an accelerometer. The impulse force test method, yields extensive information about the frequency and attenuation behavior of the system under test. Dynamic quartz sensor elements contained within instrumented hammers are used to deliver a measurable force impulse (amplitude and frequency content) to excite a mechanical structure under test.

The stainless steel head of the impulse force hammer is equipped with quartz, low impedance force sensor which accepts impact tips varying in hardness. A selection of steel, plastic, PVC and rubber tips along with an extender mass allow the hammer to be tailored to impart to the test structure, a desired spectrum of frequencies. Shear quartz accelerometers operating in a voltage mode and featuring insensitivity to base strain, thermal transients and transverse motion are available to measure the response of the test specimens ranging from thin-walled structures to steel bridge members.

The impulse force hammer, shown in Fig. 4.15 incorporates a quartz measuring cell with built-in Piezotron low impedance electronics. The cell's voltage mode operation, guarantees a stable signal transmission insensitive to ambient influences. A wide selection of single or multi-channel couplers are available to provide power and signal processing for the hammer and accelerometers.

Figure 4.15: Kistler 9724A5000 impulse force hammer

The basic technical characteristics of the impulse force hammer are given in Table 4.5.

Table 4.5: Characteristics of the impulse force hammer

Technical characteristic	Unit	Value
Force Range	*N*	0…5000
Maximum Force	*N*	12500
Sensitivity (nom.)	*mV / N*	1
Resonant Frequency	*kHz*	27
Frequency Range (with steel impact tip (-10dB))	*Hz*	6900
Rigidity	*kN / μm*	0.8
Temperature Range Operating	*°C*	–20…70
Output		
Voltage F.S.	*V*	±5
Bias nom.	*VDC*	11
Impedance	Ω	<100
Source		
Voltage	*V*	20…30
Constant Current	*mA*	2…20
Hammer Head Dimensions		
Diameter	*mm*	23
Length	*mm*	89
Weight	*g*	250

4.5.4 Accelerometers

The accelerometer shown in Fig. 4.16 is a KISTLER PiezoBEAM Accelerometer Type 8632C10 in hard anodized aluminum cube shaped housing with high sensitivity piezoelectric measuring element, built-in charge amplifier and low-impedance voltage output. Their sensitivity is very high despite lightweight construction and the cube shaped housing of the ground isolated accelerometer allows a flexible mounting onto the structure to be measured.

The patented PiezoBEAM sensor is insensitive to transverse acceleration and base strain. The built-in charge amplifier provides a voltage proportional to the acceleration. The low impedance output assures high immunity to noise and insensitivity to cable motion. It is capable to operate directly from internal power sources found in most signal analyzers like a Kistler coupler.

Figure 4.16: PiezoBEAM Accelerometer Type 8632C10

The basic technical characteristics of the PiezoBEAM Accelerometer are given in Table 4.6.

Table 4.6: Characteristics of the PiezoBEAM Accelerometer

Technical characteristic	**Unit**	**Value**
Range	g	± 10
Sensitivity	mV / g	500
Frequency Range	Hz	0.8 ... 5000
Operating Temperature	^{o}C	0...65
Mass	g	7
Resonant Frequency (mounted)	kHz	≈ 22
Time Constant	s	≈ 1
Transverse Sensitivity	%	< 1
Output Impedance	Ω	≤ 500
Supply		
Constant Current	mA	2...18
Bias Voltage	VDC	12

4.5.5 Power Supply

The power supply for both the impulse force hammer and the accelerometers is provided by a Kistler power supply coupler Type 5134A. It is shown in Fig. 4.17 and it is a 4-channel AC power coupler and amplifier. It also includes selectable high pass filters and gain. The 5134A microprocessor controlled coupler provides power and signal processing to four channels of any voltage mode piezoelectric sensor operating with constant current excitation (2-wire system). An LCD display and keyboard allows easy selection of gain and filters for each channel individually. LEDs show the unit's status and signal error in the case of a detected problem with bias voltage or the cable integrity.

Figure 4.17: Kistler power supply coupler Type 5134A

The basic technical characteristics of the power supply coupler Type 5134A are given in Table 4.7

Table 4.7: Characteristics of the power supply coupler Type 5134A

Technical characteristic	**Unit**	**Value**
Sensor supply	*mA*	4
Gain setpoints (±0.5%)	%	1, 2, 5, 10, 20, 50, 100
Frequency range	*Hz*	0.036…30*k*
Lowpass filters		
2-pole Butterworth 2nd order	*dB / octave*	−12
Cut-off frequencies (-3dB)	*Hz*	100, 1*k*, 10*k*, 30*k*
Frequency accuracy	%	±7
Highpass filters (2 pole passive)	*dB / octave*	−12
Cut-off frequency (-3dB)	*Hz*	0.036
Time constant	*s*	3.5
Frequency accuracy	%	±10
Output voltage	V	±10
Current	*mA*	±5
Impedance	Ω	≈100
Zero offset	*mV*	<25
Temperature range operating	*°C*	0…50
Voltage between power and signal ground	V_{rms}	<50
Line voltage	*VAC*	230
Line frequency	*Hz*	48…62
Consumption	*VA*	14
Weight	*kg*	1.75

4.5.6 Data Acquisitioning Software

LabVIEW (short for **Lab**oratory **V**irtual **I**nstrumentation **E**ngineering **W**orkbench) is a platform and development environment for a visual programming language from National Instruments. LabVIEW is commonly used for data acquisition, instrument control and industrial automation on a variety of platforms. The programming language

used in LabVIEW, called G, is a dataflow programming language. Execution is determined by the structure of a graphical block diagram shown in Fig. 4.18, on which the programmer connects different function-nodes by drawing wires. These wires propagate variables and any node can execute as soon as all its input data become available. Since this might be the case for multiple nodes simultaneously, G is inherently capable of parallel execution.

LabVIEW ties the creation of user interfaces (called front panels) into the development cycle. LabVIEW programs/subroutines are called virtual instruments (VIs). Each VI has three components: a block diagram, a front panel, and a connector pane. The last is used to represent the VI in the block diagrams of other, calling VIs. Controls and indicators on the front panel allow an operator to input data into or extract data from a running virtual instrument. However, the front panel can also serve as a programmatic interface. Thus a virtual instrument can either be run as a program, with the front panel serving as a user interface, or, when dropped as a node onto the block diagram, the front panel defines the inputs and outputs for the given node through the connector pane. This implies each VI can be easily tested before being embedded as a subroutine into a larger program.

The graphical approach also allows non-programmers to build programs simply by dragging and dropping virtual representations of lab equipment with which they are already familiar. The LabVIEW programming environment, with the included examples and the documentation, makes it simple to create small applications.

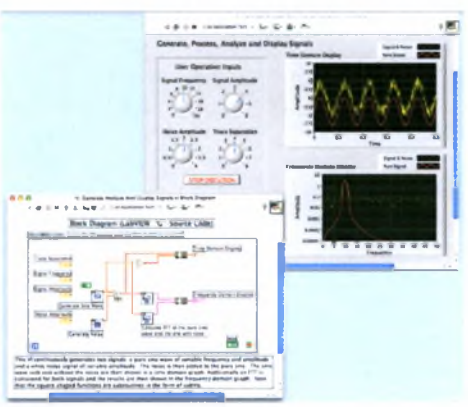

Figure 4.18: Screenshot of a simple LabVIEW 8.5e program that generates, synthesizes, analyzes and displays waveforms, showing the block diagram and front panel

4.6 System Identification

One of the most important and challenging tasks in control synthesis and analysis is the development of an accurate mathematical model of the structural system under consideration, including both the structure and the associated control devices.

There are several methods by which to accomplish this task. One approach is to analytically derive the system input/output characteristics by physically modeling the plant. Often this technique results in complex models that do not correlate well with the observed response of the physical system.

An alternative approach to developing the necessary dynamical model of the structural system is to measure the input/output relationships of the system and construct a mathematical model that can replicate this behavior. This approach is termed system identification in the control systems literature. The steps in this process are as follows:

(i) collect high quality input/output data (the quality of the model is tightly linked to the quality of the data on which it is based),
(ii) compute the best model within the class of systems considered, and
(iii) evaluate the adequacy of the model's properties.

For linear structures, system identification techniques fall into two categories: time domain and frequency domain. Time domain techniques such as the recursive least squares (RLS) system identification method is superior when limited measurement time is available. Frequency domain techniques are generally preferred when significant noise is present in the measurements and the system is assumed to be linear and time invariant.

In the frequency domain approach to system identification, the first step is to experimentally determine the transfer functions (frequency response functions) from each of the system inputs to each of the outputs. Subsequently, each of the experimental transfer functions is modeled as a ratio of two polynomials in the Laplace domain and they are used to form a state space representation for the structural system.

A block diagram of the structural system to be identified is shown in the Fig. 4.19. The input is the ground excitation $\ddot{x}_g$ and the measured system output is the absolute

acceleration at the highest point of the structure $\ddot{x}_h$. Thus a 1×1 transfer function matrix must be identified to describe the characteristics of the system.

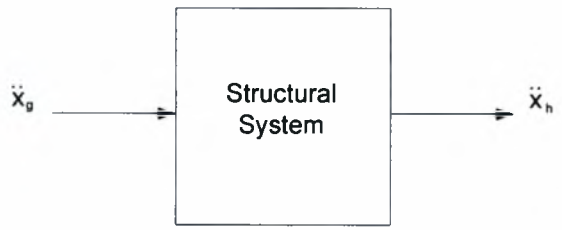

Figure 4.19: System identification block diagram

4.7 Data Acquisitioning Analysis and Problems

We use Fast Fourier Transforms (FFT) for experimental determination of transfer functions. Its main advantage of that method is the simultaneously estimation of transfer functions over a band of frequencies. We have to independently excite each of the system inputs over the frequency range of interest. Assuming the two continuous signals (input, $u(t)$, and output, $y(t)$) are available, the transfer function is determined by dividing the Fourier transforms of the two signals, as follows:

$$H_{yu}(j\omega)=\frac{\tilde{y}(\omega)}{\tilde{u}(\omega)} \tag{4.12}$$

where $\tilde{u}(\omega)$ is the Fourier transform of the input signal $u(t)$ and $\tilde{y}(\omega)$ is the Fourier transform of the output signal $y(t)$.

However, experimental transfer functions are usually determined from discrete-time data. The continuous-time records of the specified system input and the resulting responses are sampled at N discrete time intervals with an A/D converter, yielding a finite duration, discrete-time representation of each signal ($u(nT)$ and $y(nT)$, where T is the sampling period and $n=1,2\ldots N$). For the discrete case, Eq. (4.12) can be written as

$$H_{yu}(jk\Omega) = \frac{\tilde{y}(k\Omega)}{\tilde{u}(k\Omega)} \tag{4.13}$$

where $\Omega = \omega_s / N$, ω_s is the sampling frequency, $k = 0, 1 \ldots N-1$. The discrete Fourier transforms are obtained via standard digital signal processing methods. This discrete frequency transfer function can be thought of as a frequency sampled version of the continuous transfer function in Eq.(4.12).

Accurate data acquisition and processing techniques are important in the effective modeling and reliable evaluation of structural control systems. Often models are identified based on experimentally obtained data, and the quality of the resulting model is closely linked to the quality of the data on which it is based. Inaccurate recording of the system responses may lead to modeling errors and control designs which are ineffective or even unstable when implemented. Additionally, to evaluate the performance of a control system, it is necessary to obtain an accurate record of the structural responses. To obtain high-quality data, a good understanding of the sampling process and certain phenomena associated with processing the data is important.

In practice, one collection of samples of length N does not produce very accurate results. Better results are obtained by analyzing multiple collections of samples of the same length that are available by repeating the experiment.

Although most of the sensors used in structural control systems are analog devices, data acquisition is usually performed with a digital computer. The quality of the resulting transfer functions is heavily dependent upon the specific manner in which the data are obtained and the subsequent processing. To be recorded on a computer, the analog signals must be discretized in time and in magnitude, which inevitably results in errors in the time and frequency domain representations of the measured signals. The processing of the recorded data can also introduce additional errors. If the sources of these errors are identified and understood, the effects of the recorded data can be minimized.

Three important phenomena associated with data acquisition and digital signal processing are *aliasing*, *quantization error* and *spectral leakage*. The sources of each of these phenomena are discussed in the following sections (Dyke (1996)).

4.7.1 Quantization Error

The device that allows the digital computer to sample the analog signal provided by a sensor is the analog-to-digital (A/D) converter. An A/D converter can be viewed as being composed of a sampler and a quantizer. The sampler discretizes the signal in time, and the quantizer discretizes the signal in magnitude. In sampling a continuous signal, the quantizer must truncate, or round, the magnitude of the continuous signal to a digital representation in terms of a finite number of bits. Typically, data acquisition boards have A/D converters with 8, 12 or 16 bits, corresponding to dynamic ranges of 48, 72 and 96 dB, respectively. A simple example demonstrating the effect of quantization on a sinusoidal signal is shown in Fig. 4.20. Here, the dotted line is the actual signal being measured and the solid line represents a quantized version of the signal. Each value of the signal is rounded to one of ten discrete levels, resulting in significant errors in the quantized signal.

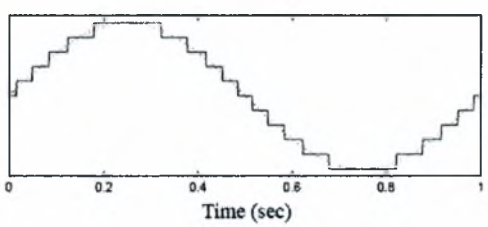

Figure 4.20: The effect of quantization

The difference between the actual value of the signal and the quantized value is considered to be a noise which adds uncertainty in the measurement. To minimize the effect of this noise, the truncated portion of the signal should be small relative to the actual signal. Thus, the maximum value of the signal should be as close as possible to, but not exceed, the full scale voltage of the A/D converter. If the maximum amplitude of the signal is known, an analog input amplifier can be incorporated before the A/D converter to accomplish this and thus reduce the effect of quantization. Once the signal is processed by the A/D system, it can be divided numerically in the data analysis program

by the same ratio that it was amplified by at the input to the A/D converter to restore the original scale of the signal.

4.7.2 Aliasing

The second component of the A/D converter is the sampler, which discretizes the analog signal in time. Often the frequency domain representation of the signal is determined (with a FFT) and errors can be introduced in the frequency domain if appropriate filtering of the signal is not performed before the signal is sampled. According to Nyquist sampling theory, the sampling rate must be at least twice the largest significant frequency component present in the sampled signal to obtain an accurate frequency domain representation of the signal. If this condition is not satisfied, the frequency components above the Nyquist frequency $(f_c = 1/(2T))$, where T is the sampling period, are aliased to lower frequencies. Once the signal has been sampled, it is no longer possible to identify which portion of the signal is due to the higher frequencies. The phenomenon of aliasing is demonstrated in Fig. 4.21 where two sinusoidal signals are shown with frequencies of 1Hz and 9Hz. If both of these signals are sampled at 10Hz, the signals have the same values at the sampling instants. Although the two signals do not have the same frequency, the frequency domain representations of the sampled versions of the signals is identical, as shown in Fig 4.21 To ensure that aliasing does not occur, the sampling frequency is chosen to be greater than twice the highest frequency in the measured signal.

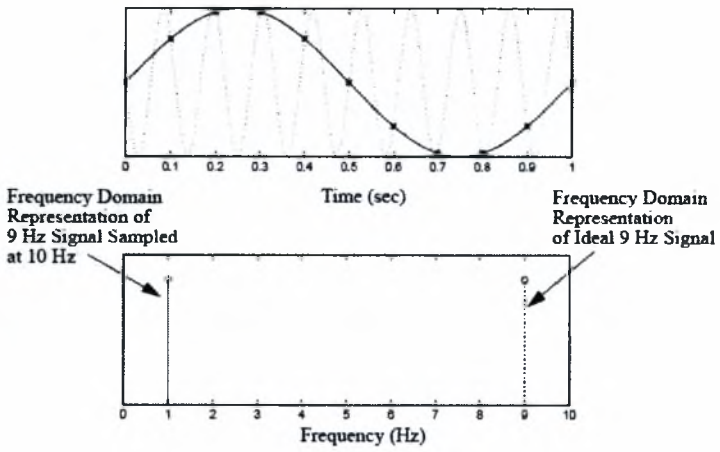

Figure 4.21: The effect of aliasing

In reality, no signal is ideally bandlimited, and a certain amount of aliasing will occur in the sampling of any physical signal. To reduce the effect of this phenomenon, analog low-pass filters can be introduced prior to sampling to attenuate the high frequency components of the signal that would be aliased to lower frequencies. Since a transfer function is the ratio of the frequency domain representations of an output signal of a system to an input signal, it is important that anti-aliasing filters with identical phase and amplitude characteristics be used for filtering both signals. Such phase/amplitude matched filters prevent incorrect information due to the filtering process from being present in the resulting transfer functions.

4.7.3 Spectral Leakage

Errors may also be introduced in the frequency domain representation of a signal due to the processing of the data. In processing the discrete-time data to determine the frequency domain representation of the signal, a finite number of samples are acquired and an FFT is performed. This process introduces a phenomenon associated with Fourier analysis known as spectral leakage. Spectral leakage is an effect in the frequency analysis of signals where small amounts of signal energy are observed in frequency components that

do not exist in the original waveform. The term *leakage* refers to the fact that it appears as if some energy has "leaked" out of the original signal spectrum into other frequencies.

4.8 Modal Analysis Method

One of the objectives of the experiment is to compute the modal characteristics of the structure or its components used to build up the structure. For this, we use impulse hammer tests to collect data that we feed to a modal analysis software to estimate the modal characteristics of the structural component that is tested. Herein, the modal characteristics that we are interested in are the modal frequencies ω and the modal damping ratios ζ. The structures that are tested are **(a)** the Main System attached to a fixed base and **(b)** the Secondary Systems also attached to fixed bases.

The Hammer Test Method is a straight forward method and yields good results under most conditions. This testing technique makes use of the fact that when a (mechanical) structure is excited by means of a Dirac pulse, the structure responds with all its eigenvalues (i.e. natural frequencies and damping). In practice, a true Dirac pulse does not exist since its theoretical duration is zero. In general, as the impact duration increases, the range of excited frequencies decreases. Impact tips mounted to a force impulse hammer consist of different materials (steel, plastic, various rubbers), each yielding different excitation durations and different excitation frequency ranges. Depending upon the frequencies of interest of the structure under test, the appropriate impact tip is mounted to the hammer.

A typical experimental setup is shown in Fig. 4.22. It consists of the structure to be tested with the test sensor, a signal conditioner (e.g. charge amplifier) which converts the test sensor's signal to an analog voltage signal, a force impulse hammer with signal conditioner and a two channel dynamic signal analyzer. This analyzer decomposes a time signal, consisting of multiple frequencies, into its individual frequencies. The excitation signal of the hammer and the response signal of the test specimen are acquired in the time domain by the two channel analyzer (Bernhard (1998)).

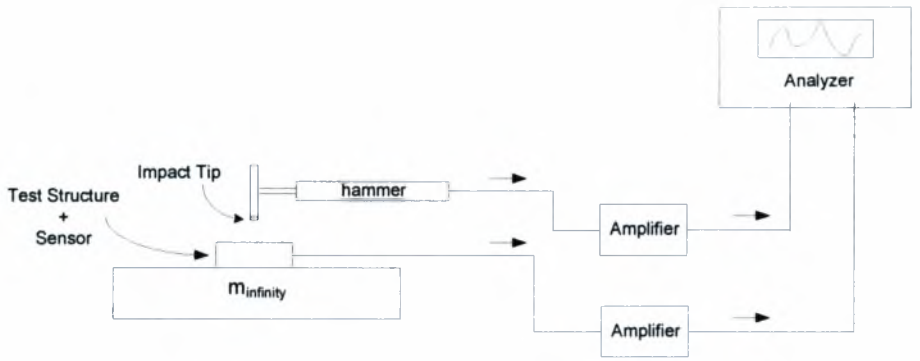

Figure 4.22: Experimental setup of hammer test

As long as a structure to be tested is linear and time independent, the ambient and boundary conditions are the same and the place of excitation (i.e. the spot, where the impact tip of the hammer contacts the test specimen) is identical, the hammer test method yields repeatable results each time the test is conducted. If over time subsequent frequency analysis yields significantly different results, the test specimen has likely experienced structural changes like cracks or other damage. Nonlinearities are difficult to detect by means of hammer testing.

The estimation of the modal characteristics using measured vibration data is based on a least squares minimization of the measure of fit given by

$$E(\psi)=\sum_{k=1}^{N_\omega} tr\left[\left(\left(\mathrm{H}k\Delta\omega;\psi\right)-\hat{\mathrm{H}}(k\Delta\omega)\right)^{*T}\left(\mathrm{H}(k\Delta\omega;\psi)-\hat{\mathrm{H}}(k\Delta\omega)\right)\right] \tag{4.14}$$

between the Transfer Function $\hat{\mathrm{H}}(k\Delta\omega)\in C^{N_0\times 1}$ estimated from the measured output acceleration and input excitation time histories and the Transfer Function $\mathrm{H}(k\Delta\omega;\psi)\in C^{N_0\times 1}$ predicted by a modal model, where N_0 is the number of measured degrees of freedom (DOF), $\Delta\omega$ is the discretization step in the frequency domain, $k=\{1,\cdots,N_\omega\}$ is the index set corresponding to frequency values $\omega=k\Delta\omega$, N_ω is the number of data in the indexed set, and ψ is the parameter set to be estimated. Assuming

general non-classically damped modes, the Transfer Function $\mathrm{H}(k\Delta\omega;\psi)$ based on the modal model of the structure is given by (Gauberghe (2004))

$$\mathrm{H}(\omega,\psi)=\sum_{r=1}^{m}\left[\frac{\boldsymbol{\phi}_r\boldsymbol{g}_r^{T}}{(j\omega)-\lambda_r}+\frac{\boldsymbol{\phi}_r^{*}\boldsymbol{g}_r^{*T}}{(j\omega)-\lambda_r^{*}}\right]+\frac{1}{(j\omega)^2}\boldsymbol{A}+\boldsymbol{B} \tag{4.15}$$

where m is the number of contributing modes in the frequency range of interest, $\lambda_r=-\zeta_r\omega_r\pm j\omega_r\sqrt{1-\zeta_r^2}$ is the complex eigenvalue of the r-th contributing mode, ω_r is the r-th modal frequency, ζ_r is the r-th modal damping ratio, $\boldsymbol{\phi}_r\in C^{N_0}$ is the complex modeshape of the r-th mode, $\boldsymbol{A}\in R^{N_0\times 1}$, $\boldsymbol{B}\in R^{N_0\times 1}$ are real vectors accounting for the contribution of the out-of-bound modes to the selected frequency range of interest, and $\boldsymbol{g}_r\in C^{N_0}$ are the participation factors that depend on the characteristics of the modal model while the symbol u^{*} denotes the complex conjugate of a complex number u.

The modal parameter set ψ to be identified contains the parameters ω_r, ζ_r, $\boldsymbol{\phi}_r$, $\boldsymbol{g}_r$, $r=1,\cdots,m$, $\boldsymbol{A}$ and $\boldsymbol{B}$ that completely define the Transfer Function in Eq. (4.15). The total number of parameters is $2m(1+2N_0)+N_0^2$ for non-classically damped modal models.

The minimization of the objective function in Eq. (4.14) can be carried out efficiently, significantly reducing computational cost, by recognizing that the error function in that equation is quadratic with respect to the complex modeshapes $\boldsymbol{\phi}_r$ and the elements in the vectors $\boldsymbol{A}$ and $\boldsymbol{B}$. This observation is used to develop explicit expressions that relate the parameters $\boldsymbol{\phi}_r$, $\boldsymbol{A}$ and $\boldsymbol{B}$ to the vectors $\boldsymbol{g}_r$, the modal frequencies ω_r and the damping ratios ζ_r, so that the number of parameters involved in the optimization is reduced from $2m(1+2N_0)+N_0^2$ to $2mN_0$. This reduction is considerable for a relatively large number of measurement points. Applying the optimality conditions in Eq. (4.14) with respect to the components of $\boldsymbol{\phi}_r$, $\boldsymbol{A}$ and $\boldsymbol{B}$, a linear system of equations results for obtaining $\boldsymbol{\phi}_r$, $\boldsymbol{A}$ and $\boldsymbol{B}$ with respect to the $\boldsymbol{g}_r$, ω_r and ζ_r, $r=1,\cdots,m$. The resulting nonlinear

optimization problem with respect to the remaining variables $\boldsymbol{g}_r$, ω_r and ζ_r, $r = 1, \cdots, m$, is solved in Matlab using available gradient-based optimisation algorithms. The starting values required in the optimization are obtained from a two-step approach as follows. In the first step, conventional least squares complex frequency algorithms (Verboten (2002)) are employed, along with stabilization diagrams, to obtain estimates of the modal frequencies ω_r and modal damping ratios ζ_r and distinguish between the physical and the mathematical modes. These values in most cases are very close to the optimal values. In the second step, given the values of ω_r and ζ_r, the values of the residue matrices $\boldsymbol{R}_r = \boldsymbol{\phi}_r \boldsymbol{g}_r^T \in C^{N_0 \times N_0}$ in Eq. (4.15) are obtained by first recognizing that the objective function in Eq. (4.14) is quadratic with respect to $\boldsymbol{R}_r$, $\boldsymbol{A}$ and $\boldsymbol{B}$, then formulating and solving the resulting linear system of equations for $\boldsymbol{R}_r$, $\boldsymbol{A}$ and $\boldsymbol{B}$, and finally applying singular value decomposition to obtain estimates of $\boldsymbol{\phi}_r$ and $\boldsymbol{g}_r$ from $\boldsymbol{R}_r$. Usually, this two-step approach gives results that are very close to the optimal estimates. However, for closely-spaced and overlapping modes it is often recommended to solve the original nonlinear optimization problem with respect to $\boldsymbol{g}_r$, ω_r and ζ_r, $r = 1, \cdots, m$, using the estimates of the two-step approach as starting values.

CHAPTER 5

RESULTS

5.1 Introduction

This Chapter presents experimental results on the two types of the laboratory structures described in Chapter 4, for the purpose of validating the performance of the TMDs for passive control. The configurations with one and two TMDs attached on the main system are used and the effects of the TMDs in reducing the vibrations of the main system are shown by comparing the measured acceleration time histories and the corresponding transfer functions between the combined system including TMDs and the transfer function of the maim system without the TMDs attached to it. Comparisons are presented for two types of base excitations applied by the electrodynamic shaking table: (a) sinusoidal excitations with frequency close to the fundamental frequency of the main system, and (b) an earthquake excitation taken to be one of the available recordings of the El Centro Earthquake.

Experimental results conducted in this Thesis, clearly demonstrate the effectiveness of the TMDs in reducing vibrations of the main system. However, the laboratory structures, especially the TMDs, have very low damping coefficients. This low damping values makes the TMDs less effective for reducing vibrations in a frequency range relatively far from the vicinity of the fundamental frequency of the main system. Therefore, the effect of damping on the performance of the TMDs in controlling vibrations is also examined experimentally by repeating the experiments after adding damping to the system through the use of a very light insulation material.

This Chapter is organized as follows. Section 5.2 gives the modal analysis results obtained by analyzing the vibrations of the laboratory structures for four structural configurations

- Fixed base of main system without TMDs attached on it
- Fixed base of TMD structures
- Combined primary-secondary structure with one TMD attachment

- Combined primary-secondary structure with two TMD attachments

Section 5.3 validates the Passive Control performance of one and two TMDs using sinusoidal base excitation with frequency of excitation close to the fundamental frequency of the main system. Validation is based on comparison of the magnitude of the steady-state time history acceleration response measured for the main system for the cases of no TMD, one TMD and two TMDs attached to the main system. Section 5.3 validates the Passive Control performance of one and two TMDs using the earthquake base excitation. Validation is based on comparison of both acceleration time history measurements and transfer functions obtained for this broad band earthquake excitation. Such performance functions are compared for the case of no TMD, one TMD and two TMDs attached to the main system. It is demonstrated that two TMDs further reduce the vibrations of the main system as compared to one TMD. Section 5.4 examines the problem of low damping identified for the laboratory structures and re-examines the performance of the TMDs by adding extra damping into the system. It is demonstrated that the additional damping improves the performance of the TMDs for controlling the vibrations of the main system.

5.2 Modal Identification

The following structural configurations were tested using impulse hammer tests in order to obtain the modal properties of the structures

1. Fixed base of main system without TMDs attached on it
2. Fixed base TMD structures, used to control vibration as a single TMD unit attached to the main system
3. Two fixed base TMD structures, used to control vibration when both TMDs are attached to the main system
4. Combined primary-secondary structure with one TMD attachment
5. Combined primary-secondary structure with two TMD attachments

Modal identification results were obtained using the methodology presented in Chapter 4. The modal identification results are based on the forced excitation and acceleration responses measured during impulse hammer tests. These responses were processed using

available modal identification software developed in the System Dynamics Laboratory of the University of Thessaly. Also, the force from the impulse hammer and the acceleration time histories measured by the accelerometers were used, as described in Chapter 4, to obtain the transfer functions of the structural configurations that were tested. The modal identification software estimates the values of the modal frequencies and the modal damping ratios from the experimentally obtained transfer functions.

Modal identification results, including modal frequencies ω and modal damping ratios ζ, for the five structural configurations are presented in Table 5.1. Also, the values of the masses of the individual primary and secondary systems are included in this Table.

Table 5.1: Dynamic characteristics of the five structural configurations examined

<table>
<tr><th colspan="3"></th><th>ω</th><th>ζ</th><th>m</th></tr>
<tr><td colspan="3">Primary System</td><td>$\omega_p = 2.75Hz$</td><td>$\zeta = 0.19\%$</td><td>$M = 1kg$</td></tr>
<tr><td rowspan="4">Secondary System</td><td rowspan="2">1 TMD</td><td>estimated</td><td>$\omega_s = 2.35Hz$</td><td rowspan="2">$\zeta = 0.21\%$</td><td rowspan="2">$m = 0.02kg$</td></tr>
<tr><td>corrected</td><td>$\omega_{s\,cor.} = 2.73Hz$</td></tr>
<tr><td rowspan="2">2TMDs</td><td>estimated</td><td>$\omega_{s1} = 2.08Hz$
$\omega_{s2} = 2.35Hz$</td><td></td><td rowspan="2">$m_1 = m_2 = 0.01kg$</td></tr>
<tr><td>corrected</td><td>$\omega_{s1\,cor.} = 2.71Hz$
$\omega_{s2\,cor.} = 3.06Hz$</td><td></td></tr>
<tr><td rowspan="2">Combined System</td><td colspan="2">with 1 TMD</td><td>$\omega_1 = 2.35Hz$
$\omega_2 = 3.20Hz$</td><td></td><td></td></tr>
<tr><td colspan="2">with 2 TMDs</td><td>$\omega_1 = 2.27Hz$
$\omega_2 = 2.92Hz$
$\omega_3 = 3.70Hz$</td><td></td><td></td></tr>
</table>

It should be noted that the modal frequencies estimated for the TMDs in Table 5.1 are not the actual modal frequencies of the TMDs due to the significant mass of the accelerator compared to the mass of the TMDs. However, these estimated frequencies could readily be corrected to reflect the actual frequencies of the TMDs ignoring the mass of the accelerometer attached to the highest point of the TMDs during the experiments. For this, let k and m be the stiffness and the mass of a TMD and let m_s be the mass of the

acceleration sensor attached to the highest point of the TMD. Considering that the TMD behaves as a SDOF oscillator, the estimated modal frequency is given by

$$\omega_{est} = \sqrt{\frac{k}{m + m_s}} \tag{5.1}$$

The actual modal frequency, ignoring the presence of the acceleration sensor, is given by

$$\omega_{act} = \sqrt{\frac{k}{m}} \tag{5.2}$$

From these two equations it can be readily shown that the two modal frequencies are related by the expression

$$\omega_{act} = \omega_{est} \sqrt{\frac{m + m_s}{m}} \tag{5.3}$$

This expression corrects the modal frequencies estimated by the modal identification software. The corrected values of the modal frequencies for the TMDs are also given in Table 5.1. It can be seen that these values are closer to the modal frequency of the main system, validating the correct design of the experiment. Figures 5.1 to 5.4 give the Fourier transform of the accelerations measured by the acceleration sensor during the experiment for the individual components of the system, namely, the primary structure and the TMDs. Note that the peaks of the Fourier spectrum occur at the corresponding estimated modal frequencies for each subsystem.

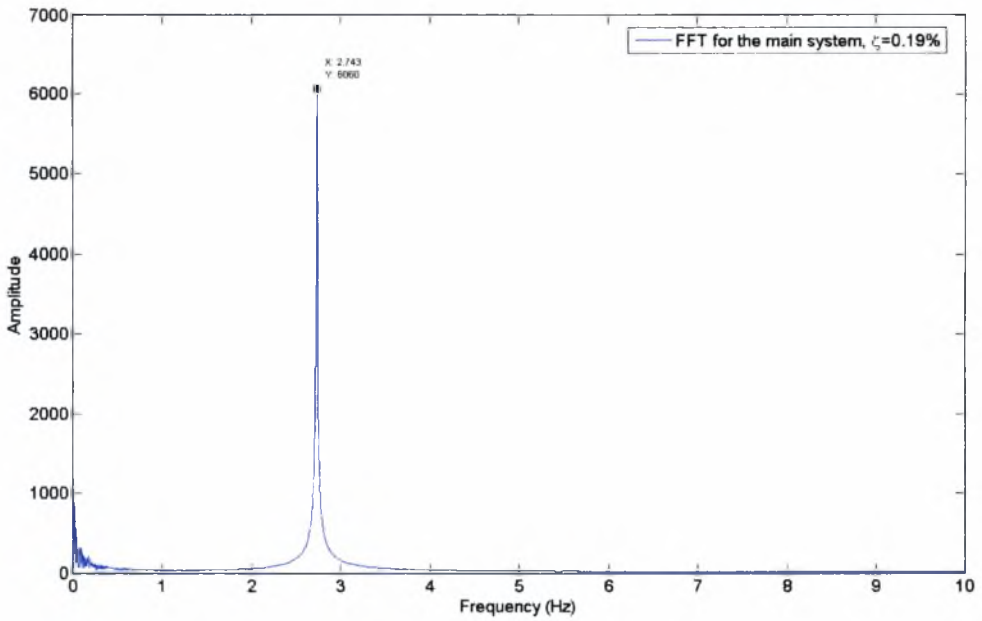

Figure 5.1: Fourier transform of the acceleration for the Primary System

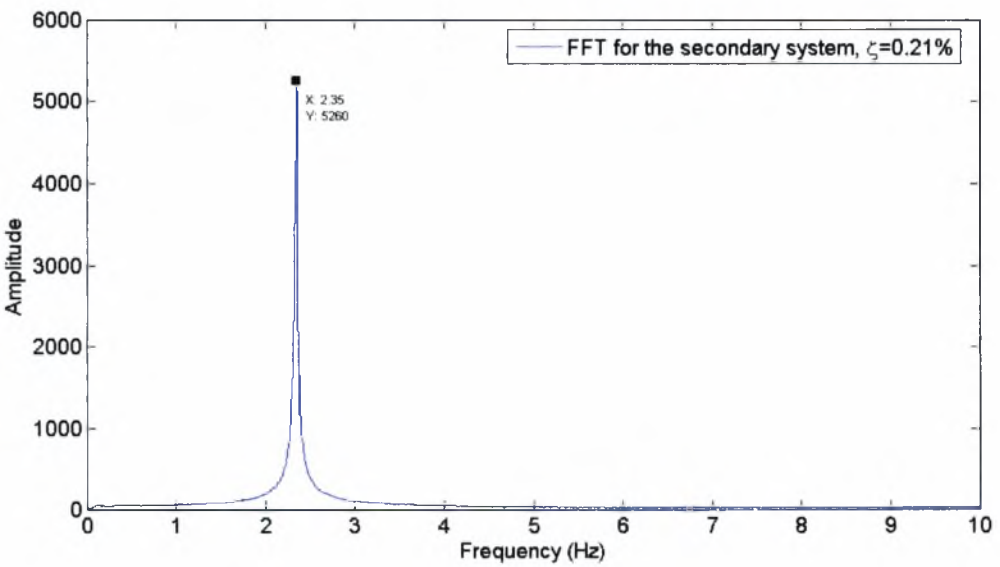

Figure 5.2: Fourier transform of the acceleration for the secondary system; case of a single TMD

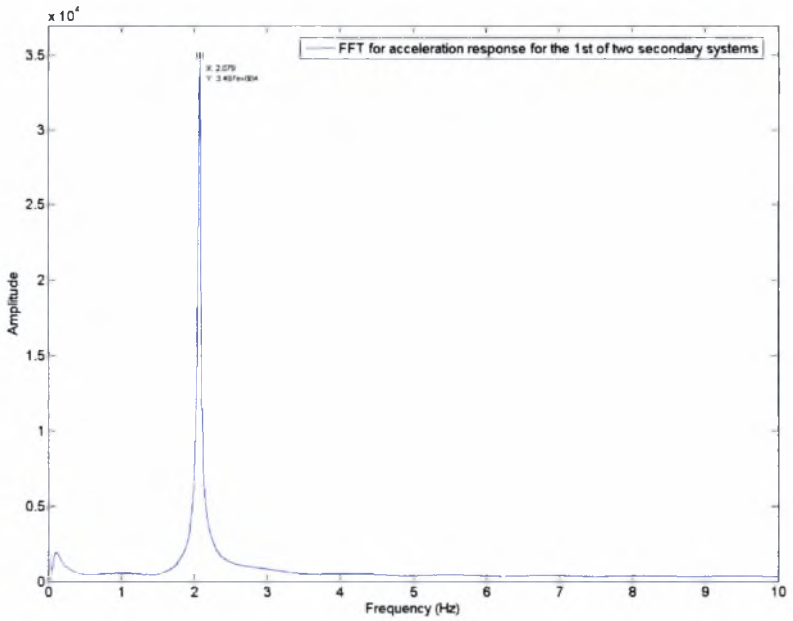

Figure 5.3: Fourier transform of the acceleration for the first TMD; case of multiple TMDs

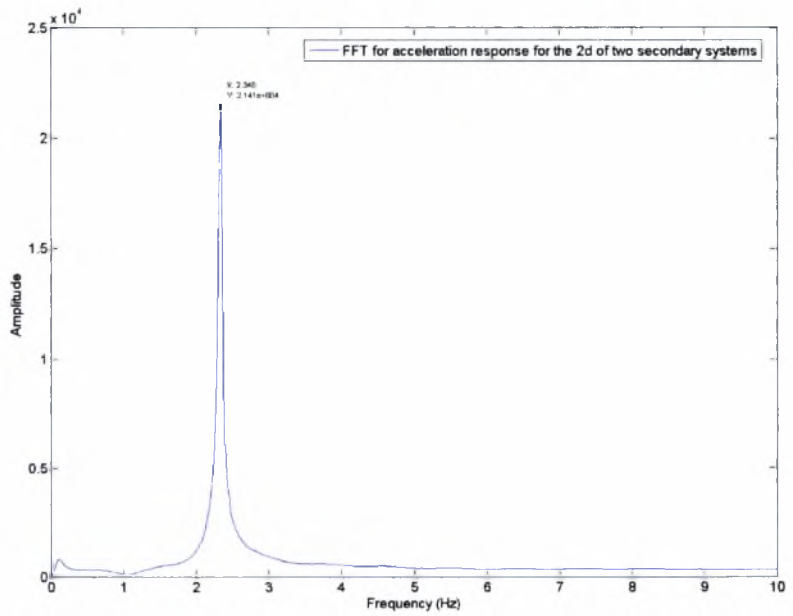

Figure 5.4: Fourier transform of the acceleration for the second TMD; case of multiple TMDs

5.3 TMD Control Effectiveness using Sinusoidal Base Excitation

The effectiveness of the TMDs to reduce the vibration of the primary structure is next examined using sinusoidal excitation applied at the base of the electrodynamic shaker. The frequency of the sinusoidal base excitation is selected to be equal to the resonant frequency of the primary structure. The experiments first conducted for the primary structure with the absence of the TMDs. Fig. 5.5 shows the sinusoidal base excitation of the primary structure as a function of time.

It is worthwhile to mention that for about the first 2-3 seconds, there is a transitional period because of inertia phenomena of the primary structure and the interaction with shaking table.

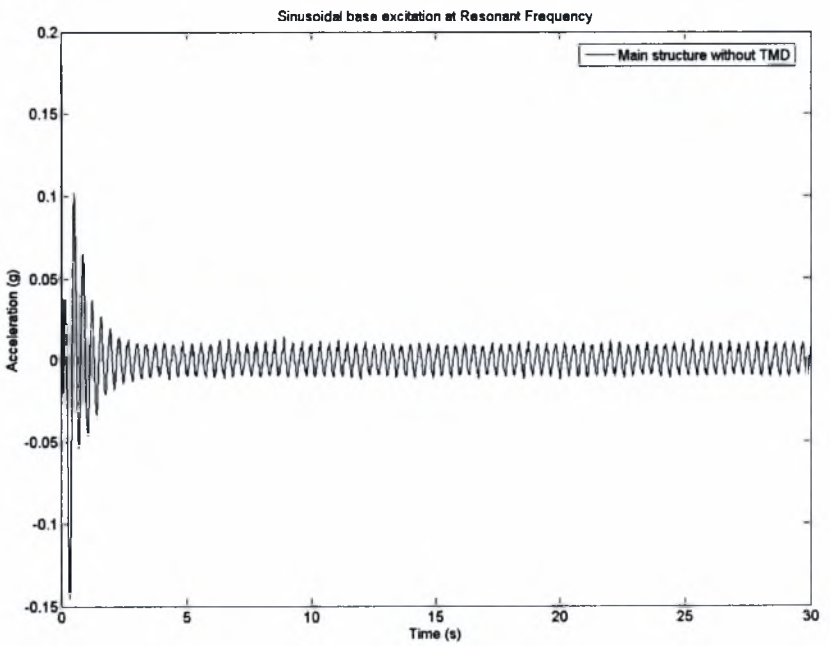

Figure 5.5: Sinusoidal base excitation measured by an accelerometer attached at the shaking table

The acceleration response of the main structure at its highest point, where the main system mass is attached as a function of time is given in Fig. 5.6.

Fig. 5.7 shows the Fourier transform of the acceleration time history of Fig. 5.6. The transient effects are evident in Fig. 5.6 for the first 2-3 seconds of the response. For time greater the 4 seconds the response has achieved is steady state. From Fig. 5.7 it is evident that only one harmonic at the excitation frequency is mainly present in the response.

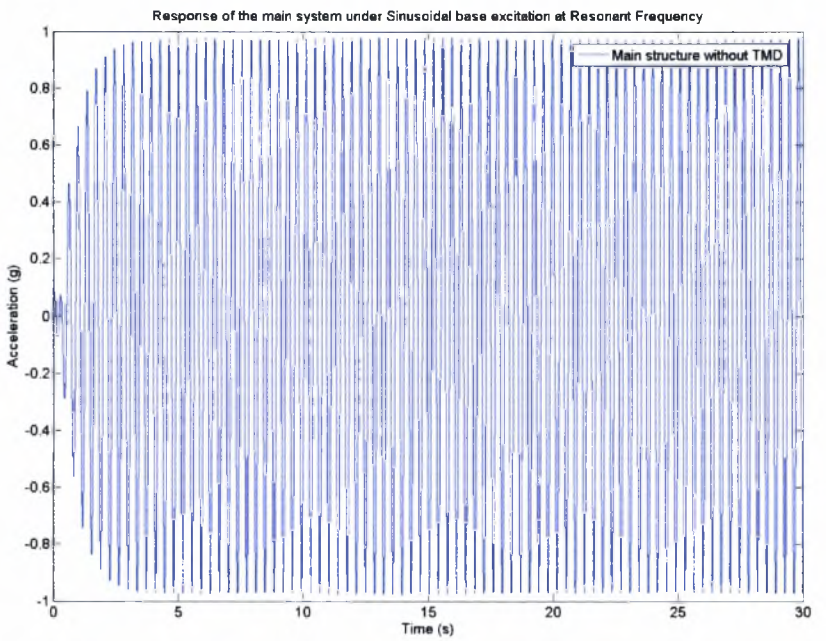

Figure 5.6: Response of the primary system subjected to sinusoidal base excitation

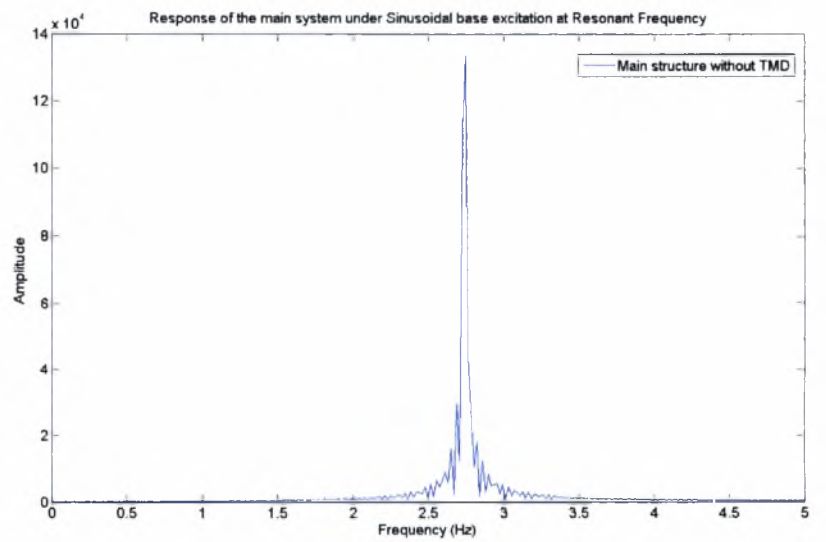

Figure 5.7: Fourier transform of the response of the primary system subjected to sinusoidal base excitation

Next, the experiments with the base harmonic excitation are conducted using the combined primary-secondary system with one TMD attached to the primary system. The acceleration response of the primary system is shown in Fig. 5.8 and is compared to the acceleration response in Fig. 5.6 obtained in the absence of the TMD.

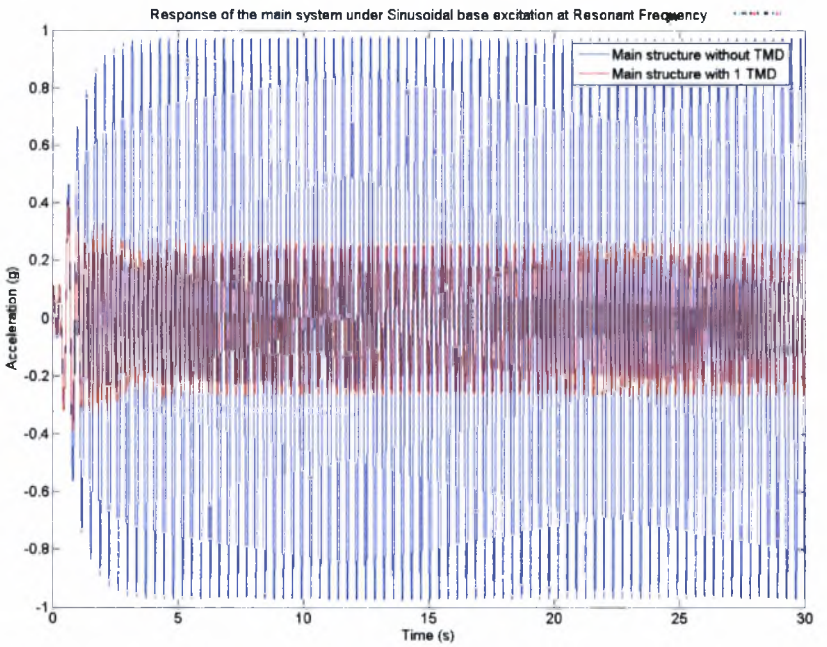

Figure 5.8: Response of the primary system subjected to sinusoidal base excitation with and without a TMD attachment

It is evident in Fig. 5.8 that a significant reduction of the response of the primary system has been achieved by attaching the TMD. Specifically, this reduction is of the order of 72%. That is the peak steady state response of the primary system with TMD attachment is 28% of peak steady state response of the primary system without TMD attachment.
Fig. 5.9 compares the Fourier transforms of the acceleration responses shown in Fig. 5.8. A similar reduction is evident in this figure as well.

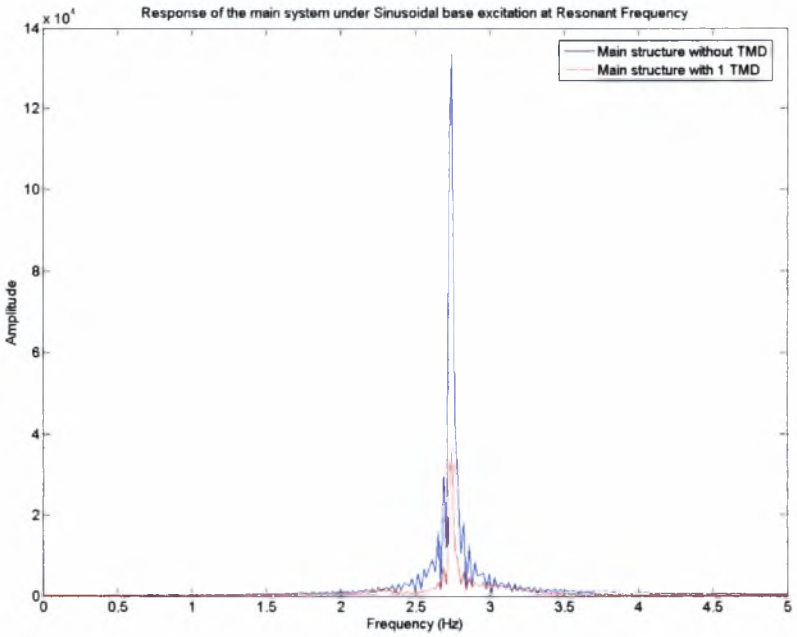

Figure 5.9: Fourier transform of the primary system subjected to sinusoidal base excitation with and without a TMD attachment

The experiment is next conducted using the combined primary-secondary system with two TMDs attached to the primary system. The acceleration response of the primary system is shown in Fig. 5.10 and is compared to the acceleration response in Fig. 5.6 obtained in the absence of TMDs.

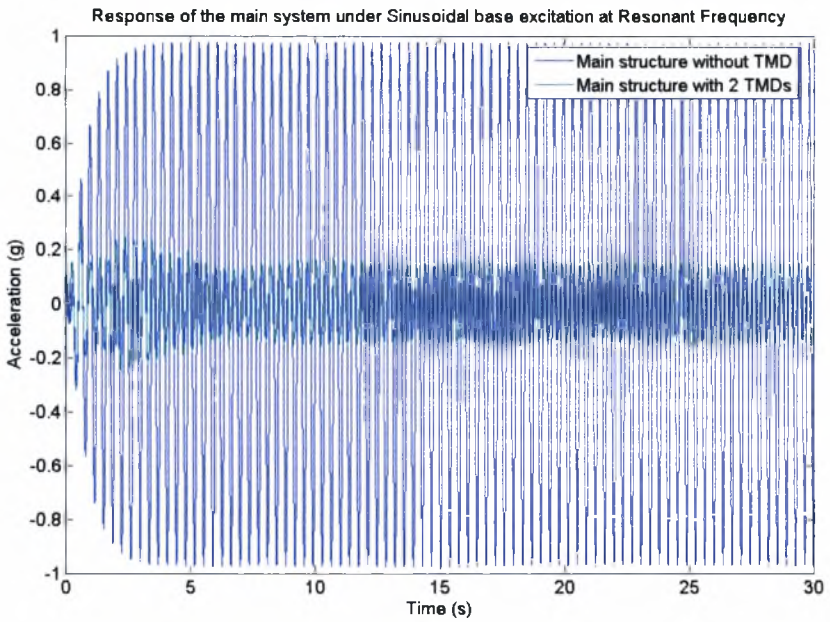

Figure 5.10: Response of the primary system subjected to sinusoidal base excitation with and without two TMD attachments

It is evident in Fig. 5.10 that a significant reduction of the response of the primary system has been achieved by attaching the TMDs. Specifically, this reduction is of the order of 84%. That is the peak steady state response of the primary system with two TMD attachments is 16% of peak steady state response of the primary system without TMD attachments.

Fig. 5.11 compares the Fourier transforms of the acceleration responses shown in Fig. 5.10. A similar reduction is evident in this figure as well.

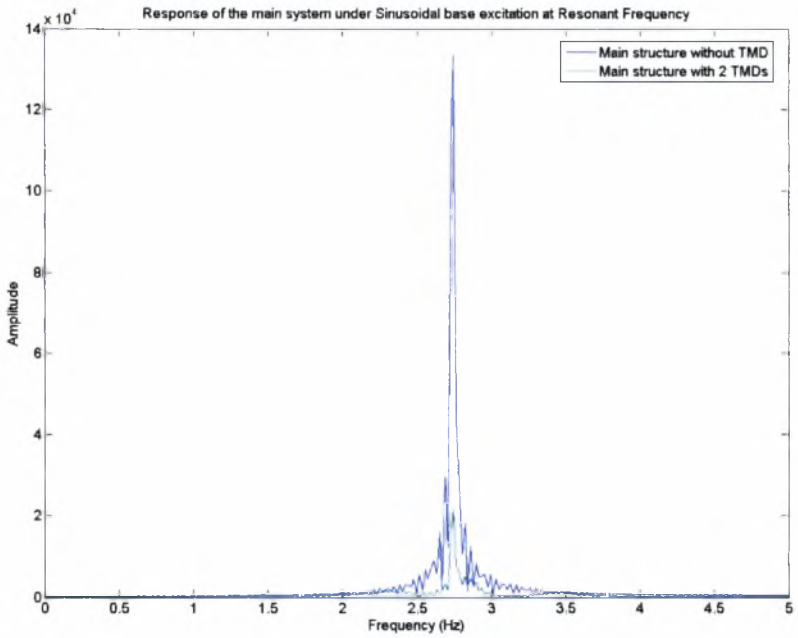

Figure 5.11: Fourier transform of the response of the primary system subjected to sinusoidal base excitation with and without two TMD attachments

At this point we compare the results obtained for the primary system without the TMD attachments with the results obtained for the primary system with one or two TMD attachments. These comparisons are shown in Fig. 5.12 for the acceleration time histories and in Fig. 5.13 for the corresponding Fourier transforms of the acceleration time histories.

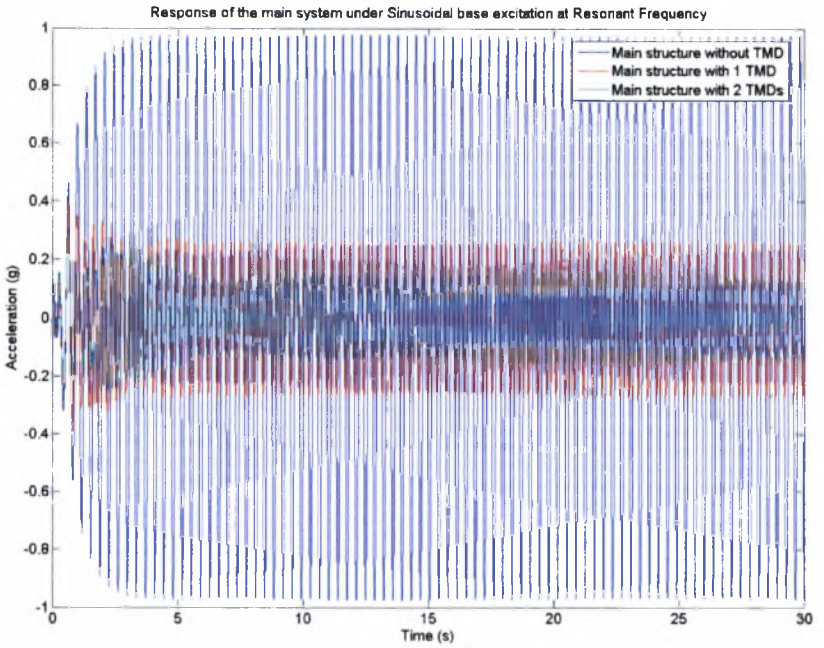

Figure 5.12: Response of the primary system subjected to sinusoidal base excitation with and without one or two TMD attachments

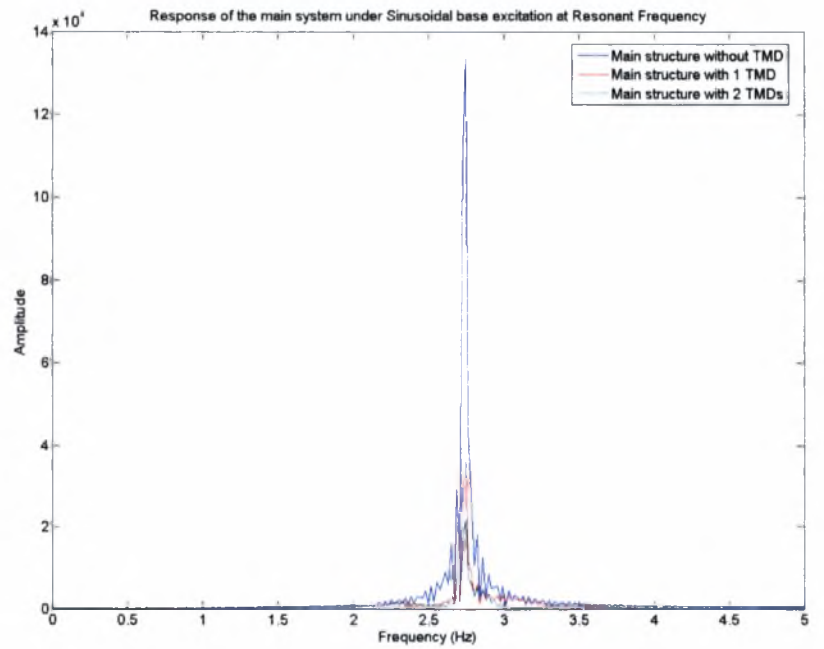

Figure 5.13: Fourier transforms of the response of the primary system subjected to Sinusoidal base excitation with and without one or two TMD attachments

The experimental results support theoretical results that state that splitting the TMD mass into two equal masses and by optimally designing TMDs with these two masses, result in reduction of the vibrations of the primary system compared to the vibrations obtained with the original single TMD attachment. In conclusion, it is expected that multiple TMDs are more effective than one TMD, provided that the sum of the masses of the multiple TMDs equals the mass of the single TMD.

5.4 TMD Control Effectiveness using Earthquake Base Excitation

The effectiveness of the TMD to reduce the vibrations of the primary structure is next examined using an earthquake excitation applied at the base of the structure with the electrodynamic shaker. Specifically, as base acceleration is selected to be one of the components available during the strong El Centro earthquake. This acceleration is shown in Fig. 5.14.

The experiment is first conducted for the primary structure without TMD attachments. The acceleration response of the primary structure is shown in Fig. 5.15. In Fig. 5.16 it is shown the Fourier transform of the acceleration time history of Fig. 5.15.

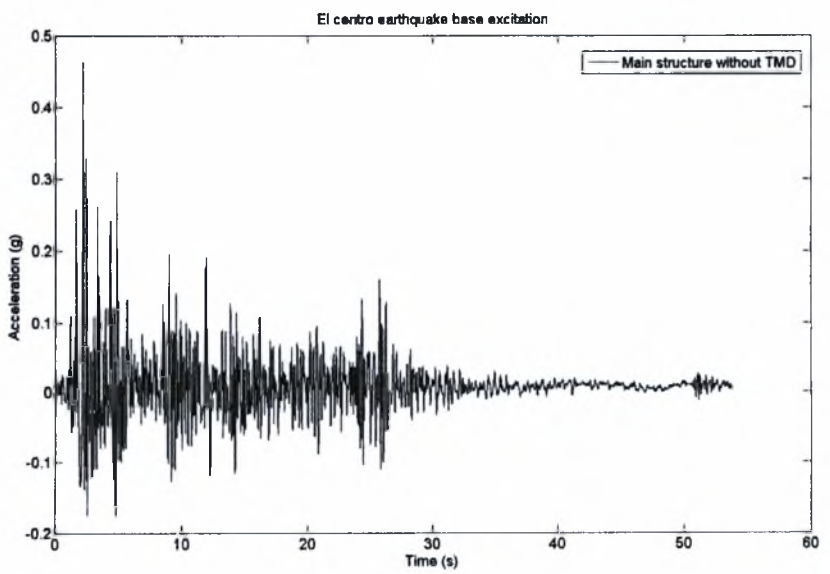

Figure 5.14: El Centro Earthquake base excitation

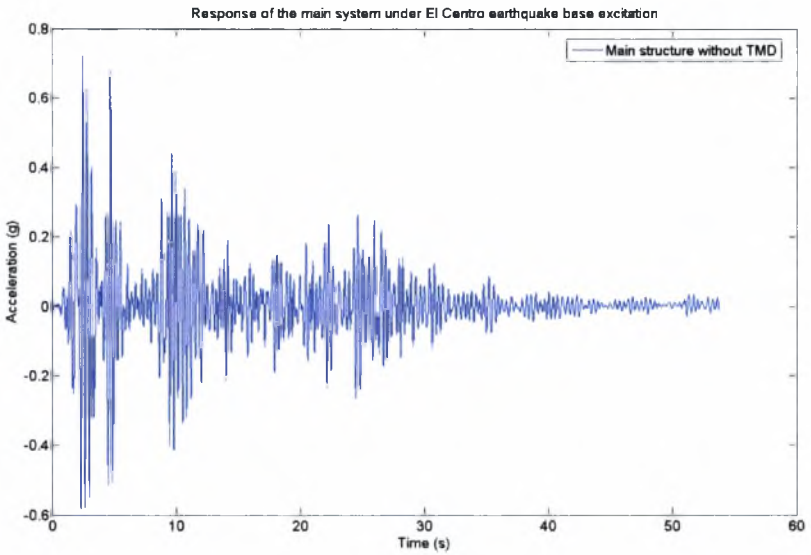

Figure 5.15: Response of the primary system subjected to El Centro earthquake base excitation

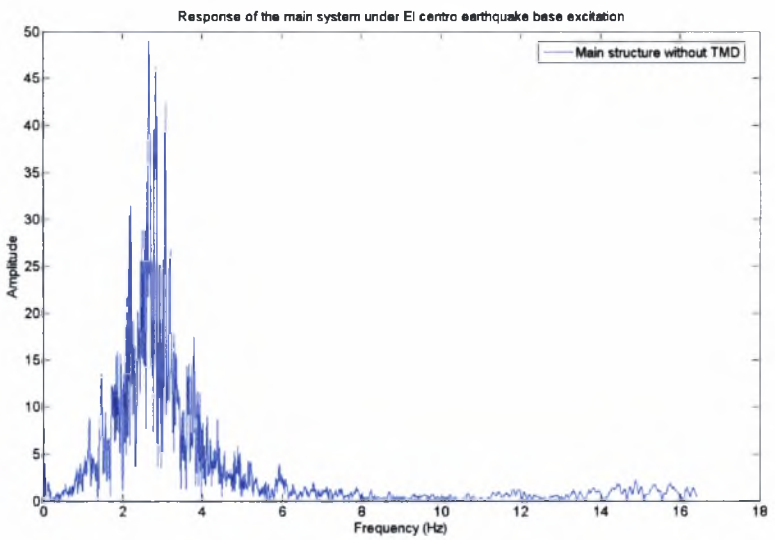

Figure 5.16: Fourier transform of the response of the primary system subjected to El Centro earthquake base excitation

The transfer function of the system, estimated experimentally as the ratio of the Fourier transform of the acceleration response to the Fourier transform of the excitation, is shown

in Fig. 5.17. As expected, in the frequency range of interest, say 0-10 Hz, the system behaves as a SDOF oscillator with resonant frequency close to the measured fundamental frequency of the primary structure without the TMD attachments.

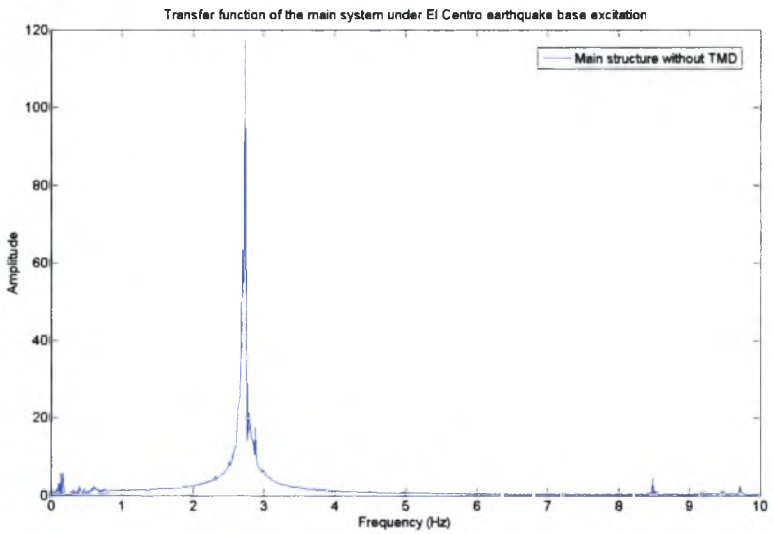

Figure 5.17: Experimental transfer function of the primary system without TMD attachments

Next, the experiment is conducted using the combined primary-secondary system with one TMD attachment to the primary system. The acceleration response of the primary system is shown in Fig. 5.18 and is compared to the acceleration response of Fig. 5.15 of the primary system without TMD attachments. Fig. 5.19 compares the Fourier transforms of the acceleration responses presented in Fig. 5.18. Finally, the transfer function between the base acceleration and the acceleration of the primary system is computed experimentally and shown in Fig. 5.20. It is clear from Fig. 5.20 that the combined primary-secondary system with one TMD behaves as a two degrees of freedom system with modal frequencies one to the left and one to the right of the fundamental frequency of the primary structure without TMD attachments. The values of the modal frequencies are reported in Table 5.1.

From the comparison of the transfer functions in Fig. 5.20, it is worth pointing out that the resonant peak of the primary system without TMD attachments has been reduced by 59% when the TMD attachment is used. This validates the effectiveness of the TMDs in

reducing the peak of the transfer function. However, for the combined system with one TMD attachment there are two resonant peaks that appear in the neighborhood of the fundamental frequency at the primary system. It is thus expected that the energy in the frequency component of the response signal in the vicinity of the fundamental frequency of the primary system will be significantly reduced when the TMD attachment is active as compared to the energy of the frequency components of the response signal of the primary system without TMD attachments. Moreover, the energy of the frequency components of the response signal obtained with the TMD will be amplified in the vicinity of the two modal frequencies of the primary-secondary system. This behavior is evident in Fig. 5.19.

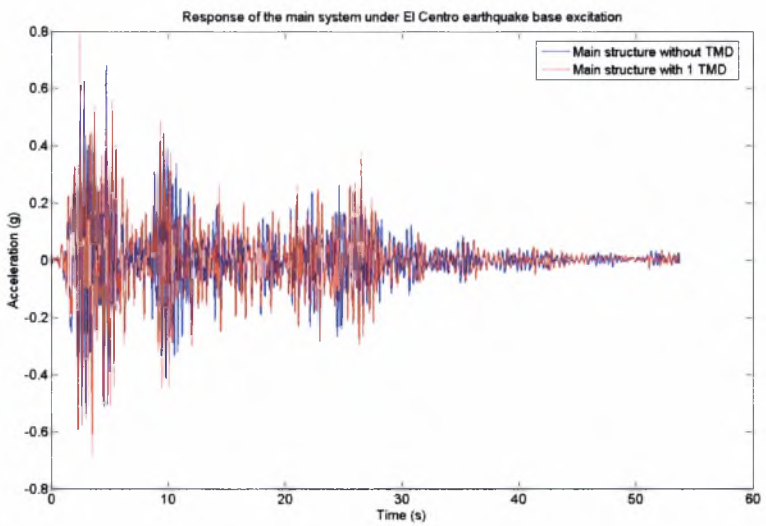

Figure 5.18: Response of the primary system subjected to El Centro earthquake base excitation with and without one TMD attachment

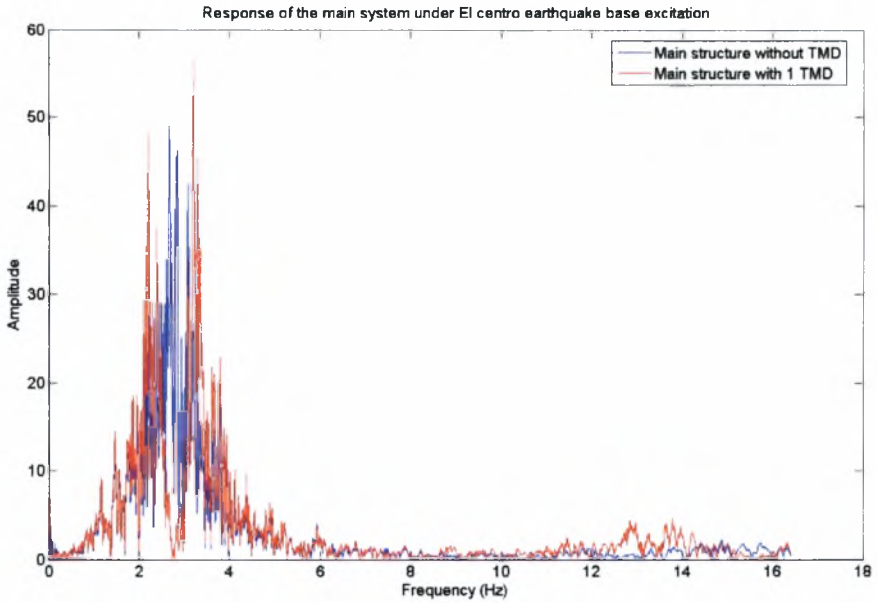

Figure 5.19: Fourier transform of the response of the primary system subjected to El Centro earthquake base excitation with and without one TMD attachment

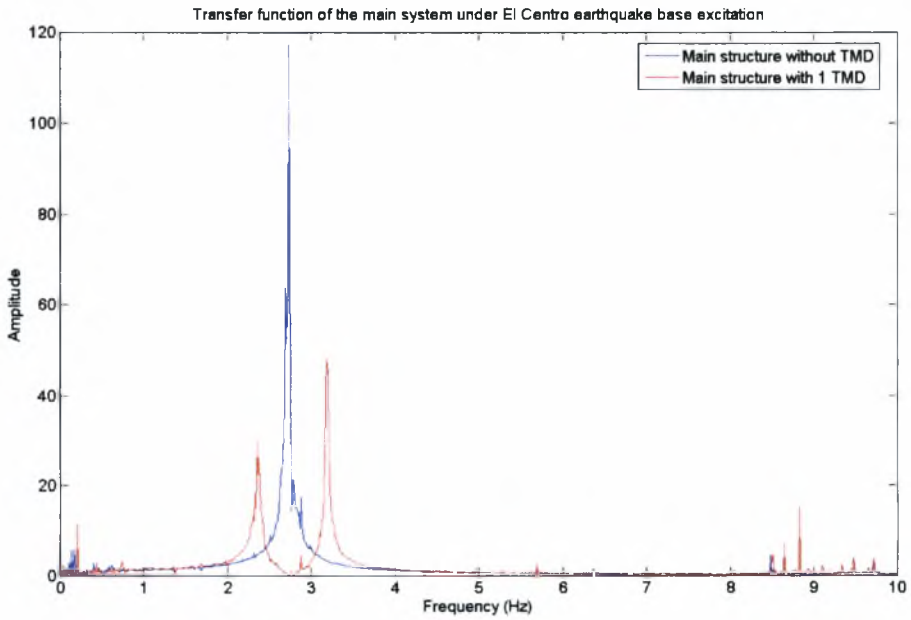

Figure 5.20: Experimental transfer function of the primary system with and without one TMD attachment

Next, the experiment is conducted using the combined primary-secondary system with two TMD attachments to the primary system and simultaneously we compare the results obtained for the primary system without the TMD attachment with the results obtained for the primary system with one or two TMDs. The acceleration response of the primary system is shown in Fig. 5.21 and is compared to the acceleration response of Fig. 5.18 of the primary system with one TMD attachment. Fig. 5.22 compares the Fourier transforms of the acceleration responses presented in Fig. 5.21. Finally, the transfer function between the base acceleration and the acceleration of the primary structure is computed experimentally and shown in Fig. 5.23. It is clear from Fig. 5.23 that the combined primary-secondary system with two TMD behaves as a three degrees of freedom system with modal frequencies one to the left and two to the right of the fundamental frequency of the primary structure without TMD attachments. The values of the modal frequencies are reported in Table 5.1.

From the comparison of the transfer functions in Fig. 5.23, it is worth pointing out that the resonant peak of the primary system without TMD attachments has been reduced about the same level as when one TMD attachment is used. However, for the combined system with two TMDs attachments there are three resonant peaks that appear in the neighborhood of the fundamental frequency at the primary system. It is thus expected that the energy in the frequency component of the response signal in the vicinity of the fundamental frequency of the primary structure will be significantly reduced when the TMD attachments are active as compared to the energy of the frequency components of the response signal of the primary structure without TMD attachments. Moreover, the energy of the frequency components of the response signal obtained with the TMDs will be amplified in the vicinity of the three modal frequencies of the primary-secondary system. This behavior is evident in Fig. 5.22.

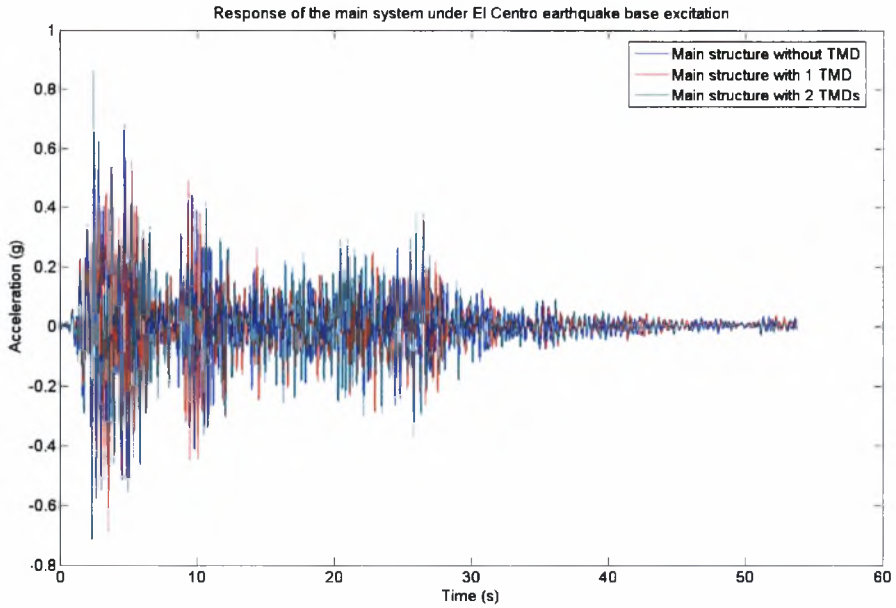

Figure 5.21: Response of the primary system subjected to El Centro earthquake base excitation with and without one or two TMD attachments

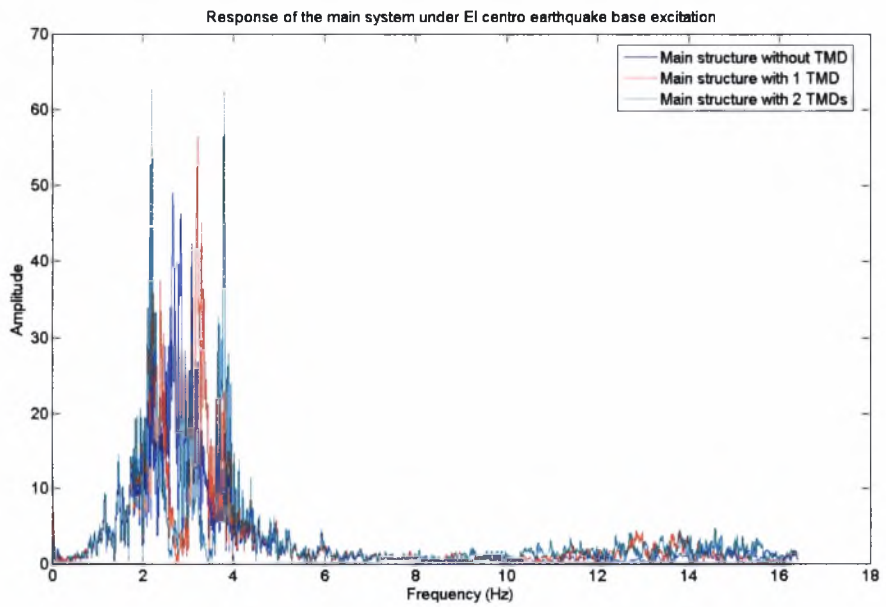

Figure 5.22: Fourier transforms of the response of the primary system subjected to El Centro Earthquake base excitation with and without one or two TMD attachments

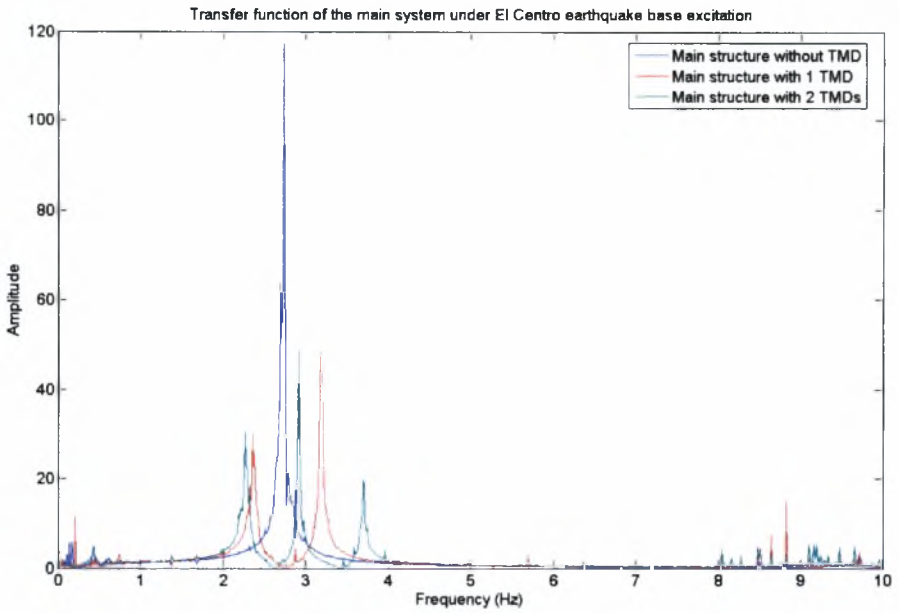

Figure 5.23: Experimental transfer function of the primary system with and without one or two TMD attachments

All the resonant peak reductions of primary system for both excitations with the effect of one and two TMDs attachments are presented in Table 5.2.

Table 5.2: Resonant peak reduction of primary system main mass M

Type of excitation	**# of TMDs**	**Resonant Peak Reduction (%)**
Harmonic excitation	1	72
Harmonic excitation	2	84
El Centro earthquake excitation	1	59
El Centro earthquake excitation	2	59

In general, for the level of very low damping values produced in these laboratory experiments, it can be conducted that the TMD attachments reduce considerably the vibrations associated with the frequency components in the vicinity of the fundamental frequency of the primary system, but amplify the vibrations associated with the frequency components in the vicinity of the modal frequencies of the combined primary-secondary

system with one and two TMD attachments. In order to achieve reduction in a broader frequency range, the damping values of the TMDs have to be increased. This, however, was difficult to implement in the laboratory experiments. An effort towards this direction was made using light insulation material and the results are presented in the next section.

5.5 Effect of Damping on TMD Effectiveness

Next, the effect of damping on the TMD effectiveness is investigated. In order to increase the damping of the TMD, the main stiffness member of the TMD was wrapped with an insulation material which is very light and it is supposed to work like a friction damper in the TMD. The TMD with the insulation material is shown in Fig. 5.24. Similarly, in order to increase the primary system damping its main stiffness member was wrapped with the same insulation material, as shown in Fig 5.25.

Figure 5.24: TMD with insulation material for extra damping

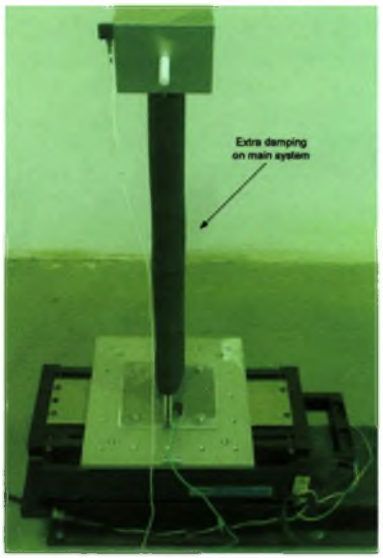

Figure 5.25: Experimental set-up of the main system with extra damping

Experiments were conducted to identify the damping of the primary system and the damping of the TMD with insulation material added on them. The damping values are given in Table 5.2 and are compared with the damping values of the primary and secondary system without the insulation material. It can be seen that the damping value of the primary system has been increased by 37% while the damping value of the TMD more than one time higher than the damping without the insulation material.

Table 5.2: Experimental measured damping ratios ζ for the main and secondary system with and without the presence of extra damping

ζ %	**Without extra damping**	**With extra damping**	**Difference (%)**
ζ_{Main}	0.19	0.26	+37%
ζ_{Sec}	0.21	0.47	+124%

Next, the passive control effectiveness of the TMD with extra damping is investigated. In the experiments conducted the base excitation is chosen to be El Centro earthquake excitation. Figs. 5.26, 5.27 and 5.28 compare the response characteristics of the main system without the presence of extra damping and with the presence of extra damping.

The experiment is first conducted for the primary structure without the TMD attachment. The acceleration responses of the primary structure are compared in Fig. 5.26, the Fourier transform of the acceleration responses are compared in Fig. 5.27 and the transfer functions are compared in Fig. 5.28.

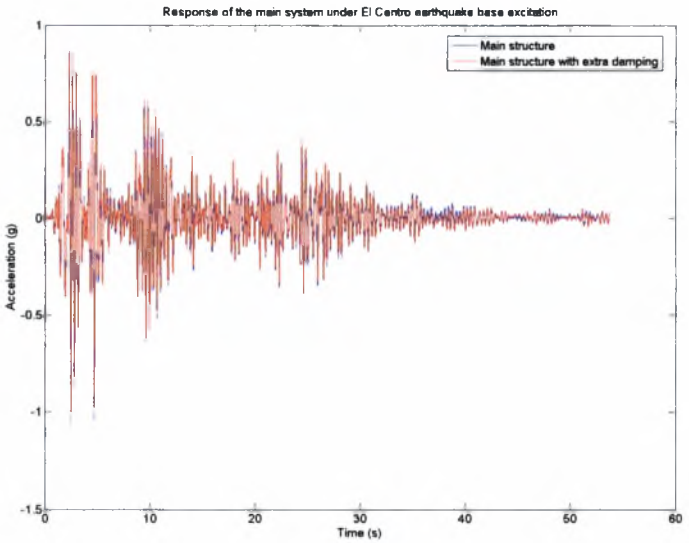

Figure 5.26: Response of the primary system subjected to El Centro earthquake base excitation with and without the presence of extra damping

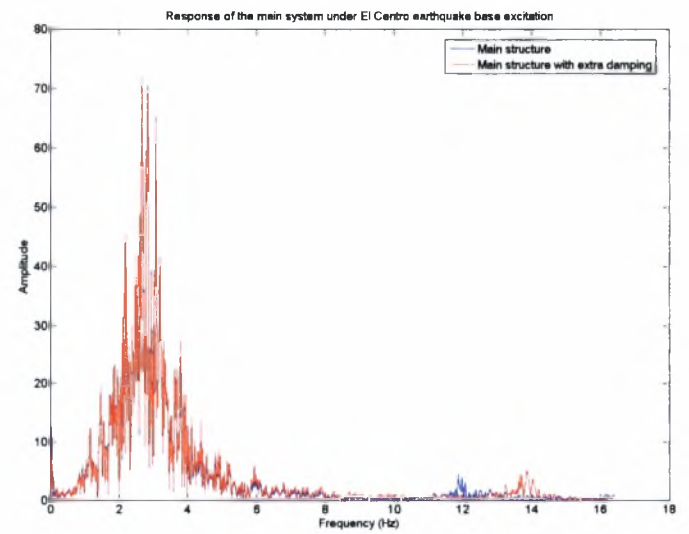

Figure 5.27: Fourier transform of the response of the primary system subjected to El Centro earthquake base excitation with and without the presence of extra damping

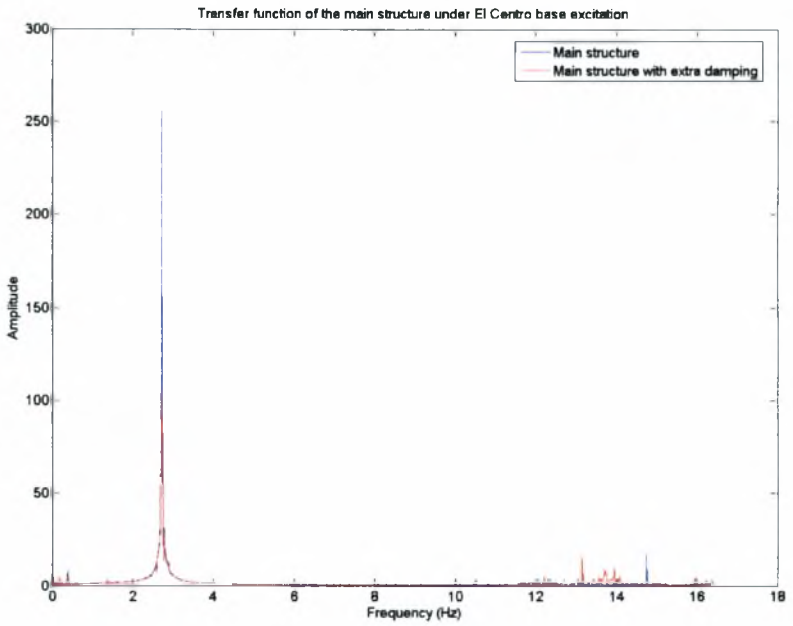

Figure 5.28: Experimental transfer function of the primary system with and without the presence of extra damping

From the peak responses of Fig. 5.28 we observe that the peak resonance response of the main system with the presence of extra damping is 59% lower than the peak resonance response of the main system without the presence of extra damping.

Next, we conducted the experiment for the combined primary-secondary system with one TMD both wrapped by insulation material for extra damping, as shown in Fig. 5.29.

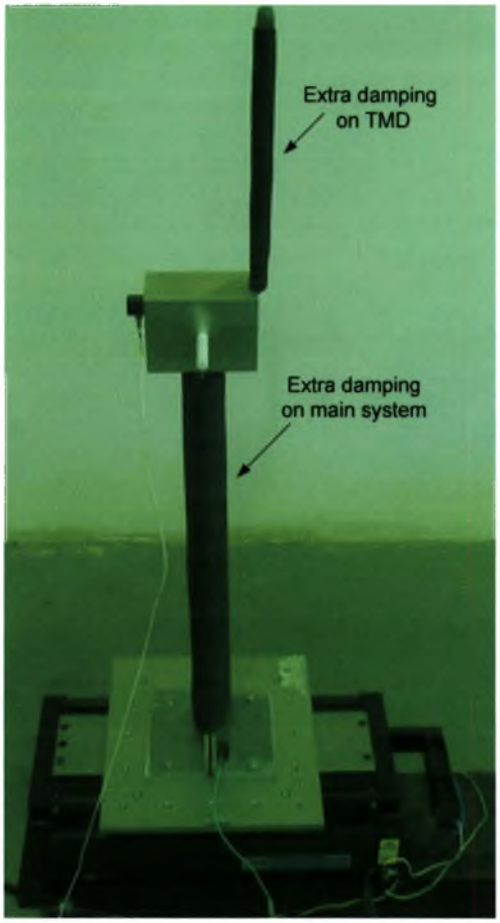

Figure 5.29: Experimental set-up of primary-secondary system with extra damping

Figs. 5.30, 5.31 and 5.32 compare the response characteristics of the main system with one TMD, without the presence of extra damping and with the presence of extra damping.

Specifically, the acceleration responses of the primary structure are compared in Fig. 5.30, the Fourier transform at the acceleration responses are compared in Fig. 5.31, and the transfer functions are compared in Fig. 5.32.

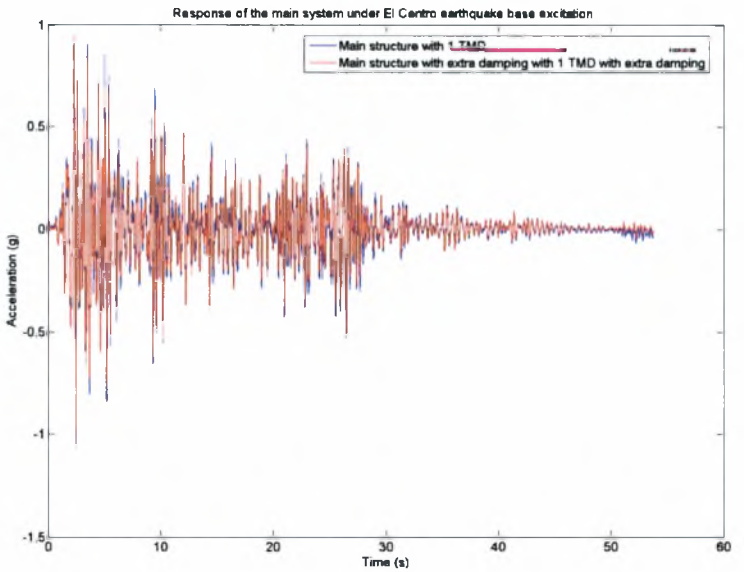

Figure 5.30: Response of the primary system with one TMD attachment subjected to El Centro earthquake base excitation with and without extra damping in the whole system

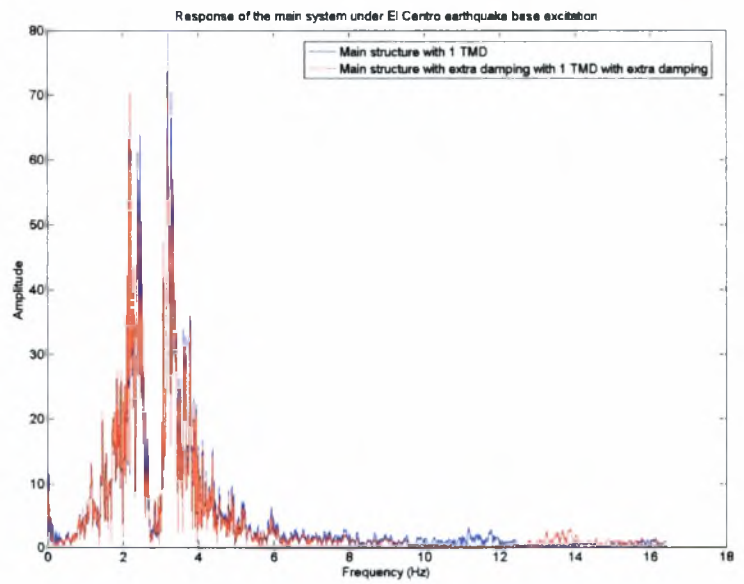

Figure 5.31: Fourier transform of the primary system with one TMD attachment subjected to El Centro earthquake base excitation with and without extra damping in the whole system

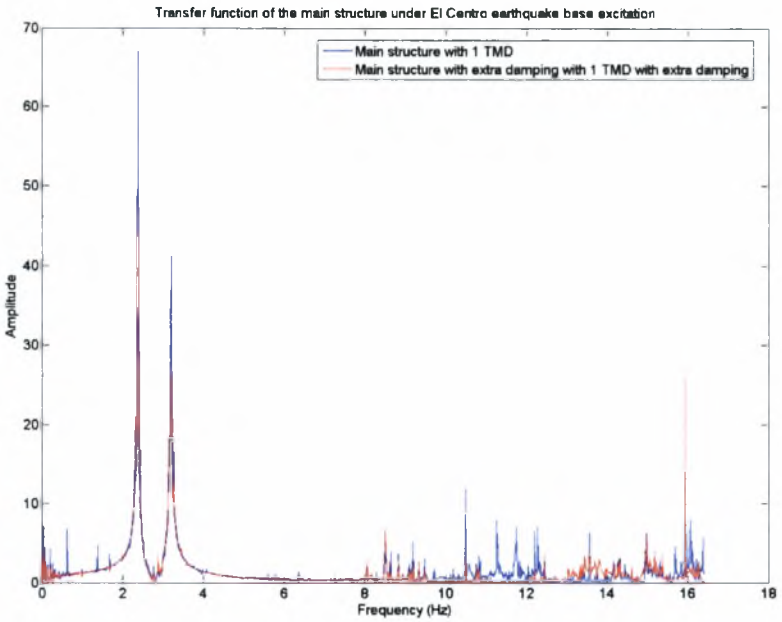

Figure 5.32: Experimental transfer function of the primary system with one TMD attachment with and without extra damping in the whole system

From the peak responses of Fig. 5.32 we observe that the peak resonance response of the main system with the presence of extra damping is 27% lower than the peak resonance response of the main system without the extra damping on the main system and on the TMD. It is thus obvious that damping may significantly contribute to the effectiveness of the TMD to control the vibrations of the primary system in the case of earthquake excitations where the frequency content of the excitation is broadband.

From the peak responses of Fig. 5.32 we observe that the peak resonance response of the main system with the presence of extra damping is 27% lower than the peak resonance response of the main system without the extra damping on the main system and on the TMD. It is thus obvious that damping may significantly contribute to the effectiveness of the TMD to control the vibrations of the primary system in the case of earthquake excitations where the frequency content of the excitation is broadband.

CHAPTER 6

CONCLUSIONS

6.1 Concluding Remarks

In this thesis, the effectiveness of Passive Control Systems and more specifically Tuned Mass Damper (TMD) and Multiple Tuned Mass Damper (MTMD) for reducing the vibrations of a single degree of freedom (SDOF) system subjected to sinusoidal and earthquake base excitation were analyzed and experimentally verified.

The equations of motion that describe a single degree of freedom (SDOF) system (primary system) with the presence either one TMD or multiple TMDs (secondary system) connected in parallel with the main SDOF system were presented and a methodology for the optimal selection and design of the parameters of the TMD was introduced.

Two combined primary-secondary systems were developed for a laboratory experiment. The first system was used to simulate the behavior of a primary system under the operation of one TMD and the second system was used to simulate the behavior of the primary system under the operation of two TMDs installed in parallel with the primary system. The structural details of the systems and the experimental equipment and software used for performing the experiments were presented in details. Additionally, experimental modal analysis methodology for identifying the modal parameters of the structure (modal frequencies, damping ratios) using the frequency response functions of the structure response was introduced.

Experimental results on the two types of the laboratory structures for the purpose of validating the performance of the TMDs for Passive Control were presented. Validation of Passive Control performance was based on comparison of the magnitude of the time history acceleration response and transfer functions obtained for this broad band earthquake excitation measured for the primary structure for the cases of no TMD, one TMD and two TMDs attached to the primary structure.

Comparisons were presented for two types of base excitations applied by the electrodynamic shaking table:

(a) sinusoidal excitations with frequency close to the fundamental frequency of the primary structure, and

(b) an earthquake excitation selected to be one of the available recordings of the El Centro Earthquake.

Due to low damping of the laboratory experimental structures was resulted in making the TMDs less effective for reducing vibrations in a frequency range relatively far from the vicinity of the fundamental frequency of the primary structure. The effect of damping on the performance of the TMDs in controlling vibrations was also examined experimentally by repeating the experiments after adding damping to the system through the use of a very light insulation material.

It was demonstrated that two TMDs further reduce the vibrations of the primary structure as compared to one TMD. It was demonstrated that the additional damping improves the performance of the TMDs for controlling the vibrations of the primary structure.

6.2 Future Work

Some recommendations for future studies related to this work are as follows:

- Passive Control Systems like Tuned Liquid Dampers (TLD) and Tuned Liquid Column Dampers (TLCD) may be developed and their effectiveness in controlling vibration of the primary system could be investigated.
- Active structural control concepts should also be developed. Specifically, a novel concept for active structural control is under development by the author for actively controlling vibrations of structures using air and water jet pulsers. Significant progress has been made with the experimental setup which is analogous to the present experimental setup. Immediate steps include the investigation and application of the controller based on Pulse Width Modulation (PWM) Control Theory.

- Throughout this dissertation the structural system was assumed to remain in the linear region, but the structure will inevitably become nonlinear at some point due to excessive excitation levels. Methods of analyzing and controlling the structures in these non-linear situations should be developed.
- Before structural control systems are implemented in full-scale structures (tall buildings, bridges etc.), guidelines and codes will be necessary for the design of structures which employ control systems. The requirements of these guidelines and codes should be considered.

References

Abe M., Fujino Y. "Dynamic characterization of multiple tuned mass dampers and some design formulas." *Earthquake Engrg. and Sturct. Dyn.*, **(23)** 813–835 (1994).

Adeli H. "Hybrid Control of Smart Structures," *6th International Congress on Advances in Civil Engineering, 6-8 October 2004, Bogazici University, Istanbul, Turkey.*

Adeli H., Kim H. "Recent Advances and Novel Concepts for Motion Control of Bridges and Highrise Buildings under Extreme Winds and earthquakes," *Asian Journal of Civil Engineering (Building and Housing)*, **7** (4) 335-342 (2006).

Aiken I.D., Kelly J.M. "Earthquake simulator testing and analytical studies of two energy-absorbing systems for multistory structures." *Report No.UCB/EERC-90/03, University of California, Berkeley, CA* (1990).

Aprile A., Inaudi J.A., Kelly J.M. "Evolutionary model of viscoelastic dampers for structural applications." *J. Engrg. Struct.*, **(123)** 551–560 (1997).

Arima F., Miyazaki M., Tanaka H., Yamazaki Y. "A study on building with large damping using viscous damping walls." *Proc. 9th World Conf. on Earthquake Engrg., Tokyo,* **(5)** 821–826 (1988).

Balendra T., Wang C.M., Rakesh G. "Effectiveness of TLCD on various structural systems," *Engineering Structures*, **21** 291-305 (1999).

Bernhard B. "Basic Theory of the Hammer Testing," *Kistler Instrumente AG Winterthur, Switzerland* (1998).

Buckle I.G., Mayes R.L. "Seismic isolation history, application, and performance – a would view." *Earthquake Spectra*, **(6)**161–201 (1990).

Chang C.C., Qu W.L. "Unified Dynamic Absorber Design Formulas for Wind-Induced Vibration Control of Tall Buildings," *Structural Design of Tall Buildings*, **7** 147-166 (1998).

Chang C.C. "Mass dampers and their optimal designs for building vibration control," *Engineering Structures*, **21** 454-463 (1999).

Chen G., Wu J. "Optimal Placement of Multiple Tuned mass Dampers for seismic Structures," *Journal of Structural Engineering*,127 **(9)** 1054-1062 (2001).

Chowdhury A. H., Iwuchukwu M. D. "The past and future of seismic effectiveness of tuned mass dampers," *Proc. 2nd Int. Symposium Struct. Control (Leipholz, H. H. E.ed)*, Martinus Nijhoff Publishers, 105-127 (1987).

Clark A.J. "Multiple passive tuned mass damper for reducing earthquake induced building motion." *Proc. 9th World Conf. on Earthquake Engrg.*, **(5)** 779–784 (1988).

Clark P.W., Aiken I.D., Tajirian F., Kasai K., Ko E., Kimura I. "Design procedures for buildings incorporating hysteretic damping devices." *Proc. Int. Post-SmiRT Conf. Seminar on Seismic Isolation, Passive Energy Dissipation and Active Control of Vibrations of Structures*, **(1)** 317–337 (1999).

Colajanni P., Papia M.. "Hysteretic characterization of friction-damped braced frames." *J. Struct. Engrg.*, ASCE, **(123)** 1020–1028 (1997).

Constantinou M.C., Symans M.D., Tsopelas P., Taylor D.P. "Fluid viscous dampers in applications of seismic energy dissipation and seismic isolation." *Proc. ATC-17-1 Seminar on Seismic Isolation, Passive Energy Dissipation, and Active Control,* **(2)** 581–591 (1993).

Constantinou M.C., Symans M.D. "Experimental study of seismic response of buildings with supplemental fluid dampers." *Struct. Design Tall Bldgs.*, **(2)** 93–132 (1993).

Crosby P., Kelly J.M., Singh J. "Utilizing viscoelastic dampers in the seismic retrofit of a thirteen story steel frame building." *Structures Congress XII*, Atlanta, GA, 1286–1291 (1994).

Currie I.G. "Fundamental Mechanics of Fluids," *Third Edition, Marcel Dekker, Inc.* (1974).

Dargush G.F., Soong T.T. "Behavior of metallic plate dampers in seismic passive energy dissipation system." *Earthquake Spectra* 11 **(4)** 545-568 (1995).

Den Hartog J.P. *Mechanical Vibrations*, New York:McGraw-Hill, Inc (1947).

Dyke S.J., Spencer Jr. B.F., Quast P., Sain M.K., Kaspari Jr. D.C., Soong T.T. "Experimental Verification of Acceleration Feedback Control Strategies for an Active Tendon System," *Report of the U.S. Center for Earthquake Engineering Research, Buffalo, New York*, Technical Report NCEER-94-0024, (1994).

Dyke S.J., Spencer Jr. B.F., Quast P., Kaspari D.C., Sain M.K. "Implementation of an AMD Using Acceleration Feedback Control," *Microcomputers in Civil Engineering: Special Issue on Active and Hybrid Structural Control* 11 **(5)** 289-366 (1996).

Dyke S.J., Spencer Jr. B.F., Sain M.K., Carlson J.D. "An experimental study of MR Dampers for seismic Protection," *Smart Materials and Structures: Special Issue on Large Civil Engineering* **7** 693-703 (1998).

Ferry J.D. *Viscoelastic properties of polymers*, New York, John Wiley (1980).

Filiatrault A., Cherry S. "Seismic design spectra for friction-damped structures." *J. Struct. Engrg.*, ASCE, **(116)** 1334–1355 (1990).

Filiatrault A., Tremblay R., Kar R. "Performance evaluation of friction spring seismic damper." *J. Struct. Engrg.*, ASCE, **(126)** 491–499 (2000).

Fujino Y., Pacheco B.M., Chaisari P., Sun L.M. "Parametric studies on tuned liquid damper (TLD) using circular container by free-oscillation experiment," *JSCE structural eng./earthquake eng.* **5** (2), 381-391 (1988).

Fujino Y., Sun L.M., Pacheco B.M., Chaisari P. "Tuned liquid damper (TLD) for suppressing horizontal motion of structures," *J. eng. Mech.* ASCE, **118** 2017-2030 (1992).

Fujino Y., Soong T.T., Spencer Jr. B.F. "Structural Control: Basic Concepts and Applications," *Proceedings of the 1996 ASCE Structures Congress, Illinois, April 15-18 1996.*

Gao H., Kwok K.S.C., Samali B. "Characteristics of Multiple Tuned Liquid Column Dampers in Suppressing Structural Vibrations," *Engineering Structures*, **21** 316-331 (1999).

Gauberghe B. "Applied frequency-domain system identification in the field of experimental and operational modal analysis," *PhD Thesis, Vrije Universiteit Brussel, Belgium* (2004).

Haroun M. A., Pires J. A. ''Active orifice control in hybrid liquid column dampers.'' *Proc., 1st World Conf. on Structural Control*, Vol. I, Los Angeles (1994).

Higgins C., Kasai K. "Experimental and analytical simulation of wind response for a full-scale VE-damped steel frame." *J. Wind Engrg. and Industrial Aerodynamics*, **(77)** 297–313 (1998).

Hochrainer M.J., Ziegler F. "Control of tall building vibrations by sealed tuned liquid column dampers," *Structural Control and Health Monitoring*, **13** 980-1002 (2006).

Housner G.W., Bergman L.A., Caughey T.K., Chassiakos A.G., Claus R.O., Masri S.F., Skelton R.E., Soong T.T., Spencer Jr. B.F., Yao J.T.P. "Structural control: past, present and future," *Journal of Engineering Mechanics*, **123** (9) 897-971 (1997).

Igusa T., Xu K. "Wide band-response characteristics of multiple subsystems with high modal density", *Proc. 2nd int. conf. stochastic struct. dyn.* Florida, U.S.A. (1990).

Igusa T., Xu K. "Vibration reduction characteristics of distributed tuned mass dampers", *Proc. 4th int. conf struct. dyn.: recent advances,* 596-605 (1991).

Jangid R.S. "Optimum multiple tuned mass dampers for base-excited undamped system." *Earthquake Engrg. and Struct. Dyn.*, **(28)** 1041–1048 (1999).

Jansen L.M., Dyke S.J. "Semi-Active Control strategies for MR Dampers: A Comparative Study," *J. Engrg Mech.*, ASCE, **126** (8) 795-803 (2000).

Kobori T., Koshika N., Yamada K., Ikeda Y. "Seismic-Response-Controlled Structures with Active Mass Driver System, Part 1: Design," *Earthquake Engrg. and Struct. Dynamics* **20** 135–149 (1991a).

Kobori T., Koshika N., Yamada K., Ikeda Y. "Seismic-Reponse-Controlled Structures with Active Mass Driver System, Part 2: Verification," *Earthquake Engrg. and Struct. Dynamics* **20** 151–166 (1991b).

Kobori T., Takahashi M., Nasu T., Niwa N., Ogasawara, K. "Seismic response controlled structure with active variable stiffness system." *Earthquake Engrg. and Struct. Dyn.*, **22** 925–941 (1993).

Kumar R.A., Sohn C.H., Gowda B.H.L. "Passive Control of Vortex Induced Vibrations: An Overview," *Recent Patents on Mechanical Engineering*, **(1)** 1-11 (2008).

Kwok K.C.S., Samali B. "Performance of tuned mass dampers under wind loads," *Engineering Structures*, **17** (9) 655-667 (1995).

Lametrie C.W. "A Literary Review of Structural Control: earthquake Forces," *Technical Research Paper, Parsons Brinckerhoff Automotive Division*, (2001).

Levy R., Marianchik E., Rutenberg A., Segal F.. "Seismic design methodology for friction damped braced frames." *Earthquake Engrg. and Struct. Dyn.*, **(29)** 1569–1585 (2000).

Li C., Reinhorn A.M. "Experimental and analytical investigation of seismic retrofit of structures with supplemental damping: part 2-friction devices." *NCEER Rep. 95-0009, State University of New York at Buffalo, Buffalo, NY* (1995).

Li C. "Performance of multiple tuned mass dampers for attenuating undesirable oscillations of structures under the ground acceleration." *Earthquake Engrg. and Struct. Dyn.*, **(29)** 1405–1421 (2000).

Lou Y., Lutes L.D., Li J.J. ''Active tuned liquid damper for structural control.'' *Proc., 1st World Conf. on Wind Engineering*,Vol. I, Los Angeles (1994).

Makris N. "Fractional derivative model for viscous damper." *J. Struct. Engrg.*, ASCE, **(117)** 2708–2724 (1991).

Makris N., Dargush G.F. "Generalized boundary element formulation for dynamic analysis of viscoelastic system." *Proc. 1st World Conf. on Struct. Control*, 73–81 (1994).

Makris N., Hill D., Burton S., Jordan M. "Electrorheological Fluid Dampers for Seismic Protection of Structures." *Proc. SPIE Conf. on Smart Struct. and Materials* (I. Chopra, Ed.), San Diego, California, 184–194 (1995).

Makris N., Burton S.A., Hill D., Jordan M. "Analysis and Design of an Electrorheological Damper for Seismic Protection of Structures," *J. Engrg Mech.*, ASCE **122** (10) 1003-1011 (1996).

Makris N. "Rigidity-Plasticity-Viscosity: Can ER dampers protect base-isolated structures from near-source ground motions?," *J. Earth. Eng. and Struct. Dyn.*, **26** (5) 571-591 (1997).

Miyazaki M., Mitsusaka V. "Design of a building with 20% or greater damping." *Proc. 10th World Conf. on Earthquake Engrg., Madrid.* 4143–4148 (1992).

Modi V.J., Munshi S.R. "An efficient liquid sloshing damper for vibration control," *Journal of Fluids and Structures*, **12** 1055-1071 (1998).

Nims D.K., Richter P.J., Bachman R.E. "The use of the energy dissipating restraint for seismic hazard mitigation." *Earthquake Spectra*, **(9)** 467–489 (1993).

Nyawako D., Reynolds P. "Technologies for Mitigation of Human-induced Vibrations in Civil Engineering Structures," *The Shock and Vibration Digest*, **39** 465-493 (2007).

Ou J.P., Wu B. "Experiment comparison of the properties of friction and mild steel yielding energy dissipators and their effects on reducing vibration of structure under earthquake." *Earthquake Engrg. and Engrg. Vib.*, **(15)**45–62 (1995).

Pall A.S., Marsh C. "Response of friction damped braced frames." *J. Struct. Div.,* ASCE, **(108)** 1313–1323 (1982).

Papadimitriou C. "Mechanical Vibrations," *University of Thessaly, Dept. of Mechanical and Industrial Engineering*, (2006).

Rahul H., Soong T.T. "Parametric study and simplified design of tuned mass dampers," *Engineering Structures*, **20** (3) 193-204 (1998).

Reinhorn A.M., Li C., Constantinou M.C. "Experimental and analytical investigation of seismic retrofit of structures with supplement damping, part I: fluid viscous damping devices." *Technical Report NCEER-95-0001, NCEER, Buffalo, NY* (1995).

Reinhorn A.M., Li C. "Experimental and analytical investigation of seismic retrofit of structures with supplement damping, part III: viscous damping wall." *Technical Report NCEER-95-0013, NCEER, Buffalo, NY* (1995).

Sadek F., Mohraz B., Taylor A.W., Chung R.M. "A method of estimating the parameters of tuned mass dampers for seismic applications." *Earthquake Engrg. and Struct. Dyn.*, **(26)** 617–635 (1997).

Scholl R.E. "Design criteria for yielding and friction energy dissipators." *Proc. ATC 17-1 on Seismic Isolation, Energy Dissipation, and Active Control*, **(2)** 485–495 (1993).

Shen K.L., Soong T.T. "Modeling of viscoelastic dampers for structural applications." *J. Engrg. Mech.*, ASCE, **(121)** 694–701 (1995).

Soong T.T., Dargush G.F. "Passive Energy Dissipation Systems in Structural Engineering," *John Wiley & Sons, England,* (1997).

Soong T.T., Spencer Jr. B.F. "Supplemental energy dissipation: state-of-the-art and state-of-the-practice." *Engineering Structures*, **24** (3) 243-259 (2002).

Spencer Jr. B.F, Sain MK "Controlling buildings: a new frontier in feedback," *IEEE Control Systems Magazine, Sp Issue Emerging Technologies* **17** (6) 19–35 (1997).

Spencer Jr. B.F., Dyke S.J., Sain M.K., Carlson J.D. "Phenomenological model of a magnetorheological damper," *J. Engrg. Mech.* ASCE, 123 **(3)** 230-238 (1997).

Spencer Jr. B.F., Soong, T.T. "New application and development of active, semi-acitve and hybrid control techniques for seismic and non-seismic vibration in the USA." *Proc. Int. Post-SMiRT Conf. Seminar on Seismic Isolation, Passive Energy Dissipation and Active Control of Vib. of Struct.*, **1** 467–488 (1999).

Spencer Jr. B.F., Nagarajaiah S. "State of the Art of Structural Control," *Journal of Structural Engineering, Forum, ASCE*, (2003).

Sun L.M., Fujino Y., Pacheco B.M., Chaisari P. "Nonlinear waves and dynamic pressures in rectangular TLD-simulation and experimental verification," *JSCE structural eng./earthquake eng.* **6** (2), 251-262 (1989).

Symans M.D., Constantinou M.C., Taylor D.P., Garnjost K.D. "Semi-Active Fluid Viscous Dampers for Seismic Response Control," *Proc. Of the First World Conference on Structural Control, Pasadena, CA.,*(1994).

Symans M.D., Constantinou M.C. "Seismic testing of a building structure with semi-active fluid damper control system." *Earthquake Engrg. And Struct. Dyn.*, **26** 757–777 (1997).

Symans M.D., Constantinou M.C. "Semi-Active Control Systems for Seismic Protection of Structures: a state-of-the-art-review," *Engineering Structures*, **21** 469-487 (1999).

Tamura Y., Fuji K.M., Sato T., Wakahara T., Kosugi M. "Wind Induced Vibration of Tall Towers and Practical Applications of Tuned Sloshing Dampers," *Proceedings of Symposium/Workshop on the Serviceability of Buildings,* Ottawa, Canada, **1** 228-241 (1988).

Tamura Y. "Application of Damping Devices to suppress Wind-induced Responses of Buildings," *Journal of Wind Engineering and Industrial Aerodynamics*, **74-76** 49-72 (1998).

Taylor D.P., Constantinou M.C. "Fluid dampers for applications of seismic energy dissipation and seismic isolation." *Proc. 11th World Conf. on Earthquake Engrg., Acapulco, Mexico* (1996).

Tsai K.C., Chen H.W., Hong C.P., Su Y.F. "Design of steel triangular plate energy absorbers for seismic-resistant construction." *Earthquake Spectra*, **(9)** 505–528 (1993).

Tsai H.C., Lin G.C. "Optimum tuned mass dampers for minimizing steady-state response of support excited and damped system." *Earthquake Engrg. and Struct. Dyn.*, **(22)** 957–973 (1993).

Uang C.M., Bertero V.V. "Use of energy as a design criterion in earthquake–resistant design," *Report No. UCB/EERC-88/18, University of California, Berkeley*, (1988).

Verboven P. "Frequency domain system identification for modal analysis," *PhD Thesis, Vrije Universiteit Brussel, Belgium* (2002).

Wada A., Huang Y.H., Iwata M. "Passive damping technology for buildings in Japan." *Progress in Struct. Engrg. and Mat.*, **(2)** 1–15 (1999).

Wakahara T., Ohyama T., Fuji K., Suppression of wind-induced vibration of a tall building using the tuned liquid damper, *J. Wind Eng. Ind. Aerodyn.* **41-44** 1895-1906 (1992).

Whittaker A., Aiker I., Bergman D., Clark P., Cohen J., Kelly J., Scholl R. "Code requirements for the design and implementation of passive energy dissipation systems." *Proc. ATC 17-1 on Seismic Isolation, Energy Dissipation, and Active Control*, **(2)** 497–508 (1993).

Xia C., Hanson R.D. "Influence of ADAS element parameters on building seismic response." *J. Struct. Engrg.*, ASCE, **(118)** 1903–1918 (1992).

Xu K., Igusa T. "Vibration control using multiple tuned mass dampers," *J. Sound and Vib.* 175 **(4)** 491-503 (1994).

Yamaguchi H., Harnpornchai N.. "Fundamental Characteristics of Multiple Tuned Mass Dampers for Suppressing Harmonically Forced Oscillations," *Earthquake Engineering and structural Dynamics*, **22** 51-62 (1993).

Yang G., Spencer Jr. B.F., Carlson J.D., Sain, M.K. "Large-scale MR fluid dampers: modeling, and dynamic performance considerations." *Engineering Structures*, **24** (3) 309-323 (2002).

Yao J.T.P. "Concept of structural control," *J. Struct. Div.* ASCE **98** 1567-1574 (1972).